

**INVESTIGATION OF CONTROLLING FACTORS ON CELLULAR AND
SOFT TISSUE PRESERVATION IN FOSSILS FROM WHITE RIVER
GROUP OF NEBRASKA AND SOUTH DAKOTA**

A Thesis
Submitted to
the Temple University Graduate Board

In Partial Fulfillment
of the Requirements for the Degree
MASTER OF SCIENCE

by
Brian Kibelstis
August 2024

Thesis Approvals:

Dennis O. Terry, Jr, Thesis Advisor, Earth and Environmental Science
David E. Grandstaff, Earth and Environmental Science
Allison R. Tumarkin-Deratzian, Earth and Environmental Science
Paul V. Ullman, University of North Dakota

ABSTRACT

Recovery of soft tissues, such as original cells, blood vessels, and proteinaceous fibers, from fossil bone is becoming more frequent, but the factors that control such exceptional preservation are not well understood. This study assesses the influence(s) exerted on soft tissue preservation by several possible controlling factors. Specifically, this study assesses biomechanical function, apatite recrystallization, bone tissue density, taxonomic identity, and depositional environment as possible controls on the quantity and quality of preservation of endogenous microstructures. Six bones derived from three taxa from the Paleogene White River Group of South Dakota and Nebraska – namely an oreodont from the Oligocene Brule Formation and a brontothere and tortoise from the Eocene Chadron Formation – were subsampled for cortical and trabecular bone, which were then assessed via demineralization, thin sectioning, transmitted light and scanning electron microscopy (SEM), X-ray diffraction (XRD), and energy-dispersive X-ray spectroscopy (EDS). Bones belonging to each clade were acquired from bonebeds to minimize intraspecific variation in taphonomic history, and (where possible) similar skeletal elements were selected from each skeleton to similarly minimize differences in biomechanical function between corresponding samples.

Initial demineralization analyses showed high yields of potentially endogenous cells and soft tissues in all three taxa: only two subsamples lacked structures morphologically consistent with osteocytes, and microstructures visually consistent with vertebrate blood vessels and fibrous matrix were recovered from all 12 subsamples of the six fossils. Variation in the dominant tissue type corresponded with taxonomic identity and bone type and was independent of biomechanical function, as defined in this study,

but this assertion requires a larger dataset to be conclusive. Apatite crystallinity loosely correlated with osteocyte preservation, but the association was less robust than the taxonomic identity. Transmitted light microscopy of histological thin sections revealed varying levels of histological alteration among the bones. SEM-EDS analyses of demineralized microstructures identified apparent zeolite mineralization and zeolite crystals within the majority of blood vessel fragments, although some examples of hollow vessels were found which were identified to be composed primarily of silicon, oxygen, and carbon. Elemental mapping of thin sections via SEM-EDS revealed evidence of double-medium diffusion through Haversian canals and trabecular voids, as well as a dominance of enlarged, recrystallized bioapatite crystals. Observed variations in thin section and SEM also suggest different taphonomic histories for the three clades, particularly the oreodont samples, as certain features observed in thin sections were not observed in SEM. The demineralization data indicate a potential correlation between taxonomic identity and soft tissue preservation, but geochemical and thin section analyses suggest geochemical processes controlling mineralization may have a greater influence on the abundance of microstructures recovered through demineralization assays.

ACKNOWLEDGEMENTS

First and foremost, I would like to thank my advisor, Dr. Dennis Terry, for his guidance and support throughout this study – none of this would have happened without him. I would also like to thank my other committee members for their help in completing this study – Dr. Allison Tumarkin-Deratzian, for getting me through more than a few histologic and taphonomic roadblocks; Dr. David Grandstaff, for teaching me more about geochemistry in one semester than I had thought possible; and Dr. Paul Ullmann, for providing the guidance needed to ensure our initial assays were successful and for his continued involvement despite some major changes in the span of only two years.

Outside of my committee, I would also like to thank Dr. Steven Chemtob and Dr. Kristyn Voegele for their material help with producing additional solvent for my demineralization assays – much of my later research would not have been possible without them. Dr. Dmitriy Dikin's expertise was indispensable to my SEM and EDS analyses, without which I would not have any geochemical data. I would also like to acknowledge Jim Ladd, Jesse Thornburg, and Minh Nguyen for the logistical support that ensured this study could be completed. I would like to thank the Delaware Valley Paleontological Society, which funded my SEM work via their Paul Bond Scholarship. Funding for this research was also provided by a grant from the National Park Service to D. Terry (PMIS-154957). Fossils used for this study were collected over the past two decades by D. Terry under various permits from the National Park Service (Badlands National Park, SD: BADL-2012-SCI-0016 and BADL-2019-SCI-0012), U.S. Forest Service (Toadstool Geologic Park, NE: Challenge Cost-share Agreement 05-PA-11020700), and Bureau of Land Management (Flagstaff Rim, WY: PA09-WY-179).

TABLE OF CONTENTS

	Page
ABSTRACT.....	ii
ACKNOWLEDGEMENTS.....	iv
LIST OF FIGURES.....	vi
LIST OF TABLES.....	vii
CHAPTER	
1. INTRODUCTION.....	1
2. BACKGROUND.....	3
2.1 Lithologic Description of the White River Group.....	3
2.2 Cellular and Soft Tissue Preservation in the Vertebrate Fossil Record.....	4
2.3 Apatite Crystallinity in Fossil Bone.....	5
2.4 Geochemistry.....	6
3. METHODS.....	8
3.1 Sample Collection and Selection.....	8
3.2 Demineralization and Transmitted-Light Microscopy.....	9
3.3 Histologic Thin Sections.....	11
3.4 X-Ray Diffraction and Crystallinity Indices.....	12
3.5 Scanning Electron Microscopy and Energy Dispersive X-Ray Spectroscopy..	12
4. RESULTS.....	14
4.1 Demineralization and Transmitted-Light Microscopy.....	14
4.2 Histologic Thin Sections.....	15
4.3 X-Ray Diffraction and Crystallinity Indices.....	17
4.4 Scanning Electron Microscopy and Energy Dispersive X-Ray Analysis.....	18
5. INTERPRETATIONS AND DISCUSSION.....	25
5.1 Endogenous Structure Counts and Biomechanical Function.....	25
5.2 Taxonomy.....	26

5.3 Apatite Recrystallization.....	27
5.4 Histology.....	28
5.5 SEM.....	30
6. CONCLUSION.....	36
REFERENCES CITED.....	39
APPENDICES	
A. FOSSIL BONE IMAGES.....	43
B. DEMINERALIZATION PRODUCTS.....	44
C. THIN SECTION IMAGES.....	47
D. X-RAY DIFFRACTION DATA.....	52
E. SEM IMAGES AND EDS DATA.....	83
F. SEM-EDS MAPPING.....	88

LIST OF FIGURES

Figure	Page
1. White River Group Section and Map.....	3
2. HCl Wash Mass Change.....	10
3. Demineralized Cells and Tissues.....	14
4. Thin Section Plate.....	16
5. SEM-EDS Scan of a Potential Blood Vessel Infill.....	19
6. SEM Images of Sectioned Fossil Bone.....	21
7. EDS Maps.....	23
8. EDS Line Scan.....	24
9. Thin Section of Fungally-Degraded Bone.....	29
10. Oreodont Limb Section.....	30
11. SEM Microstructure Images.....	33
12. SEM Images Interpreted as Fungal Hyphae.....	35
13. Pre-Subsampling Images of the Six Fossil Bones Used for This Study.....	43
14. “Set 1” Demineralization Wells.....	45
15. “Set 2” Demineralization Wells.....	46
16. Thin Section Image Of Brontothere Rib.....	47
17. Calcite-Infilled Trabecular Voids Within the Brontothere Phalanx.....	48
18. Thin Section Image of the Oreodont Dentary.....	49
19. Thin Section Image of the Cortical Region of the Tortoise Peripheral.....	50
20. Thin Section Image of the Cortical Region of the Tortoise Scapula.....	51
21. X-Ray Diffractograms for Brontothere Rib Subsamples.....	77

Figure	Page
22. X-Ray Diffractograms for Brontothere Phalanx Subsamples.....	78
23. X-Ray Diffractograms for Oreodont Dentary Subsamples.....	79
24. X-Ray Diffractograms for Oreodont Limb Bone Subsamples.....	80
25. X-Ray Diffractograms for Tortoise Peripheral Subsamples.....	81
26. X-Ray Diffractograms for Tortoise Scapula Subsamples.....	82
27. Structures and EDS Spectra from the Brontothere Phalanx Cortical Bone.....	83
28. Preserved Vessel from Brontothere Phalanx Trabecular Bone.....	84
29. Structures and EDS Spectra from the Oreodont Limb Cortical Bone....	85
30. Structures and EDS Spectra from the Oreodont Limb Trabecular Bone.....	86
31. Structures and EDS Spectra from the Oreodont Dentary Cortical Bone.....	87
32. Brontothere Rib EDS Map Set.....	88
33. Oreodont Limb Bone EDS Line Scan.....	89
34. Tortoise Peripheral EDS Map Set.....	90

LIST OF TABLES

Table	Page
1. Sample Codes.....	8
2. Demineralization Tissue Bins.....	15
3. Histological Indices.....	17
4. Crystallinity Indices.....	18
5. Elemental Abundances In Microstructures.....	20
6. Demineralization “Set 1” Count Data.....	44
7. Brontothere Subsample XRD Data, Background Subtracted.....	52
8. Oreodont Subsample XRD Data, Background Subtracted.....	60
9. Tortoise Subsample XRD Data, Background Subtracted.....	68

CHAPTER 1

INTRODUCTION

Recognition of the preservation of endogenous cells and soft tissues (e.g., proteinaceous fibers, vascular tissues) in fossilized bone is a relatively recent event (e.g., Schweitzer, 1995; Schweitzer & Horner, 1999; Schweitzer et al., 2007). Since a famous discovery of endogenous soft tissues in *Tyrannosaurus rex* (Schweitzer et al., 2005), similar structures have been found in fossils of a wide variety of extinct taxa, including other non-avian dinosaurs, crocodylians, turtles, pre-mammalian synapsids, and mammals (e.g., Armitage, 2022; Gallucci, 2020; Schweitzer, 1995; Schweitzer et al., 2007; Voegelé et al., 2022; Woolslayer et al., 2022). However, the wide variety of species, environments, and time periods from which these soft tissues have been recovered raises questions about what geologic, taphonomic, and environmental factors determine the preservation of these structures. Little work has been conducted thus far toward answering these questions, and most of the studies conducted have failed to show strong correlations between the preservation of endogenous cells and soft tissues and any geologic or environmental variable (Cadena & Schweitzer, 2014; Gallucci, 2020; Woolslayer et al., 2022; Ullmann & Schweitzer, 2023).

This study aims to assess multiple potential controls and proxies by which the preservation of endogenous cells and soft tissues may be predicted or controlled. Tested variables include biomechanical function, cortical vs. trabecular bone, taxonomic identity, extent of apatite recrystallization, elemental composition, and quality of histologic preservation of bone structures. Techniques used include bone demineralization, histologic thin-section, X-ray diffraction (XRD), transmitted light

microscopy, scanning electron microscopy (SEM), and energy dispersive X-ray spectroscopy (EDS) to compare data from fossil bones from the White River Group of South Dakota and Nebraska to identify any potential correlations between the tested factors and the preservation of endogenous cells and soft tissues.

CHAPTER 2

BACKGROUND

2.1 Lithologic Description of the White River Group

The samples for this study are from outcrops of the Paleogene White River Group exposed in South Dakota and Nebraska. This sequence of strata preserves evidence of terrestrial ecosystems from the Late Eocene and Early Oligocene Epochs (~35.5–30 Ma) and is primarily composed of mudstones and siltstones that incorporate volcanoclastic sediments (Larson & Evanoff, 1998). Fossils used in this study were collected from two formations of the White River Group: the Eocene Chadron Formation and the Oligocene Brule Formation (Fig. 1).

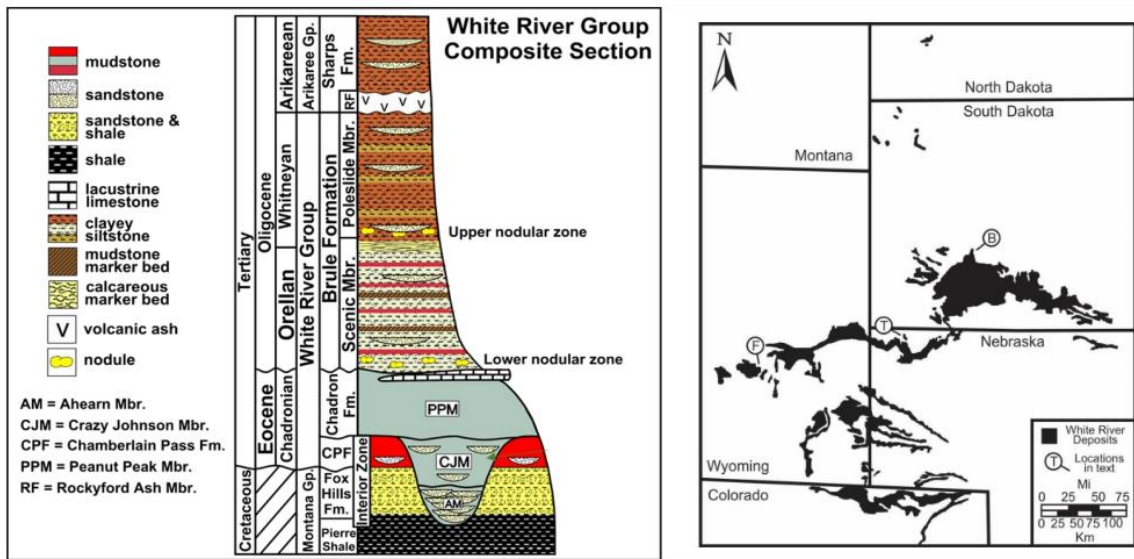


Figure 1. White River Group Section and Map. Composite section and map of White River Group deposits, including sites of previous studies. Fossils used in this study originate from the uppermost Chadron and lower Brule formations and were collected at Toadstool Geologic Park (T) and Badlands National Park (B). Modified from Terry (2001) and Gallucci (2020).

The Chadron Formation is composed primarily of sandstones and pedogenically altered mudstones. These strata are interpreted to have been deposited in forested, fluvial

settings under a warm, humid climate (Terry, 2001; Gallucci, 2020). By contrast, the overlying Oligocene Brule Formation consists of mudstones that coarsen up-section into siltstones, which have typically been interpreted as recording a transition to a drier, eolian environment consistent with a plains biome, contrasting with the preceding forest cover of the Late Eocene (LaGarry, 1998; Terry, 2001; Zanazzi et al, 2007; Lukens, 2013). Both formations contain a notable volcanoclastic component, primarily associated with explosive volcanism in Utah and Nevada beginning ~35.5 Ma (LaGarry, 1998; Larson & Evanoff, 1998).

2.2 Cellular and Soft Tissue Preservation in the Vertebrate Fossil Record

Soft tissues have historically been assumed to decay prior to fossilization, leaving only the hard parts of an organism, such as bones or shells, to be preserved as fossils (Schweitzer et al., 2019). Many well-known macroscopic soft parts, such as the feathers of *Archaeopteryx* or body outlines of ichthyosaurs (Owen, 1841; Meyer, 1862), have been preserved as impressions or carbonized films. Direct preservation of endogenous cells and soft tissues, in contrast, was not meaningfully substantiated until the 1990s (e.g., Schweitzer, 1995; Schweitzer & Horner, 1999).

Over the last twenty years, endogenous tissues have been recovered from a wide variety of taxa, depositional environments, and time. Early examples were recovered from bones of a *Tyrannosaurus rex* buried in channel sandstones of the Hell Creek Formation (Schweitzer, 1995; Schweitzer & Horner, 1999). Preserved cells and soft tissues have also recently been recovered from marine crocodylians and turtles from the Maastrichtian–Paleocene Hornerstown Formation of southern New Jersey (Voegelé et al., 2022), mammalian bones from the Eocene–Oligocene White River Group of South

Dakota and Nebraska (Gallucci, 2020; Woolslayer et al., 2022), and synapsid fossils from the Permian of Oklahoma (Armitage, 2022). As can thus be seen, preservation of endogenous cells and soft tissues has been shown to be fairly common, and the frequency with which endogenous cells and soft tissues are now being found raises questions regarding the factors that influence their preservation (Gallucci, 2020; Barker et al., 2021; Armitage, 2022; Voegelé et al., 2022; Woolslayer et al., 2022). Possible factors that have been proposed as influences on soft tissue preservation include taxonomic identity (Cadena, 2016), geologic age (Wiersma et al., 2021), depositional environment / entombing lithology (Barker et al., 2021), and differences in taphonomic history (Woolslayer et al., 2022). Investigations thus far have failed to show any strong correlations and, in some cases, have even demonstrated independence from these factors (Gallucci, 2020; Woolslayer et al., 2022; Ullmann & Schweitzer, 2023).

2.3 Apatite Crystallinity in Fossil Bone

Bone is composed of collagen fibers and carbonate-hydroxyapatite crystallites. During fossilization, the apatite crystals often recrystallize, growing larger, more ordered, and ultimately transitioning into a more stable phase (e.g., fluorapatite), primarily through the incorporation of fluorine (Huttenlocker et al., 2013; Keenan, 2016). Apatite crystallinity analysis utilizes X-ray diffraction (XRD) to assess the size and ordering of apatite crystallites in a given sample, which is quantified using a Crystallinity Index (CI) calculated from ratios of XRD peak heights associated with hydroxyapatite with higher CI values indicating greater degrees of recrystallization (Person et al., 1995). An initial study by Person et al. (1995), which analyzed bones ranging in age from the Late Triassic to near-modern, reported an inverse relationship between CI values in bone and preserved

endogenous organic molecules. A later assessment by Gallucci (2020), however, presented evidence disputing the correlation of CI values and preservation of endogenous cells and tissues, finding such materials in fossilized bones regardless of the calculated CI. As such, the exact influence of apatite recrystallization on the preservation of endogenous soft tissues within bone remains unclear.

2.4 Geochemistry

Wiemann et al. (2018) proposed that oxidizing conditions were favorable to preserving endogenous cells and soft tissues. These conditions are commonly found in the White River Group (Retallack, 1983; Larson & Evanoff, 1998; Terry, 2001), from which fossil bones have yielded an abundance of such cells and soft tissues (Gallucci, 2020; Woolslayer et al., 2022). Other studies, however, suggest reducing or iron-rich environments favor soft tissue preservation (Ullmann et al., 2019; Voegele et al., 2022; Zhao et al., 2023). Optical analyses of White River Group fossils have shown a distinct lack of visible iron in preserved cells and soft tissues in comparison to similar structures from other geologic formations, suggesting that the abundance of iron may not be a primary controlling factor in the preservation of these structures (Ullmann et al., 2019; Gallucci, 2020; Woolslayer et al., 2022).

Geochemical analysis of fossil bone is commonly performed via laser-ablation inductively coupled mass spectrometry (LA-ICP-MS). This technique typically entails ablation of an edge-to-edge transect of polished bone for determination of spatial variations in elemental composition along the chosen transect (Suarez et al., 2010; Drewicz et al., 2011; Gallucci, 2020). For example, this method was used by Ullmann et al. (2020) to assess rare earth and trace element (REE, TE) concentrations in a polished

section of *Edmontosaurus* bone, showing a relative enrichment in REEs near the bone surface compared to internal regions of the bone. Similar data were collected for fossils from the White River Group and used to approximate the time period of diffusion over which bone was incorporating these elements from groundwater, in turn providing a proxy for recrystallization rate – a possible controlling factor on soft tissue preservation (Gallucci, 2020). LA-ICP-MS has also been used to reconstruct paleoredox conditions based on relative enrichment of cerium and uranium, with relative enrichment in the cerium generally indicating that fossilization occurred in a reducing environment whereas enrichment in uranium is generally suggestive of fossilization occurring under oxidizing early diagenetic conditions (Metzger et al., 2004).

CHAPTER 3

METHODS

3.1 Sample Collection and Selection

The fossils used in this study derive from existing collections (Table 1) (Terry et al., 2014). Samples selected represent multiple taxa found in the Eocene–Oligocene deposits of the White River Group in South Dakota and Nebraska. Three available taxa were chosen to cover multiple ecological niches and clades: brontotheres, representing large herbivorous mammals; oreodonts, representing smaller mammalian herbivores; and tortoises, representing reptilian herbivores. Specific bones of each taxon, deriving from weight-bearing and non-weight-bearing portions of the skeleton (i.e., limb bones vs. ribs and skull elements), were analyzed. Selected fossils were assigned secondary codes upon subsampling which indicate the source taxon, skeletal element, and bone tissue type (i.e. C for cortical, T for trabecular) (Table 1). The oreodont samples were sourced from a carbonate nodule in Oligocene siltstones of the lower Brule Formation at Badlands National Park in South Dakota, while the brontothere and tortoise samples were collected from Eocene mudstones of the Chadron Formation at Toadstool Geologic Park in northwestern Nebraska.

Table 1. Sample Codes. Catalog codes associated with the samples used in this study, as well as a summary of each taxonomic identification, skeletal element, and acronyms used to describe each associated subsample hereafter. Abbreviation: Indet., indeterminate.

Temple Catalog Code	Taxon	Anatomical Position	Study Codes
F08-915R	Brontothere	Rib, Phalanx	BRC, BRT, BPC, BPT
F12-28	Oreodont	Dentary, Indet. Limb Bone	ODC, ODT, OLC, OLT
F08-52A	Tortoise	Peripheral (Shell)	TPC, TPT
F08-52B	Tortoise	Scapula	TSC, TST

3.2 Demineralization and Transmitted-Light Microscopy

Initial assessments of cellular and soft tissue preservation were done by demineralization of bone in ethylenediaminetetraacetic acid (EDTA). Fossils were subsampled for cortical and trabecular bone, after which each subsample was weighed and then briefly washed in a 10% HCl solution to remove excess carbonate-rich sediments, rinsed in deionized water, dried, and re-weighed (Figure 2). Following these preparation steps, the samples were then placed into separate wells of two six-well polystyrene cell culture plates and incubated in enough 0.5 M EDTA pH 8.0 solution to fully cover the subsamples (typically 3–5 mL). This solution was then replaced every 48–72 hours over a period of about seven weeks (until the samples were sufficiently demineralized for visualization).

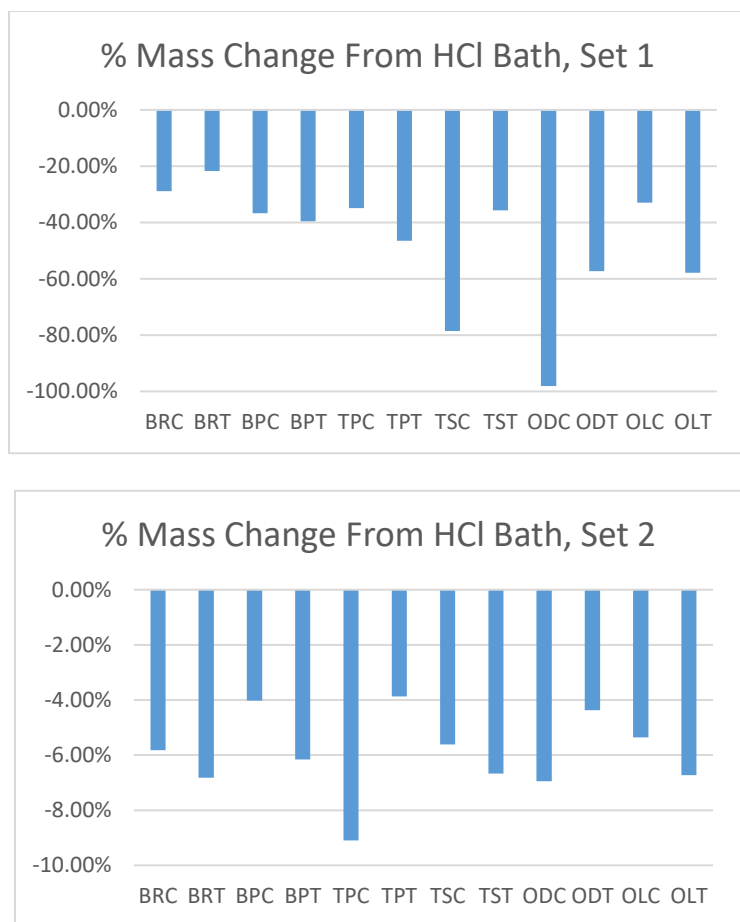


Figure 2. HCl Wash Mass Change. Percent mass change of “Set 1” (top) and “Set 2” (bottom) bone subsamples following the initial HCl wash. “Set 1” was used for initial tissue-count analysis via transmitted light microscopy, while “Set 2” was used for SEM imaging and EDS analyses. The high losses observed in “Set 1” samples of ODC and TSC resulted in individual subsamples being one to two orders of magnitude lesser in mass than other subsamples. Mass changes for “Set 2” were significantly lower, as less acid was used in the initial wash.

Resulting demineralization products were loaded onto standard microscope slides and coverslipped for transmitted light microscopy in order to assess the presence, quantity, and preservation quality of any preserved blood vessels, fibrous matrix fragments, and osteocytes. Following prior studies (e.g., Ullmann & Schweitzer, 2023) the quantity of each of these cell / tissue types was recorded as counts per slide, with relative abundances used to simplify later comparisons. Categories were defined as – slides with ≥ 50 observations of a particular organic microstructure type were marked as

“Abundant” in that microstructure type; slides with 30–49 instances were marked as “Frequent;” slides with 15–29 instances were marked as “Uncommon;” slides with 1–14 instances were marked as “Rare;” and slides in which the respective microstructure type was not observed were marked as “Absent.” When a specific tissue type reached the “Abundant” category, counting of that tissue type stopped and the number of visual sweeps across the microscope slide to reach that checkpoint was recorded for later comparisons. A consistent number of sweeps per slide – 20 ± 1 sweeps under a 20X microscope objective – produced a reliable method for comparing samples with high rates of preservation without counting features that would not result in a change in category classification. Apart from quantitative data, observations of qualitative information were also made, including the preservation state of osteocyte filopodia, the complexity of blood vessel fragment morphology (i.e. number of ramifications / branches), and the presence or absence of red-orange or other colored staining.

3.3 Histologic Thin Sections

Histologic thin sections were prepared of each of the six fossils used in this study. Samples were embedded in Hillquist® thin section epoxies, then cut and mounted to frosted slides, with some reassembly required if a specimen fractured during initial cutting. These samples were then trimmed and polished to ~100 µm thickness using 320 and 600 grit sandpaper on a lap wheel. The resulting thin sections were then analyzed under a transmitted light microscope and assigned Histological Index values to quantify their relative preservation quality (Hedges et al., 1995). Glycerin was not used in initial analyses in anticipation of geochemical assessments of these sections. The goal of this analysis was to assess any internal, micro-scale taphonomic alterations and differences

among the fossils that could not be observed externally or via other methods. Selection of this technique was prompted by observed disparities in the EDTA breakdown of samples and because histology affords a means of assessing bone tissue microstructure, which may dictate groundwater access to inner regions of a bone during diagenetic alteration, as well as to help contextualize demineralization data with the structure of each bone and provide guidance for EDS elemental mapping.

3.4 X-Ray Diffraction and Crystallinity Indices

Gallucci (2020) assessed the Crystallinity Indices (CI values) of fossil bone; however, no attempt was made to differentiate the CI values of cortical and trabecular bone. The current study made this distinction between bone tissue types, thereby generating a higher resolution dataset, by subsampling the fossils used for demineralization into cortical and trabecular subsamples (Table 1). These subsamples were then ground and homogenized into 70 μm powders using a mortar and pestle and a 70 μm mesh sieve that was washed with deionized water between samples. These powders were then loaded into a Bruker D8 Advance X-ray diffractometer and scanned using Cu α x-rays from 5–70° 2 θ . Background signal was removed within the Diffrac.EVA® software, and each resulting diffractogram was exported to Microsoft Excel and used to calculate a Crystallinity Index (Person et al., 1995), using the following formula, where H represents the height of each respective peak (eq. 1).

$$[\text{Eq. 1}] \text{ CI} = \frac{\Sigma(H[202],H[300],H[112])}{H[211]}$$

3.5 Scanning Electron Microscopy and Energy Dispersive X-ray Spectroscopy

A second batch of fossil bone subsamples (“Set 2”) were also demineralized in EDTA, following the procedure described in Section 3.2. Demineralization products from

this batch were allowed to demineralize over approximately 10 weeks after which they were washed five to six times with deionized water to stabilize them for SEM analyses. Demineralization products were then pipetted onto a silicon wafer for SEM visualization. Samples were analyzed in secondary electron imaging mode and via energy dispersive X-ray spectroscopy (EDS) using a Quanta™ 450 FEG microscope. Oxford Instruments® Aztec® software was used to determine bulk element composition, with silicon being excluded from the initial analyses to improve the visibility of less abundant elements (and to ensure minimal detection of any signals from the underlying silicon wafer plate).

A second set of EDS analyses were conducted using thin sections of the bones to create elemental maps of key structures within the original, undissolved bone, namely cortical-trabecular transitions, primary and secondary osteons, and trabecular voids infilled by secondary (permineralizing) mineral phases. These images were specifically used to determine whether diagenetic interactions with groundwater took place entirely from the outer surface of the bone or if groundwater interacted with the bone through infiltration of internal pathways as well (i.e. through the central medullary cavity; cf., Goodwin et al., 2007). EDS line scans were also utilized to assess possible changes in composition as a function of distance from the cortical margin. These analyses were thus used to assess the overall diagenetic history of the fossils, particularly regarding multi-phase mineralization and alteration, as well as to identify any signs of double-medium diffusion (DMD, *sensu* Kohn, 2008) of groundwater through internal conduits such as Haversian canals and trabecular voids.

CHAPTER 4

RESULTS

4.1 Demineralization and Transmitted-Light Microscopy

Each subsample was analyzed for three varieties of soft tissue – blood vessels, osteocytes (bone cells), and fibrous matrix (the ultrastructural proteinaceous component of bone tissue) – on a counts-per-slide basis, with these quantitative results being categorized for later comparison (Figure 3). My categorized demineralization data are provided below in Table 2, with the raw count data provided in the Appendices.

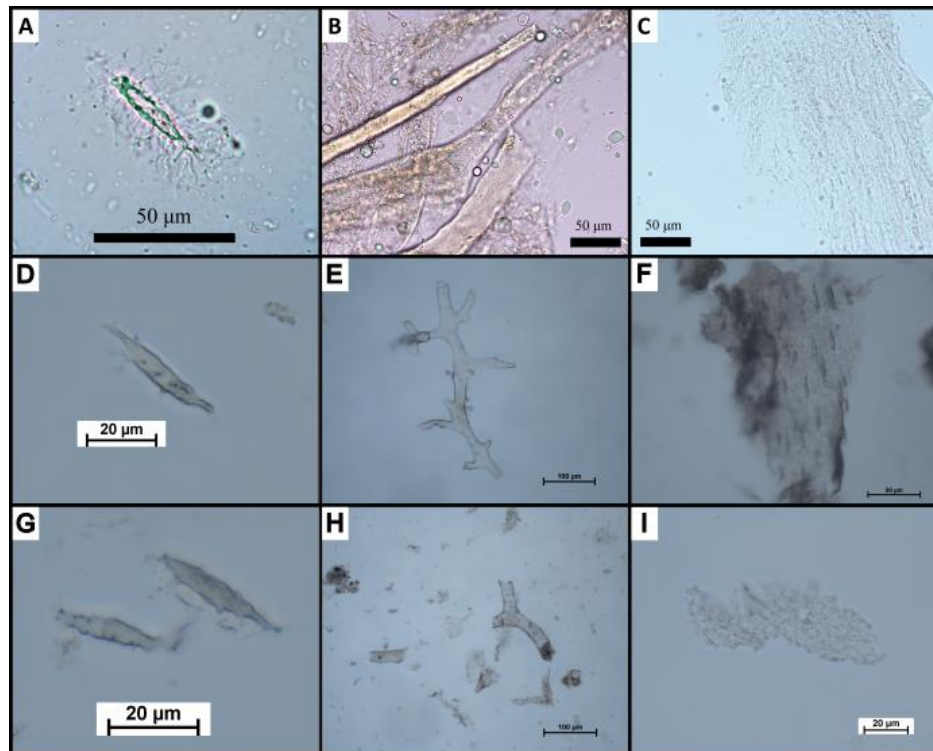


Figure 3: Examples of Demineralized Cells and Tissues: Transmitted light images of endogenous cells and soft tissues obtained by demineralizing fossil and modern bone. A-C from Ullmann et al. (2019) sourced from modern Alligator mississippiensis. D and F-H are sourced from tortoise bones from the White River Group, and E and I are from oreodont bones. The left column shows structures morphologically consistent with osteocytes, the center column shows structures morphologically consistent with blood vessels, and the right column shows structures morphologically consistent with sheets of fibrous matrix.

Table 2. Demineralization Results. Summary of cellular and soft tissue recovery from my optical demineralization analysis (“Set 1” samples).

Sample	Fibrous Matrix	Osteocytes	Blood Vessels
BRC	Frequent	Rare	Abundant
BRT	Abundant	Rare	Uncommon
BPC	Rare	Rare	Abundant
BPT	Uncommon	Rare	Frequent
ODC	Rare	Rare	Rare
ODT	Uncommon	Rare	Abundant
OLC	Uncommon	Absent	Abundant
OLT	Frequent	Absent	Abundant
TPC	Frequent	Abundant	Abundant
TPT	Uncommon	Abundant	Rare
TSC	Uncommon	Frequent	Rare
TST	Frequent	Abundant	Abundant

4.2 Histologic Thin Sections

Transmitted light microscopy of thin sections prepared from the six fossils in this study was used to assess the meso-scale structure and preservation quality of the bones (Figure 4). Some observations were consistent across all samples, namely the presence of Haversian canals and associated structures (i.e., primary and secondary osteons), as well as blocky calcite infilling both these canals and other voids in trabecular regions of many of the specimens. Other observations indicated differential preservation between samples, with brontothere specimens exhibiting less well-preserved histology than the oreodont and tortoise fossils, as well as a far greater abundance of osteocyte lacunae in thin sections of the oreodont specimens than were observed in their associated demineralized samples. The brontothere thin sections lacked the apparent and well-preserved osteocyte lacunae observed within both the oreodont and tortoise slides, instead exhibiting a less detailed preservation on the millimeter scale. This difference is highlighted in Figure 4 through comparison of images A, C, D, and H: each shows varying degrees of preservation of Haversian canals. Trabecular voids in Figure 4-I also show multi-stage

infilling with secondary minerals, with micritic calcite lining the edges of trabecular voids, followed by later infilling with blocky calcite and lesser amounts of other minerals such as barite and chalcedony.

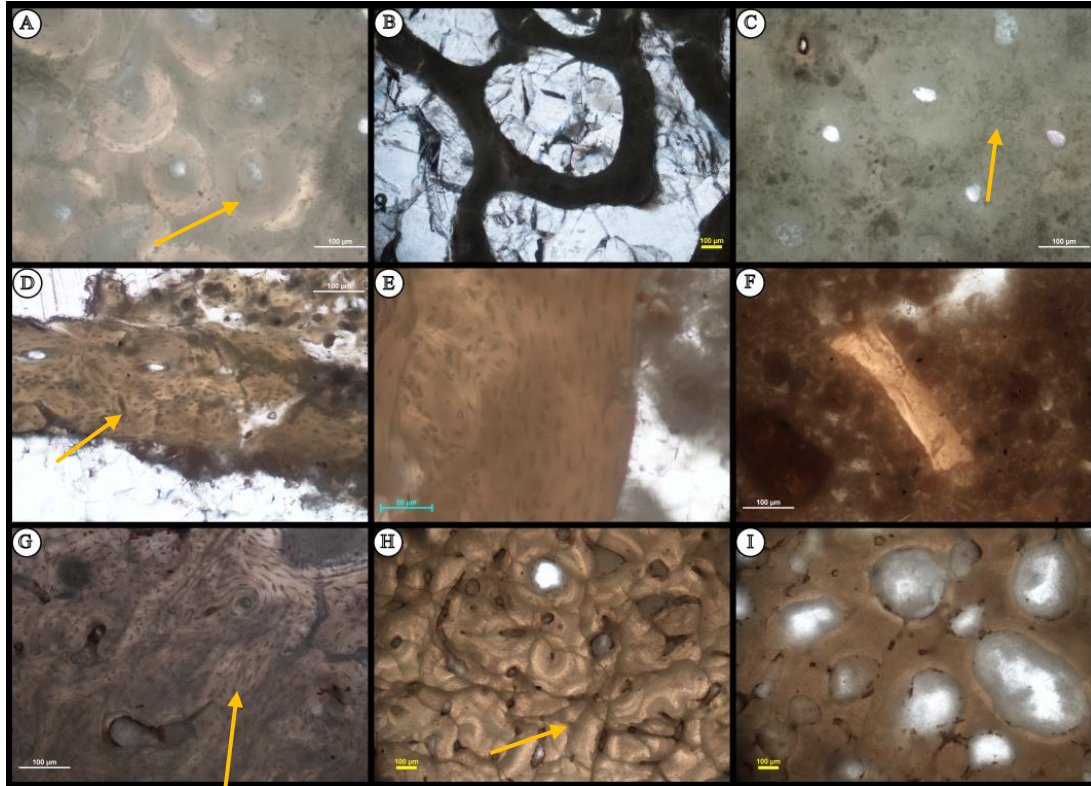


Figure 4. Thin Section Plate. Photomicrographs of fossil bones assessed in this study. Panels A-C show calcite-permineralized Haversian canals and trabecular voids in the brontothere rib specimen, as well as less detailed preservation of osteons compared to oreodont and tortoise specimens. Panels D and E show osteocytes in the oreodont dentary, while F shows an isolated fragment of bone within sediment infill in the marrow cavity of the oreodont limb bone. G-I show Haversian and trabecular structures in tortoise bone (G and I are from the tortoise peripheral, H from the scapula), as well as evidence of preserved osteocytes. Arrows point to osteons associated with Haversian canals; note the lack of osteocyte lacunae in the osteons of panels A and C compared to panels D and G.

Each sample was also assigned a Histological Index (HI) score following the methods of Hedges et al. (1995) to quantify the quality of meso-scale preservation on a 0–5 scale, with 5 indicating near-perfect preservation. This system considers the number of original textures and structures preserved within a bone’s cortical and trabecular

tissues, as well as the presence and quantity of both osteocyte lacunae and areas of destroyed bone fabric infilled with secondary mineralization. HI values for each of the fossil bones are provided in Table 3.

Table 3. Histological Indices. Histological Index (HI) values of each fossil bone examined in this study. An HI score of 5 indicates excellent preservation, while an HI score of 0 indicates very poor preservation.

Taxon	Bone	HI	Bone	HI
Brontothere	Rib	1	Phalanx	1
Oreodont	Dentary	3	Limb Bone	2
Tortoise	Peripheral	5	Scapula	4

4.3 X-Ray Diffraction and Crystallinity Indices

Using the procedure of Person et al. (1995), CI values are given in Table 4. The full diffractograms on which these calculations are based are provided in Appendix 4. The diffractograms contain not only the expected peaks for apatite that were used in this calculation, but also notable peaks associated with calcite, which were particularly apparent in subsamples of trabecular bone. These trabecular calcite peaks each exceeded the signal intensity height of the apatite peaks, ranging from approximately three to 17 times higher. For comparison, the greatest calcite peak observed in a cortical subsample was subequal to the highest apatite peak, with all other peaks being significantly shorter, ranging from approximately 30% of the height of the highest apatite peak to just over 80% of that peak.

Table 4: Crystallinity Indices: Apatite CI values associated with each subsample. Trabecular subsamples typically exhibited higher CI values than their cortical counterparts, and tortoise subsamples yielded higher cortical CI values than those from the other two taxa.

Sample	CI (Cortical)	CI (Trabecular)
BR	0.45	0.59
BP	0.50	0.55
OD	0.45	0.89
OL	0.48	1.03
TP	0.50	0.54
TS	0.50	0.60

4.4 Scanning Electron Microscopy and Energy Dispersive X-Ray Analysis

SEM images revealed a mix of hollow features consistent with the blood vessel fragments seen via transmitted light microscopy, solid crystalline features that were also morphologically consistent with blood vessels, and solid, mesh-like material interpreted as pieces of fibrous matrix. No definitive osteocytes were identified under SEM, even in samples which yielded abundant microstructures morphologically consistent with osteocytes in transmitted light microscopy. EDS analyses generally detected a high concentration of oxygen, as well as carbon and metals including aluminum, sodium, potassium, magnesium, iron, and calcium, with some samples also registering mercury, selenium, chlorine, sulfur, zinc, and titanium (Figure 5, Table 5). Silicon was also a prominent component in each scan, but this element was excluded from the quantitative summary in Table 5 to allow clearer interpretation of the relative abundances of the rare elements.

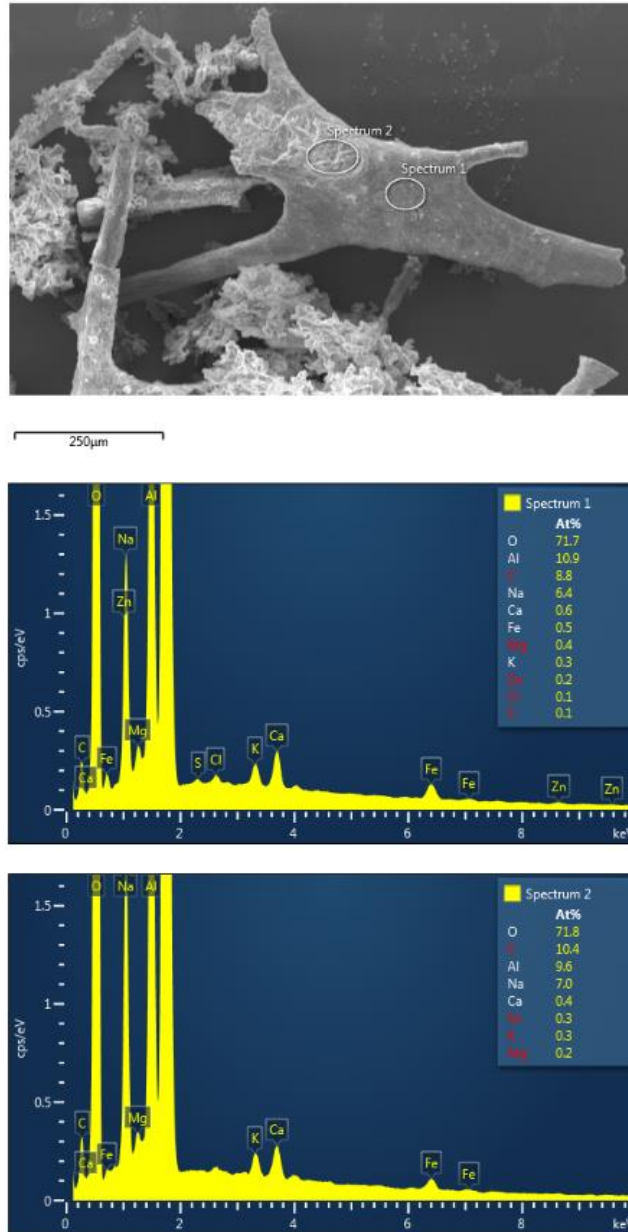


Figure 5. SEM-EDS Scan of a Potential Blood Vessel Infill. Compositional data from a preserved blood vessel (top) from the cortical region of the brontothere phalanx, highlighting the dominance of silicon (unlabeled peak at 1.8keV), oxygen, aluminum, and carbon in this microstructure. Locations of spectra shown in secondary electron image.

Table 5. Elemental Abundances in Microstructures. Summary of elemental abundances as determined by SEM-EDS. This dataset consists of 67 EDS point readings in “Set 2” samples and excludes a calibration site of blank wafer. Silicon is also excluded in this table to allow clearer interpretation of the relative abundances of rare elements. Percentages represent averages acquired from 67 recovered microstructures, and thus each column will not total to 100%.

Element	Presence (Number of sites observed)	Average Abundance at All Non-Si Sites (Atomic %)	Average Abundance at Sites Observed (Atomic %)
Oxygen	67	69.4	69.4
Aluminum	67	7.1	7.1
Carbon	66	11.1	11.3
Sodium	67	4.5	4.6
Potassium	67	0.4	0.4
Magnesium	67	1.1	1.1
Iron	63	4.7	5.0
Calcium	63	0.8	0.9
Chlorine	34	0.8	1.6
Barium	3	0.0	0.3
Mercury	1	0.0	1.6
Selenium	1	0.0	2.7
Sulfur	3	0.0	0.6
Zinc	3	0.0	0.2
Titanium	1	0.0	0.4

Elemental mapping of thin sections showed distinct visual differences between regions of bone tissue, infilling sediments, and secondary mineral phases. Elemental abundances were measured in cortical and trabecular regions of brontothere bone with a focus on Haversian canals and trabecular voids, the former identified by infilled canals surrounded by circular, osteonal bone tissue (Figure 6B, C). The tortoise bones exhibited small, dark “depressions” in some regions that are interpreted as osteocyte lacunae due to their size, shape, and locations within the bone tissue. These features appeared in both scanning and backscatter electron imaging (Figure 6G, I). Interestingly, these features were not observed in the oreodont samples, despite their clear presence observed via transmitted light microscopy of the thin sections.

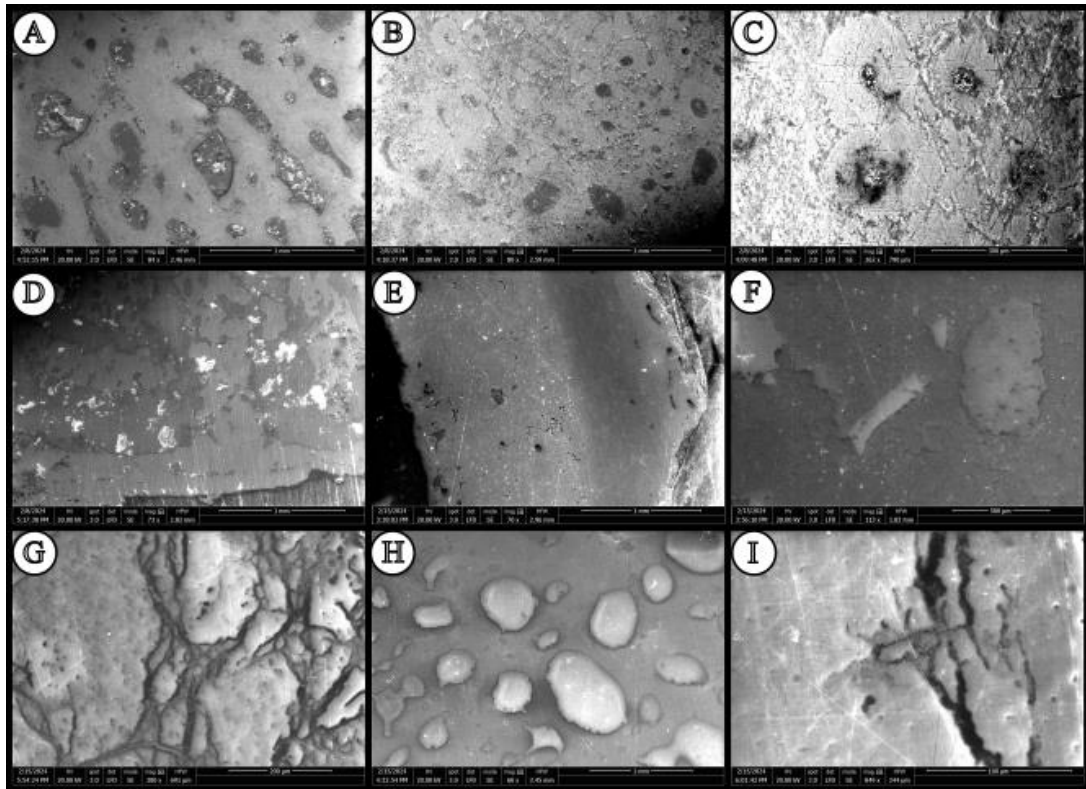


Figure 6. SEM Images of Sectioned Fossil Bone. SEM images from thin sections of each fossil bone. A: Trabecular bone in the brontothere phalanx, showing infilled voids. B, C: Haversian canals and secondary osteons in cortical bone from the brontothere rib, correlating with panel A of Figure 4. D: Cortical bone and infilled void space in the oreodont dentary, roughly corresponding to, and inverted from, panel D in Figure 4. E: Cortical bone from the oreodont indeterminate limb bone, with the cortical margin at the top-right corner of the panel. F: A bone fragment within sediment infill of the oreodont indeterminate limb bone, correlating with image F of Figure 4. G, I: Fractured bone cortical tissues in the tortoise scapula showing a pitted texture. H: Trabecular bone in the tortoise peripheral, correlating with panel I of Figure 4.

Elemental mapping revealed additional information about the diagenetic history of the bones. Strong phosphorus signatures aligned with regions of bone across all samples, which when combined with widespread calcium and oxygen signals is consistent with carbonate-rich fluorapatite being the primary mineral present in each fossil bone (as indicated by my XRD results). Trabecular voids and Haversian canals had comparable concentrations of calcium and oxygen to the bone tissues but lacked any major phosphorus signal, instead showing concentrated carbon, indicating that most

infills were composed of calcite, with one trabecular void in the brontothere phalanx containing barite crystals among the permineralizing calcite. Silicon was observed to be faintly distributed throughout many of the specimens but was most concentrated in the brontothere bones around Haversian canals (Figures 7, 8). Oreodont specimens had silicon signatures limited to voids in bone, often overlapping with upticks in oxygen and aluminum, suggesting a likely zeolite infill; unlike the brontothere specimens, these silicon signatures did not penetrate significantly into the bone tissue. The tortoise specimens showed a third pattern in their silicon signatures: like the oreodont specimens, silicon was found to be abundant within several voids in the bone but it did not coincide with similar abundance of aluminum. Silicon was spatially associated with the “depressions” representing osteocyte lacunae identified under SEM. Voids in the tortoise specimens were found to be filled with either calcite or quartz, with some sites possessing mostly quartz within voids near the cortical margin, and calcite in the interior of the bone.

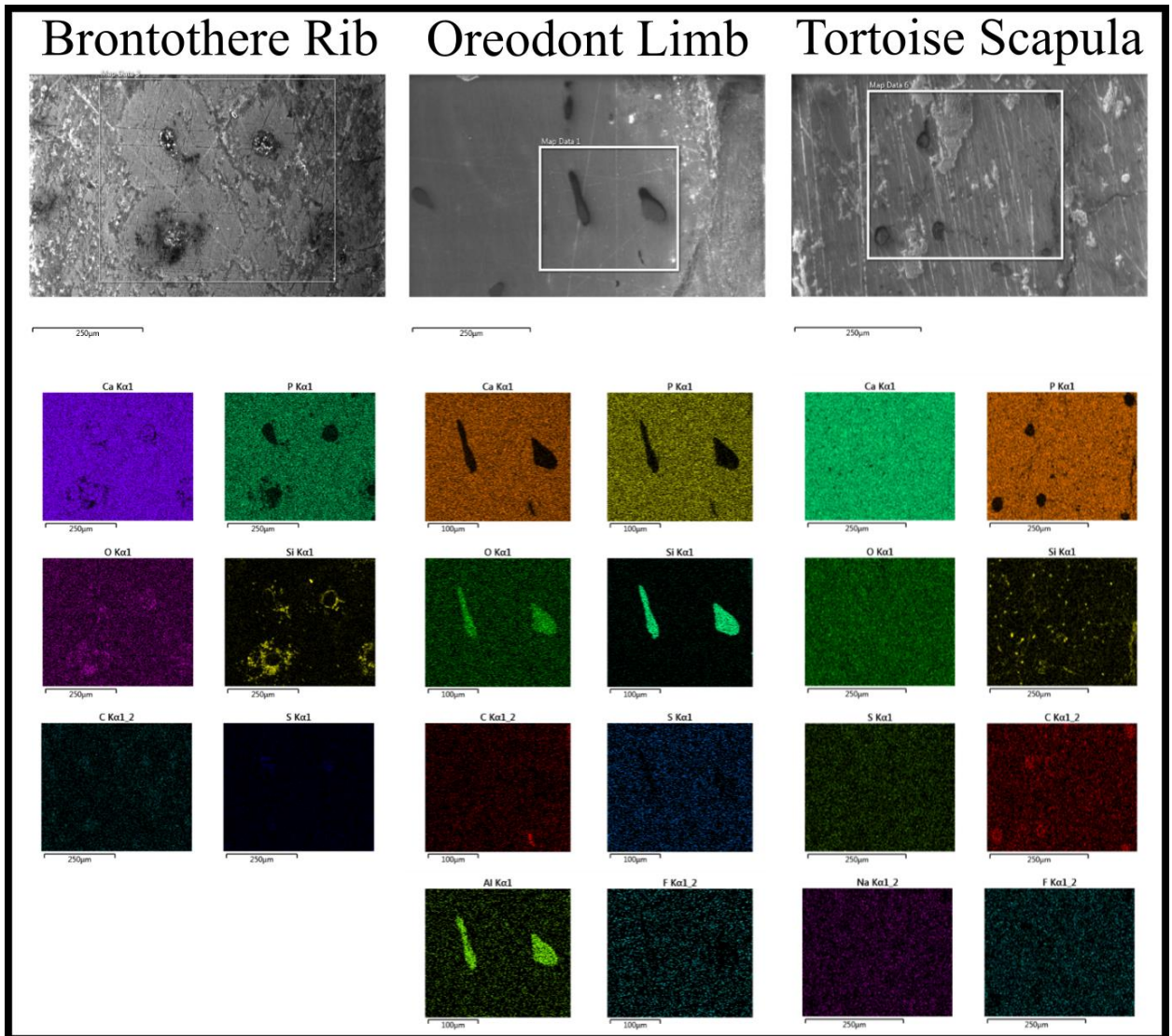


Figure 7. EDS Maps. SEM scans of fossil brontothere, oreodont, and tortoise bones highlighting the spatial distributions of the major identified elements. Phosphorus consistently corresponds with regions of bone tissue, whereas other elements, such as silicon and aluminum, are often concentrated within voids. In the tortoise specimens, silicon is primarily identified within small pits or “depressions” identified as osteocyte lacunae, suggesting either silicification of osteocytes or their emptied lacunae in that sample (see Chapter 5).

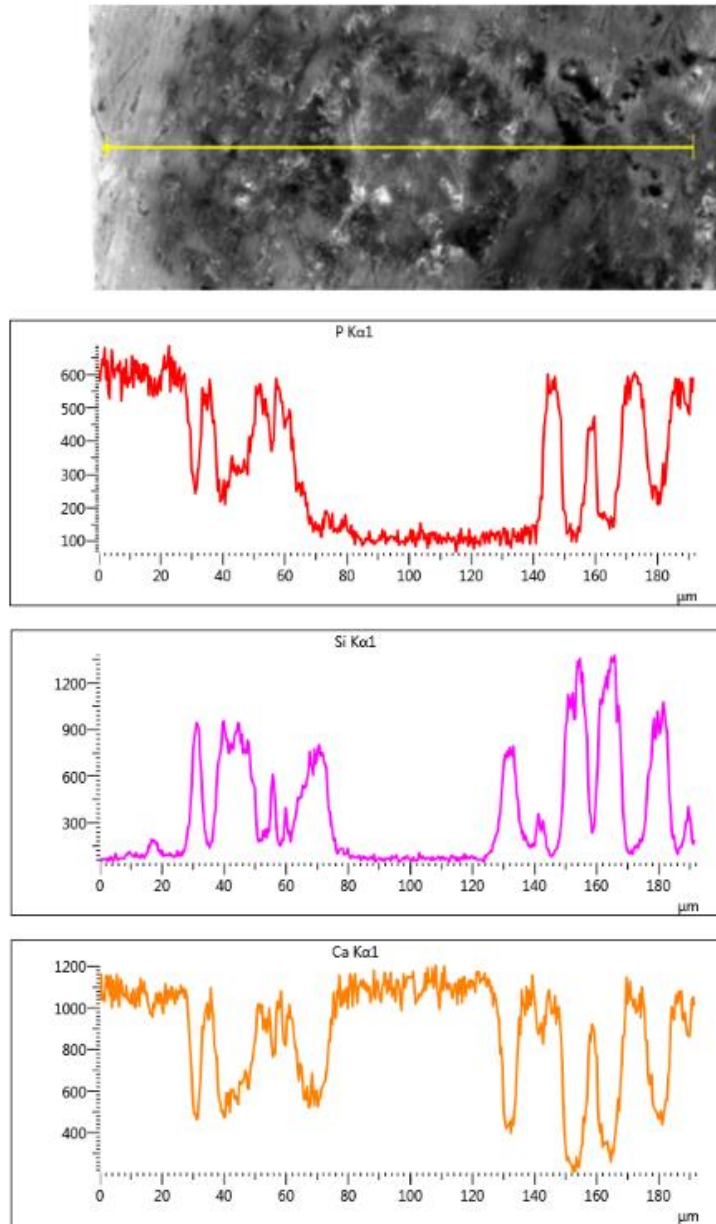


Figure 8. EDS Line Scan. Line scan crossing an osteon and its central Haversian canal in the brontothere rib. Spikes in silicon signal intensity coincide with edges of voids in the bone, as well as decreases in phosphorus and calcium, suggesting incorporation of quartz into fossilized bone tissue around the edges of the voids, while calcite forms in the void interior.

CHAPTER 5

INTERPRETATIONS AND DISCUSSION

5.1 Endogenous Structure Counts and Biomechanical Function

The initial demineralization assay was primarily designed to assess the possible role of biomechanical function in controlling soft tissue preservation. The resulting counts of preserved microstructures morphologically consistent with endogenous cells and soft tissues were higher than anticipated, necessitating the use of higher numbers for the abundance categories used in several other, recent demineralization studies (e.g., Ullmann et al., 2019; Voegelé et al., 2022). Prior category cutoffs that assign the highest value at 20 counts for a given microstructure would not have provided sufficient differentiation within this dataset for examining patterns among the six fossil specimens; therefore, the lower boundary of the highest category used in this study (“Abundant”) was set at 50 counts for any microstructure type. Even with this higher cutoff, 11 of the 36 bone subsample-microstructure observation pairs still hit this top category (Table 2). It is possible that such disparity in structure counts is due to differences in sample geologic age, as, for instance, both Ullmann et al. (2019) and Voegelé et al. (2022) studied bones of Maastrichtian (72–66 Ma) age, whereas this study examined bones spanning the Eocene–Oligocene Transition (~34 Ma). This explanation would be consistent with at least one previous study which found slightly greater degradation of recovered cells and soft tissues from geologically older specimens (Schweitzer et al., 2007).

No strong connection was found between microstructure recovery patterns and biomechanical function of the source skeletal element in this study. Corresponding samples taken from weight-bearing and non-weight-bearing skeletal elements – including

cortical or trabecular subsamples of each – did not yield substantial variation in the quantities of individual microstructure types, with most pairs (13 out of 18) either remaining within the same abundance category or an adjacent one, and multiple pairs with multi-category differences were at least partially confounded by sample size, specifically involving sample ODC, which had a significantly smaller mass than the other subsamples post-HCl wash. A correlation among mammalian fossils was observed for the oreodont and brontothere bones between bone tissue type (cortical vs. trabecular) and which microstructure types were most prevalent in the resulting demineralization products. Trabecular subsamples from fossils of these two taxa yielded higher quantities of fibrous matrix than the corresponding cortical subsamples, whereas the latter instead preserved blood vessels in greater abundance, excepting only sample ODC due to the aforementioned reduction in initial mass.

5.2 Taxonomy

My initial demineralization counts showed a strong correlation between source taxon and the preservation of microstructures morphologically consistent with vertebrate osteocytes within the bone samples (Table 2). Mammalian samples yielded few osteocytes, with sample ODC yielding the highest number of osteocytes among this group, with a count of seven. By contrast, the tortoise subsample with the fewest observed osteocytes in demineralization products was subsample TSC, with 38. TSC, like ODC, was also notably lesser in mass than most of the other samples, and thus it can be reasonably extrapolated that the abundance of potential osteocytes in TSC would most likely cross into the Abundant category if a subsample of equal mass to the other tortoise subsamples were demineralized; however, since this inference represents pure

extrapolation, and the starting mass difference is far less than that associated with ODC, the direct count of 38 is used in this study. It should also be mentioned that thin section analyses focused on the osteocyte lacunae of these bones corroborated osteocyte counts for the brontothere and tortoise bones within demineralization products, but found osteocyte lacunae to be present in much greater abundance than expected (based on the demineralization results) within the oreodont slides.

In addition to disparities in apparent osteocyte preservation, other soft tissue morphotypes were also differentially preserved among the six fossils. Mammalian bones yielded the greatest relative abundance of microstructures morphologically consistent with pieces of fibrous matrix and blood vessels from both cortical and trabecular subsamples. This trend was not seen in the tortoise bones. Among the four tortoise subsamples, one yielded more frequent preservation of all microstructure types in the cortical bone, while the other yielded similar results in the trabecular subsample, potentially indicating a different preservation trend than was observed in the mammalian bones. More specimens would need to be examined to firmly make this assertion, but the White River Group tortoise fossils thus far analyzed yield contrasting results to the observed trend within the mammalian samples in regard to bone tissue type and the types of cells / soft tissues recovered via demineralization.

5.3 Apatite Recrystallization

Subsamples of trabecular bone consistently presented higher CI values than corresponding cortical subsamples (Table 4). The lowest CI value calculated for a trabecular subsample – 0.54 for the tortoise peripheral – was notably higher than the highest CI calculated for any cortical sample – 0.50, coincidentally also from the tortoise

peripheral. This result perhaps indicates that greater recrystallization was occurring in the cancellous trabecular bone than in the denser cortex. This would suggest significant infiltration of pore fluids toward the internal cortex from the inside of the medullary cavity, allowing for more direct and thus more substantial interaction between the pore fluid and the cancellous, internal tissues of the bone. In contrast, “simple diffusion” models anticipate diffusion of fluids moving inward from the cortical margin (Kohn, 2008; Trueman et al., 2008). It is worth noting that both trabecular subsamples from the oreodont specimens (ODT and OLT) exhibited anomalously high CI values: ~0.89 and 1.03, respectively. I tentatively hypothesize that the greater extent of infilling by carbonate-rich sediments observed in the trabecular regions of the oreodont bones resulted in a masking effect that distorted the values used for CI value calculation. These were the samples with the greatest proportional disparity between the 29.5° calcite peak and the highest observed apatite peak, with the calcite peak measuring 15–17 times greater than the highest apatite peak in each diffractogram. The next greatest difference was observed in sample BRT, where the calcite–apatite peak ratio is just over half of that observed in the oreodont samples.

5.4 Histology

Histological observations both supported and contradicted the results of my other analyses. For example, the high counts of osteocytes observed in the demineralized tortoise subsamples were corroborated by observation of plentiful osteocyte lacunae in thin section. However, abundant osteocyte lacunae were also observed in the thin sections of oreodont specimens, which yielded very few osteocytes via demineralization (Table 2).

Histological analyses also revealed a spotted texture interpreted to represent fungal degradation in multiple mammalian specimens, including distinct discoloration of the internal and middle cortex in the oreodont limb bone that is visible without magnification (Figures 9, 10). This interpretation is corroborated by the discovery of fungal hyphae in demineralization products from the trabecular regions of both brontothere specimens (cf. Luo et al., 2023), where the fungal texture was observed in thin section, albeit less pronounced than in the oreodont limb bone.

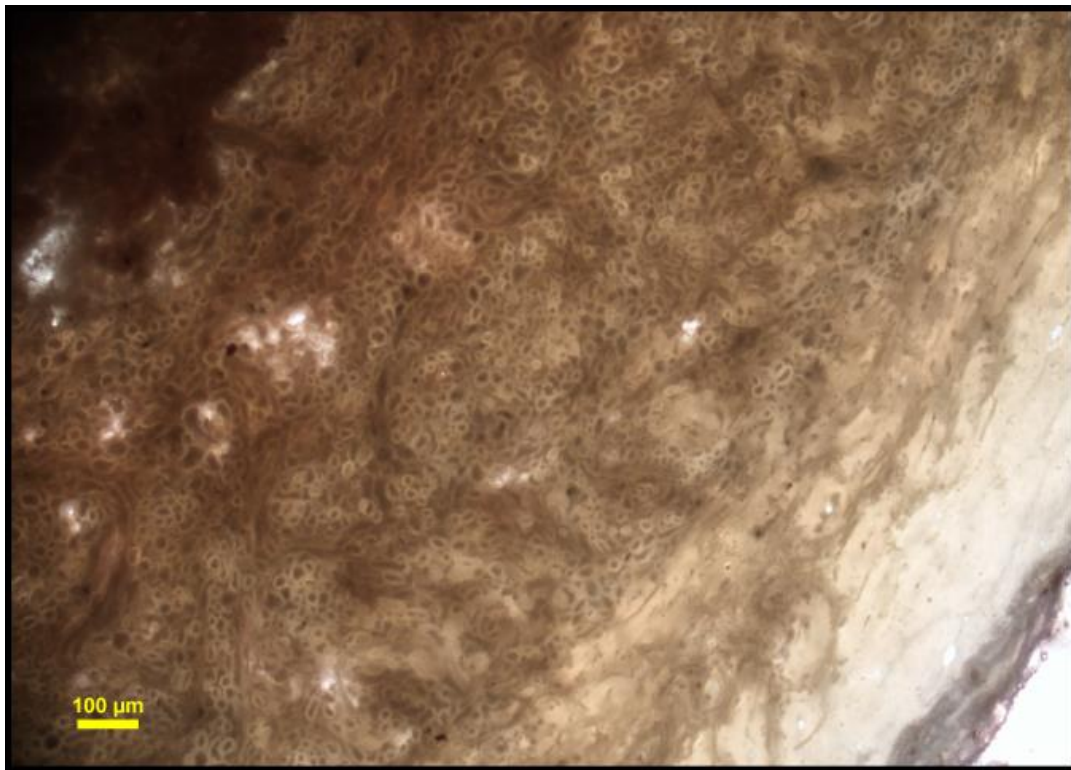


Figure 9. Thin Section of Fungally-Degraded Bone. Thin section image highlighting the spotted texture observed in the oreodont limb bone, interpreted to be the product of extensive fungal degradation, especially within the internal and middle cortex.

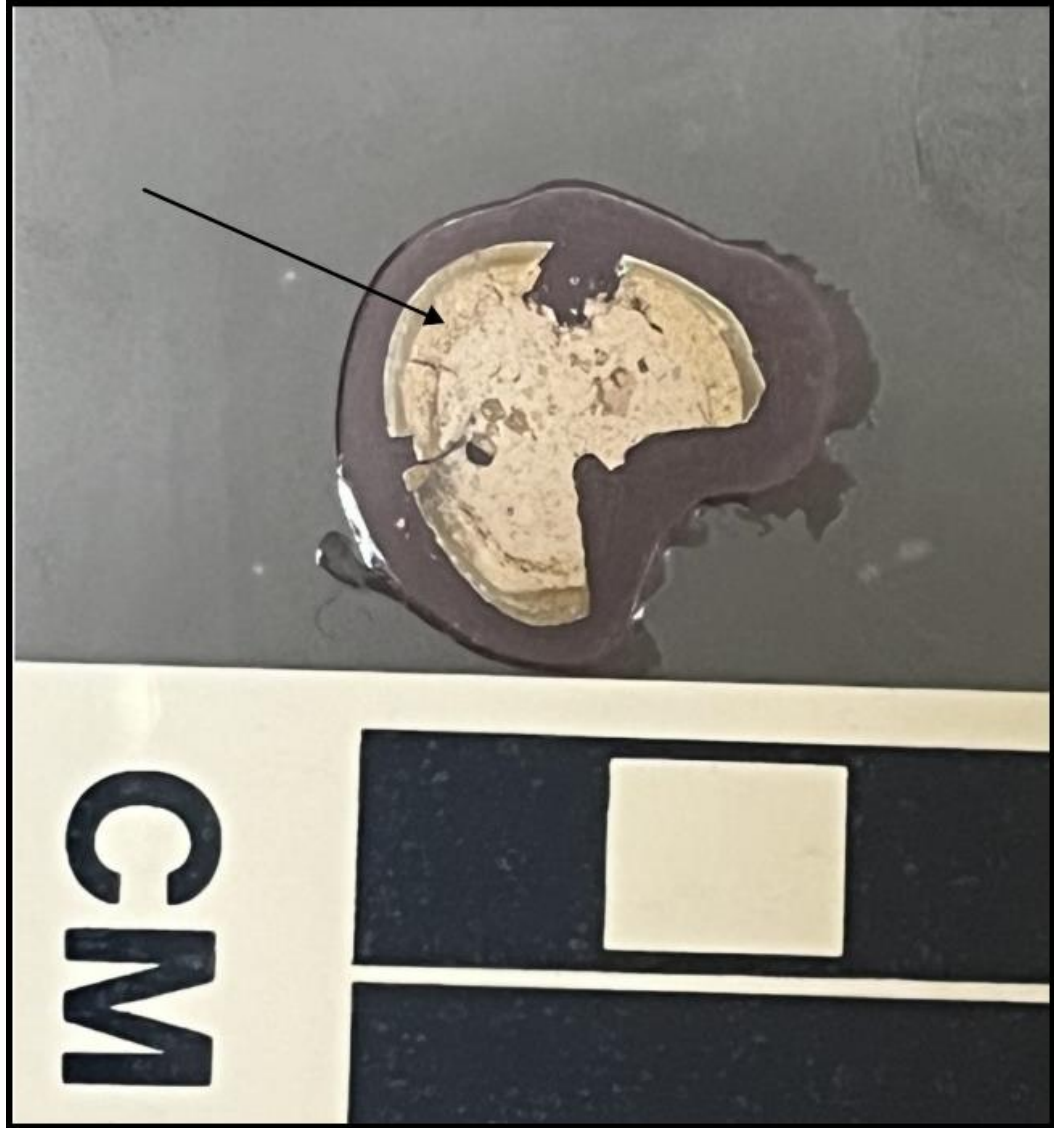


Figure 10. Oreodont Limb Section. Transverse thin section of sample OL, an oreodont limb bone that exhibits extensive fungal degradation which has discolored the internal and middle cortex, as indicated by the arrow. This image also shows how the external cortex remains darker and unaltered, as well as how the sediment infill accounts for most of the area of the specimen's cross-section.

5.5 SEM

Elemental maps revealed differential distribution of elements such as silicon, phosphorus, and carbon. Silicon is largely scattered throughout the samples, but it is also occasionally concentrated in osteonal lamellae and within voids in the bone tissue, both of which are interpreted as evidence of uptake from pore fluids percolating through these

spaces (in conjunction with diffusion from the external cortical margin). Tortoise samples in particular were also found to possess concentrated spots of silicon that correlate with structures interpreted as the locations of osteocyte lacunae, which were also identified both under transmitted light and SEM. Oreodont specimens, which also exhibited abundant osteocyte lacunae in thin section when viewed in transmitted light, interestingly did not show the same trend in SEM: *in situ* osteocyte lacunae were not identified under SEM, either by secondary electron imaging or chemical mapping. This scarcity in SEM is consistent with my initial demineralization data, even if the transmitted light observations suggest significantly greater abundance of these microstructures. This disparity is hypothesized, as with the fungal structures mentioned above, to be a diagenetic difference between the two localities from which the fossil bones were collected. Specifically, it appears that the tortoise bone silicified osteocytes or osteocyte lacunae and the oreodont likely calcified most of them, with the latter resulting in their loss during demineralization and a lack of a significant chemical signal in SEM mapping, such as those observed in the tortoise specimens.

Upticks in carbon were not uncommon within trabecular voids and Haversian canals, which is logical as they were observed in thin section to primarily be infilled with one or more forms of secondary calcite. This analysis confirmed that these open features in the bone tissue were primarily lined with micrite which subsequently became infilled by blocky calcite, indicating a shift from vadose to saturated conditions after burial (Khormali et al., 2006; Tófalo & Pazos, 2010). An isolated instance of barite crystallization in a trabecular void in the brontothere phalanx was also observed. Phosphorus mapped to bone material, indicating that diagenetic processes affecting the

bone itself were primarily oriented toward recrystallization of existing apatite within the bone, particularly in the trabecular regions (with greater surface area relative to volume), rather than replacement by other minerals, even though limited areas of apparent replacement by quartz and zeolites are observed surrounding structures like Haversian canals that would allow direct contact with infiltrating groundwater.

Abundant microstructures resembling hollow and permineralized blood vessels were observed in SEM in the brontothere and oreodont samples; the tortoise samples lacked definitive blood vessels but included possible fibrous matrix fragments. Chemical analyses of these structures via EDS generally showed them to be composed mostly of silicon, oxygen, and aluminum, indicative of potential zeolitic replacement or infiltration. This inference is corroborated by the presence of crystalline structures on and within multiple vessels (e.g., Figure 11). However, carbon values exceeding 11% (of identified non-silicon atoms) were also observed in several putative blood vessels, and hollow vessel structures were also observed, though generally with more apparent degradation than zeolite-infilled vessels.

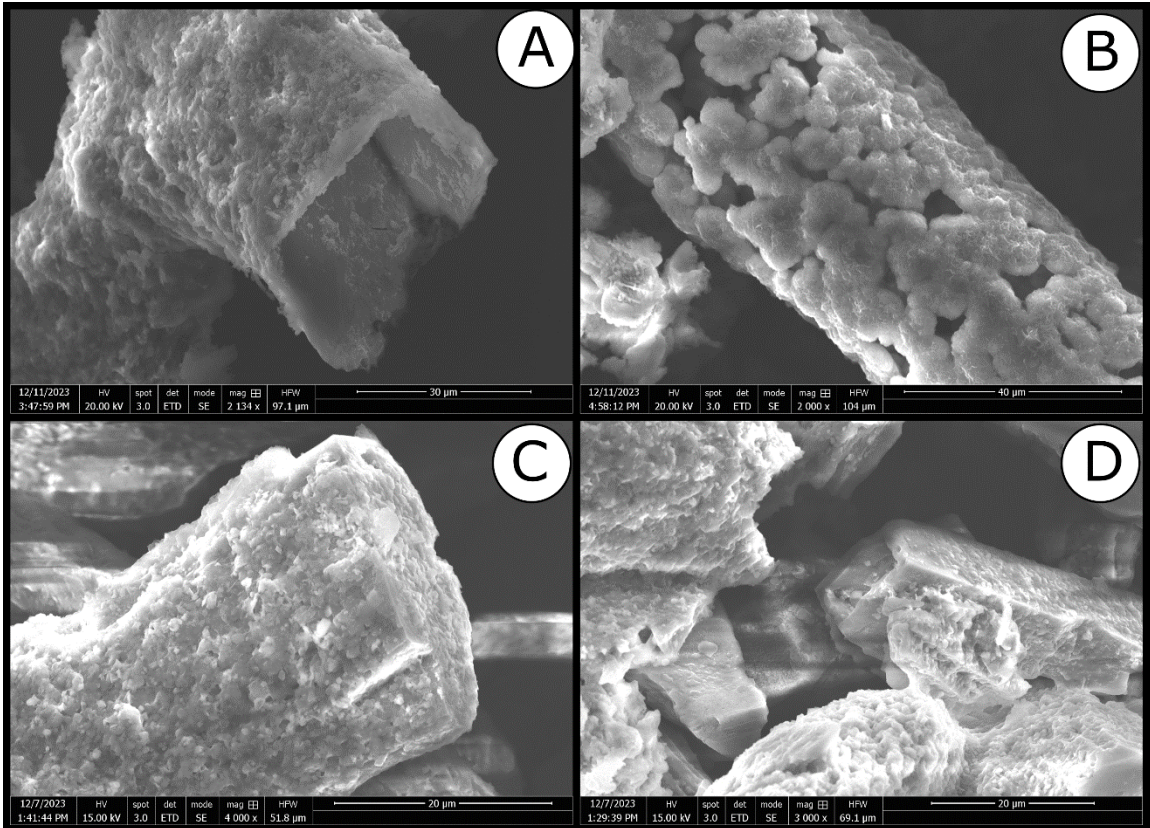


Figure 11. SEM Microstructure Images. SEM images of microstructures observed in demineralized fossil bone from the White River Group. Panel A shows a zeolite-permineralized cast of a vessel recovered from subsample BTC, whereas the vessel shown in panel B retains a hollow, if degraded, structure from subsample BRC that is also largely silicon-rich but with an accompanying higher abundance of carbon. Panels C and D are from the subsample OLC, showing another zeolitic-permineralized blood vessel cast (C) and a zeolite crystal similar in form to euhedral heulandite or clinoptilolite in the center right portion of panel D.

In addition to the potential blood vessels, other fibrous structures were observed in SEM imaging of the demineralization products. These fibers were recorded primarily within demineralization products from both brontothere specimens, specifically from their trabecular subsamples, as well as at least one additional site within demineralization products from the cortical region of the tortoise peripheral. These structures are interpreted as mineralized fungal hyphae, based on both their fibrous form (cf. Luo et al., 2023) and the degraded texture observed in thin section of the brontothere specimens

which are consistent with fungal decay (cf. Jans, 2008). Interestingly, the oreodont samples lack these structures in SEM, despite having the limb bone thin section exhibiting the greatest extent of fungal degradation (Figure 9). The hyphae appear to have been preserved as siliceous minerals based on EDS analyses (Figure 12). Hyphae were not observed in the oreodont samples, which were recovered from a carbonate nodule from Badlands National Park. It is hypothesized this is due to preservation of the hyphae in carbonate in the oreodont specimens, which would have been removed during demineralization. These presumably fungal microstructures were also not observed in elemental maps of the thin sections, and EDS analyses (including elemental mapping, point spectra, and line scans) did not show major chemical differences between fungally-degraded and unaltered bone tissues in the oreodont limb bone (Figures 9, 10).

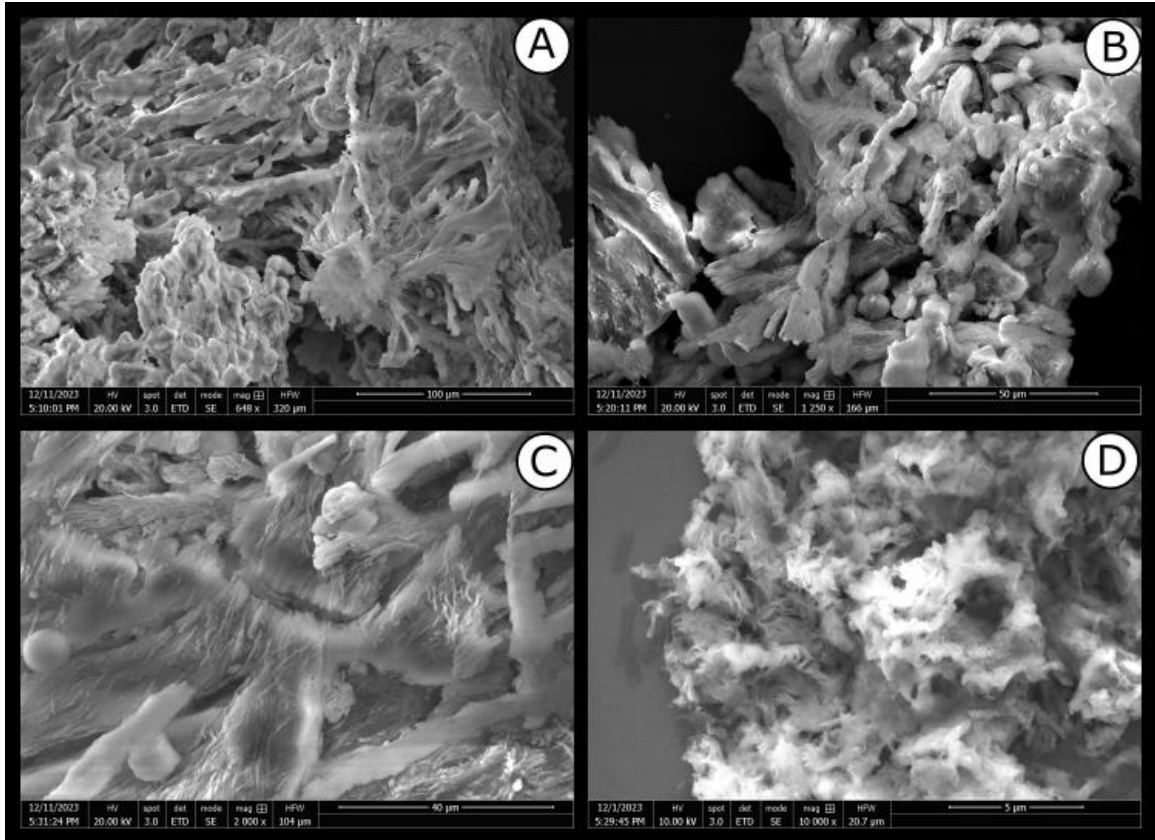


Figure 12. SEM Images Interpreted as Fungal Hyphae. Microstructures interpreted to be silicified fungal hyphae within demineralization products from several of the fossil bones. Panels A, B, and C were sourced from the trabecular region of the brontothere rib, and panel D is sourced from cortical bone of the tortoise peripheral.

CHAPTER 6

CONCLUSION

This study aimed to assess possible controlling factors on the preservation of endogenous cells and soft tissues in fossil bones, utilizing samples from the Paleogene White River Group of Nebraska and South Dakota. The overall quantity of recovered and potentially-endogenous organic microstructures was not strongly influenced by biomechanical function, depositional environment, bone tissue type, elemental chemistry, or apatite crystallinity, as high volumes of microstructures morphologically consistent with preserved cells and soft tissues were observed in all samples analyzed. Permineralized casts of osteocyte lacunae and Haversian canals were also recovered in abundance from these fossils. Other microstructures were preserved as hollow features with higher levels of carbon, but further biomolecular assays (i.e. immunofluorescence, tandem mass spectrometry) would be required to confirm the potential presence of preserved organic matter in such microstructures. Taxonomic identity and bone tissue type (cortical vs. trabecular) did appear to correlate to variability in the frequency with which specific types of potentially-endogenous microstructures were recovered, seemingly favoring osteocyte preservation in tortoise bone regardless of bone tissue type, blood vessel preservation in mammalian cortical bone, and fibrous matrix preservation in mammalian trabecular bone. However, a larger sample set is required to confirm these preliminary findings.

X-ray diffraction of powdered bone subsamples showed no strong pattern between calculated CI values and potentially-endogenous soft tissue preservation, but the results did include higher crystallinity indices within trabecular regions of bone in

comparison to corresponding cortical subsamples, suggesting greater recrystallization of the bioapatite in the more cancellous internal regions of each fossil. Elemental mapping via energy dispersive x-ray spectroscopy (EDS) of thin sections taken from these fossil bones also showed concentrations of silicon along and / or near the margins of Haversian canals and other internal voids, further suggesting double medium diffusion of pore fluids through these natural conduits during fossilization. This technique also highlighted differing elemental signatures between fossils from different localities, with specimens from Toadstool Geologic Park showing greater signatures of silica in elemental maps than specimens from Badlands National Park. Specifically, silicon was found to be concentrated within osteonal lamellae and within tiny “depressions” interpreted as osteocyte lacunae within the brontothere and tortoise specimens, respectively. This finding is interpreted to be an effect of the environments in which these bones fossilized, as well as a potential cause of the resistance of the brontothere subsamples to demineralization. Silicification of osteocytes or osteocyte lamellae in the tortoise bones may explain why they yielded more microstructures morphologically consistent with osteocytes via demineralization than the oreodont bones, despite similar preservation of these cellular structures being observed in transmitted light analyses of the thin sections.

Assessment of controlling factors on endogenous cell and soft tissue preservation in fossil bone allows for a better understanding of the biological and geologic processes that influence such preservation and may eventually aid paleontologists in estimating the likelihood of exceptional preservation of such features at a fossil locality. This study provides early insight into multiple possible factors that have previously been hypothesized to affect the preservation of endogenous microstructures, and my work

should be built upon by expanding this preliminary dataset to include additional samples from these and other taxa, ages, and localities, thereby facilitating even more comprehensive examination of potential controlling factors on this type of exceptional preservation. Additionally, it would be intriguing to investigate whether the microstructures recovered in this study retain possible organic matter and biomolecules by repeating demineralization assays and then proceeding to antibody-based identification methods as in Cleland et al. (2015), and / or protein extractions and peptide sequencing, as in Schroeter et al., (2017).

REFERENCES CITED

- Armitage, M.H., 2022, UV autofluorescence microscopy of Oklahoma Permian synapsid femur (*Dimetrodon* Cope, 1878) reveals blood clots in vascular canals: *Microscopy Today*, v. 30, no. 1, p. 18-23.
- Barker, K., Terry, D.O. Jr., and Ullmann, P.V., 2021, Recovering endogenous cells and soft tissues from fossil bones: does the depositional environment matter: *Geological Society of America Abstracts with Programs*, v. 53, no. 6.
- Cadena, E.A., and Schweitzer, M.H., 2014, A pelomedusoid turtle from the Paleocene-Eocene of Colombia exhibiting preservation of blood vessels and osteocytes: *Journal of Herpetology*, v. 48, p. 461-465.
- Cadena, E., 2016, Microscopical and elemental FESEM and Phenom ProX-SEM-EDS analysis of osteocyte- and blood vessel-like microstructures obtained from fossil vertebrates of the Eocene Messel Pit, Germany: *PeerJ* 4:e1618
- Cleland, T.P., Schroeter, E.R., Zamdborg, L., Zheng, W., Lee, J.E., Tran, J.C., Bern, M., Duncan, M.B., Lebleu, V.S., Ahlf, D.R., Thomas, P.M., Kalluri, R., Kelleher, N.L., and Schweitzer, M.H., 2015, Mass spectrometry and antibody-based characterization of blood vessels from *Brachylophosaurus canadensis*: *J Proteome Res*, v. 14, no. 12, p. 5252-5262.
- Drewicz, A.E., Grandstaff, D.E., Ash, R., and Terry D.O., Jr, 2011, Quantifying periods of fossilization in terrestrial and marine environments using rare earth elements: *Geological Society of America Abstracts with Programs*, v. 43, no. 5.
- Gallucci, J., 2020, Controls on soft tissue and cellular preservation in Late Eocene and Oligocene vertebrate fossils of the White River and Arikaree Groups. [Unpublished master's thesis]. Temple University.
- Goodwin MB, Grant PG, Bench G, Holroyd PA. 2007. Elemental composition and diagenetic alteration of dinosaur bone: distinguishing micron-scale spatial and compositional heterogeneity using PIXE. *Palaeogeography, Palaeoclimatology, Palaeoecology* 253: 458–476.
- Hedges, R.E.M., Millard, A.R., and Pike, A.W.G., 1995, Measurements and relationships of diagenetic alteration of bone from three archaeological sites: *Journal of Archaeological Science*, v.22, p. 201-209.
- Huttenlocker, A.H., Woodward, H.N., and Hall, B.K., 2013, The biology of bone, *in* Padian, K., & Lamm, E.T., eds., *Bone histology of fossil tetrapods*: University of California Press, p. 13-34.
- Jans MME. 2008. Microbial bioerosion of bone – a review. 397–413 in *Current Developments in Bioerosion*. Wisshak M and Tapanila L. Berlin, Springer-Verlag.

- Keenan, S.W., 2016, From bone to fossil: A review of the diagenesis of bioapatite: *American Mineralogist*, v. 101, no. 9, p. 1943-1951.
- Khormali, F., Abtahi, A., and Stoops, G., 2006, Micromorphology of calcitic features in highly calcareous soils of Fars Province, Southern Iran: *Geoderma*, v. 132, no. 1-2, p. 31-46.
- Kohn MJ. 2008. Models of diffusion-limited uptake of trace elements in fossils and rates of fossilization. *Geochimica et Cosmochimica Acta* 72: 3758–3770.
- LaGarry, H.E., 1998, Lithostratigraphic revision and redescription of the Brule Formation, White River Group, western Nebraska, *in* Terry Jr., D.O., LaGarry, H.E., Hunt, R.M., eds., Depositional environments, lithostratigraphy, and biostratigraphy of the White River and Arikaree Groups (Late Eocene to early Miocene, North America), Geological Society of America Special Paper 325, p. 63-91.
- Larson, E.E., and Evanoff, E., 1998, Tephrostratigraphy and source of the tuffs of the White River sequence, *in* Terry Jr., D.O., LaGarry, H.E., Hunt, R.M., eds., Depositional environments, lithostratigraphy, and biostratigraphy of the White River and Arikaree Groups (Late Eocene to Early Miocene, North America), Geological Society of America Special Paper 325, p. 1-14.
- Lukens, W.E., 2013, Paleopedology and paleogeomorphology of the Early Oligocene Orella and Whitney Members, Brule Formation, White River Group, Toadstool Geologic Park, Nebraska. [Master's thesis]. Temple University.
- Luo, M., Li, Z., Su, M., Gadd, G.M., Yin, Z., Benton, M.J., Pan, Y., Zheng, D., Zhao, T., Li, Z., and Chen, Y., 2023, Fungal-induced fossil biomineralization: *Current Biology*, v. 33, 2417-2424.
- Metzger, C.A., Terry, D.O., Jr., and Grandstaff, D.E., 2004, Effect of paleosol formation on rare earth element signatures in fossil bone: *Geology*, v. 32, no. 6, p. 497-500.
- Meyer, H., 1862, *Archaeopteryx lithographica* aus dem lithographischen Schiefer von Solenhofen: *Palaeontographica*, vol. 10, no. 2, 53-56.
- Owen, R., 1841, A description of some of the soft parts, with the integument, of the hind-fin of the *Ichthyosaurus*, indicating the shape of the fin when recent: *Transactions of the Geological Society of London*, vol. 6, p. 199-201.
- Person, A., Bocherens, H., Saliège, J.F., Paris, F., Zeitoun, V. and Gérard, M., 1995, Early diagenetic evolution of bone phosphate: an X-ray diffractometry analysis: *Journal of Archaeological Science*, v. 22, no. 2, p. 211-221.
- Retallack, G.J., 1983, Late Eocene and Oligocene paleosols from Badlands National Park, South Dakota. [Special paper]. Geological Society of America, v. 193.
- Schroeter, E.R.; DeHart, C.J.; Cleland, T.P.; Zheng, W.; Thomas, P.M.; Kelleher, N.L.; Bern, M.; Schweitzer, M.H., 2017, Expansion for the *Brachylophosaurus canadensis* Collagen I

- Sequence and Additional Evidence of the Preservation of Cretaceous Protein. *J. Proteome Res.* v. 16, 920–932.
- Schweitzer, M.H., 1995, Microstructural, elemental, and biomolecular preservation of *Tyrannosaurus rex* cancellous tissues. [PhD Dissertation]. Montana State University.
- Schweitzer, M.H., and Horner, J.R., 1999, Intravascular microstructures in trabecular bone tissues of *Tyrannosaurus rex*: *Annales de Paleontologie*, v. 85, no. 3, p. 179-192.
- Schweitzer, M. H., Schroeter, E. R., Cleland, T. P., and Zheng, W., 2019, Paleoproteomics of Mesozoic Dinosaurs and Other Mesozoic Fossils: *Proteomics*, vol. 19, no. 16.
- Schweitzer, M.H., Wittmeyer, J.L. and Horner, J.R., 2007, Soft tissue and cellular preservation in vertebrate skeletal elements from the Cretaceous to the present: *Proceedings of the Royal Society B: Biological Sciences*, v. 274, no. 1607, p. 183-197.
- Schweitzer, M.H., Wittmeyer, J.L., Horner, J.R., and Toporski, J.K., 2005, Soft-tissue vessels and cellular preservation in *Tyrannosaurus rex*: *Science*, v. 307, p. 1952-1955.
- Suarez, C.A., Macpherson, G.L., González, L.A. and Grandstaff, D.E., 2010, Heterogeneous rare earth element (REE) patterns and concentrations in a fossil bone: implications for the use of REE in vertebrate taphonomy and fossilization history: *Geochimica et Cosmochimica Acta*, v. 74, no. 10, p. 2970-2988.
- Terry, D.O., Jr., 2001, Paleopedology of the Chadron Formation of Northwestern Nebraska: implications for paleoclimatic change in the North American midcontinent across the Eocene–Oligocene boundary: *Palaeogeography, Palaeoclimatology, Palaeoecology*, v. 168, no. 1-2, p. 1-38.
- Terry, D. O., Jr., Grandstaff, D. E., Cerruti, A. D., Lator, E. F., and Lukens, W. E., 2014, Regional variability of geochemical signatures in fossils from the Paleogene White River Sequence of South Dakota, Nebraska, and Wyoming: *Abstracts of the 10th Conference on Fossil Resources, Dakoterra*, v. 6, p. 73-75.
- Tófaló, O.R., and Pazos, P.J., 2010, Paleoclimatic implications (Late Cretaceous–Paleogene) from micromorphology of calcretes, palustrine limestones, and silcretes, southern Paraná Basin, Uruguay: *J. South American Earth Sci.*, v. 29, no. 3, p. 665-675.
- Trueman, C.N., Privat, K., and Field, J., 2008, Why do crystallinity values fail to predict the extent of diagenetic alteration of bone material?: *Palaeogeography, Palaeoclimatology, Palaeoecology*, v. 266, no. 3-4, p. 160-167.
- Ullmann, P.V., Pandya, S.H. and Nellerhoe, R., 2019, Patterns of soft tissue and cellular preservation in relation to fossil bone tissue structure and overburden depth at the Standing Rock Hadrosaur site, Maastrichtian Hell Creek Formation, South Dakota, USA: *Cretaceous Research*, v. 99, p. 1-13.

- Ullmann, P.V., and Schweitzer, M.H., 2023, A statistical analysis of lithologic and other potential controls on fossil bone cellular and soft tissue preservation: *Palaios*, v. 38, no. 5, p. 246-257.
- Ullmann, P.V., Voegelé, K.K., Grandstaff, D.E., Ash, R.D., Zheng, W., Schroeter, E.R., Schweitzer, M.H., and Lacovara, K.J., 2020, Molecular tests support the viability of rare earth elements as proxies for fossil biomolecule preservation: *Scientific Reports*, v. 10, no. 15566.
- Voegelé, K.K., Boles, Z.M., Ullmann, P.V., Schroeter, E.R., Zheng, W., and Lacovara, K.J., 2022, Soft tissue and biomolecular preservation in vertebrate fossils from glauconitic, shallow marine sediments of the Hornerstown Formation, Edelman Fossil Park, New Jersey: *Biology*, v. 11, no. 1161.
- Wiemann, J., Fabbri, M., Yang, T.R., Stein, K., Sander, P.M., Norell, M.A., and Briggs, D.E., 2018, Fossilization transforms vertebrate hard tissue proteins into N-heterocyclic polymers: *Nature Communications*, v. 9, no. 1, p. 4741.
- Wiersma, K., Läbe, S., And Sander, P.M., 2021, Organic phase preservation in fossil dinosaur and other tetrapod bone from deep time, in C.T. Gee, V.E. McCoy, and P.M. Sander (eds.), *Fossilization: Understanding the Material Nature of Ancient Plants and Animals*: Johns Hopkins University Press, Baltimore, p. 16–54.
- Woolslayer, G., Terry, D.O., Grandstaff, D.E., and Ullmann, P., 2022, The effects of taphonomic variability on the preservation of cells and soft tissues in fossil bones from Badlands National Park, South Dakota: *Geological Society of America Abstracts with Programs*, v. 54, no. 3.
- Zanazzi, A., Kohn, M., MacFadden, B.J., and Terry, D.O., Jr., 2007, Large temperature drop across the Eocene-Oligocene transition in central North America: *Nature*, v. 445, p. 639-642.
- Zhao, Y., Tian, Q., Ren, G-Y., Guo, Y., and Zheng, X-T., 2023, Taphonomic analysis of the exceptional preservation of early bird feathers during the early Cretaceous period in Northeast China: *Frontiers in Earth Science*, v. 10.

APPENDIX A

FOSSIL BONE IMAGES

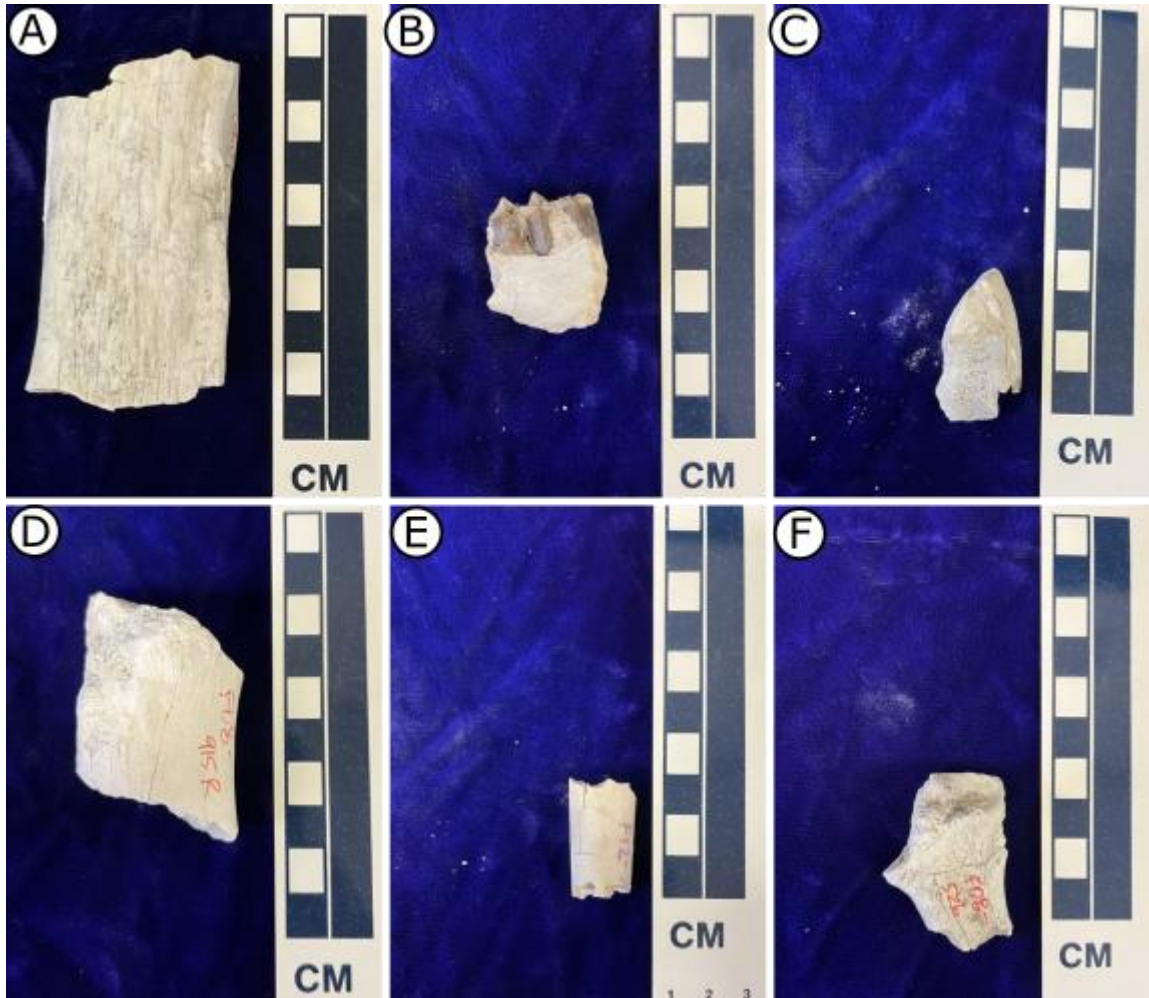


*Figure 13. Pre-Subsampling Images of the Six Fossil Bones Selected For This Study.
Panel A: brontothere rib, Panel B: oreodont dentary, Panel C: tortoise peripheral (shell), Panel D: brontothere phalanx, Panel E: oreodont limb bone, Panel F: tortoise scapula.*

APPENDIX B

DEMINERALIZATION PRODUCTS

B.1 Count Data

Table 6. Demineralization "Set 1" Count Data. Count data given as counts per slide. Sweeps (to a maximum of 50 microstructure counts) given as sweeps to 50 counts over total equivalent sweeps with a 20X microscope objective (i.e. nine sweeps to 50 vessel counts out of 20 total sweeps on the slide). Column header abbreviations: BV, blood vessel; FM, fibrous matrix; O, osteocyte.

Sample	Fibrous Matrix Count	FM Sweeps to 50 (if applicable)	Osteocyte Count	O Sweeps to 50 (if applicable)	Blood Vessel Count	BV Sweeps to 50 (if applicable)
BRC	33	-----	3	-----	50+	9/20
BRT	50+	8/21	3	-----	25	-----
BPC	5	-----	2	-----	50+	10/20
BPT	20	-----	3	-----	35	-----
ODC	21	-----	7	-----	2	-----
ODT	27	-----	5	-----	50+	6/20
OLC	20	-----	0	-----	50+	5/20
OLT	35	-----	0	-----	50+	15/21
TPC	38	-----	50+	4/24	50+	8/24
TPT	29	-----	50+	8/20	4	-----
TSC	27	-----	38	-----	14	-----
TST	33	-----	50+	1/18	50	18/18

B.2 Demineralization Product Images

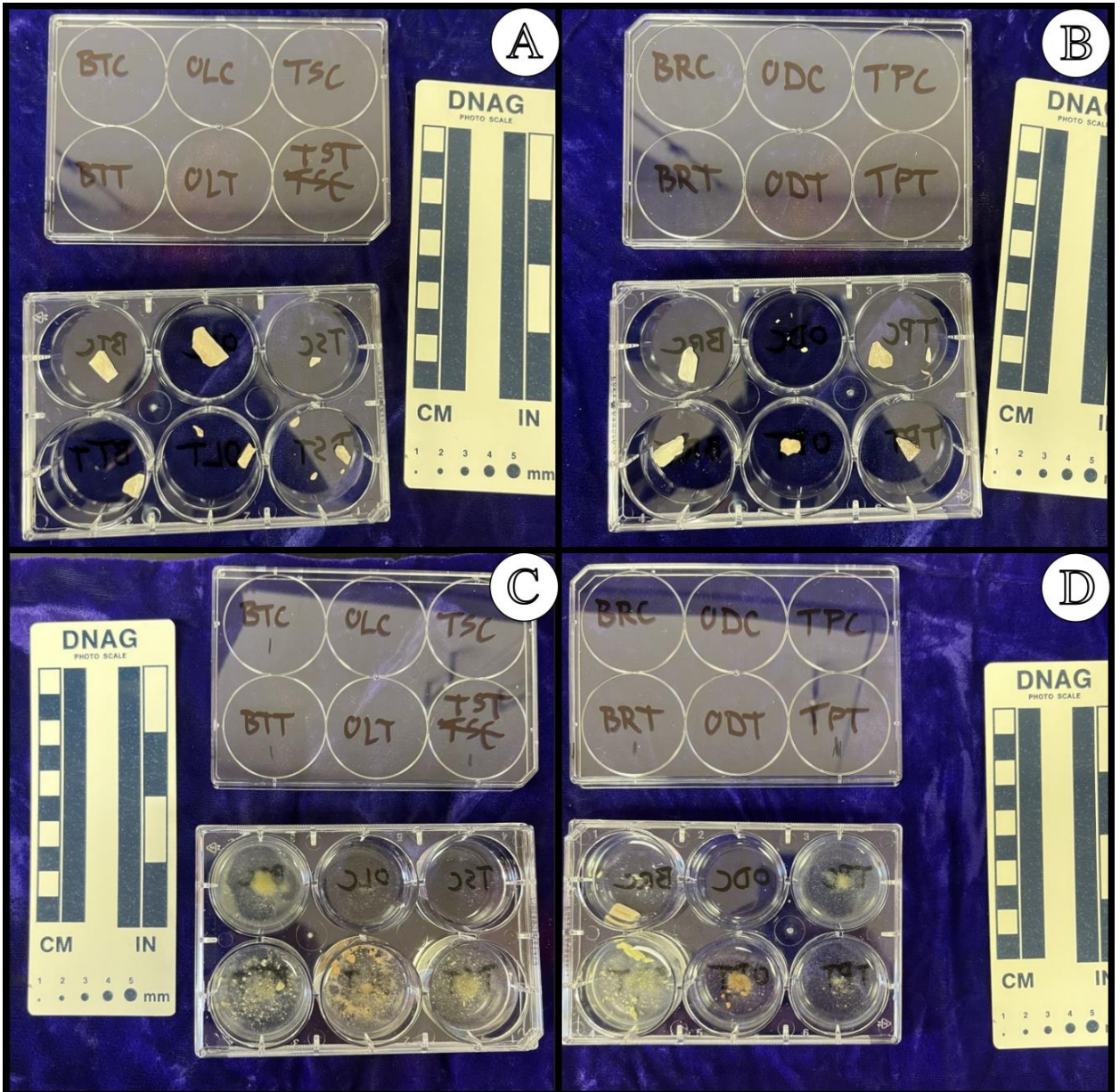


Figure 14. “Set 1” Demineralization Wells. A and B show the subsamples at the start of demineralization on Oct. 24, 2022; C and D show the same subsamples nearing the end of demineralization on Nov. 28, 2022. “Set 1” was used for initial assessment of preserved cells and soft tissues within the fossils.

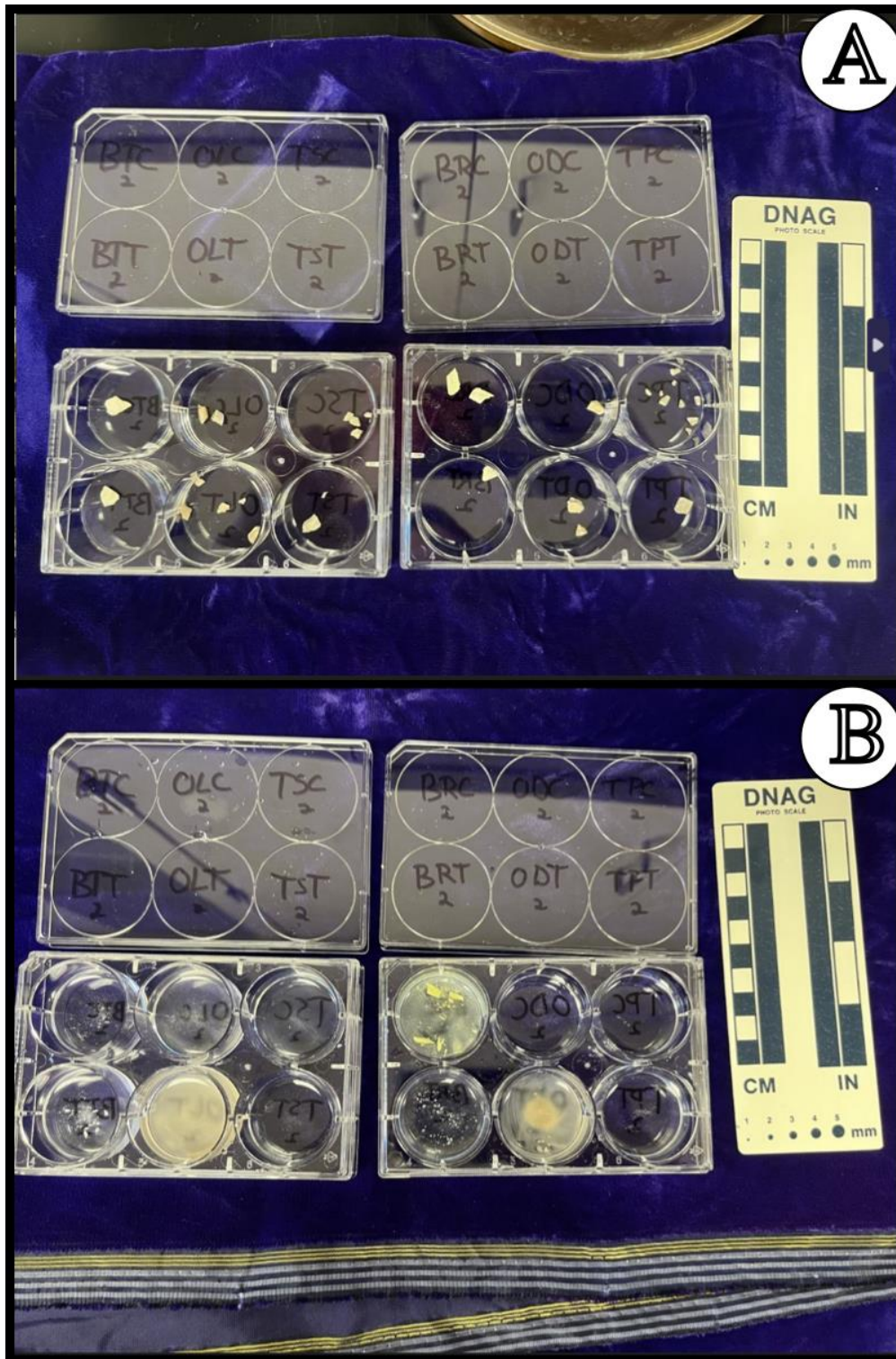


Figure 15. "Set 2" Demineralization Wells. Image A shows the subsamples at the start of demineralization on Sept. 6, 2023; Image B shows the same subsamples in deionized water on Dec. 6, 2023. EDTA was removed in preparation for SEM imaging on Nov. 17. "Set 2" was used for SEM imaging and EDS analyses of the demineralization products.

APPENDIX C

THIN SECTION IMAGES

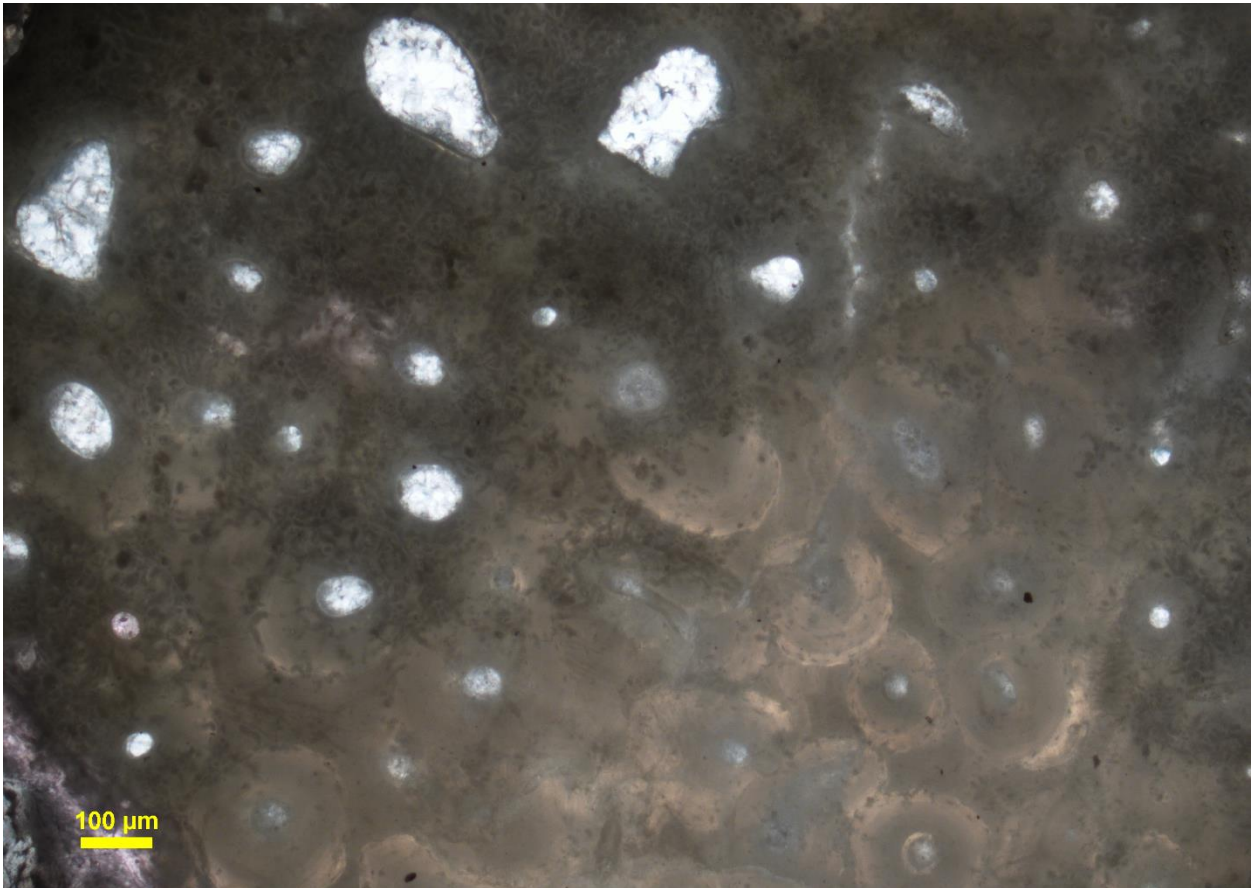


Figure 16. Thin Section Image of Brontothere Rib. This thin section shows the transition between cortical (bottom right) and trabecular (top left) tissues. Note fungal degradation, seen as a dark, punctate pattern in the bone tissue, in the trabecular region of the bone.

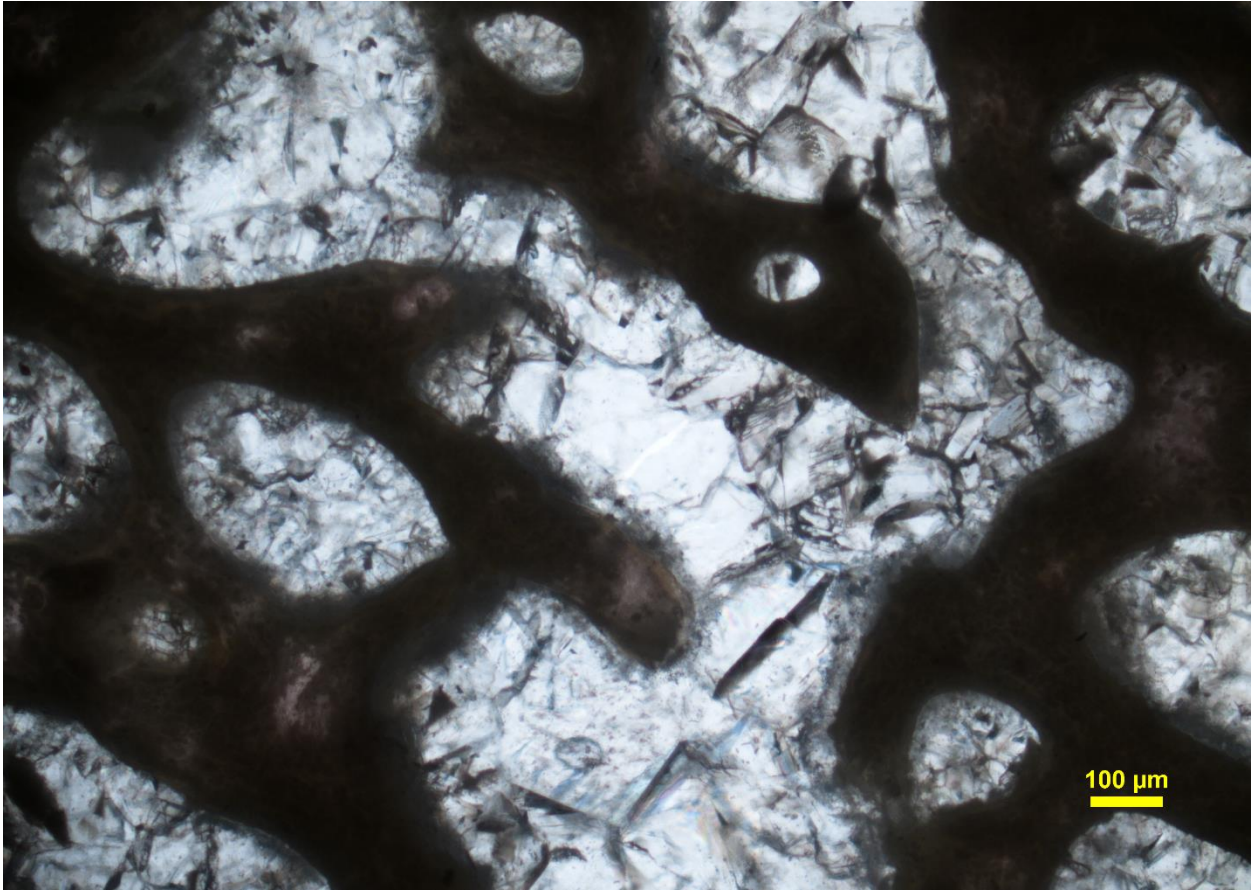


Figure 17. Calcite-Infilled Trabecular Voids Within the Brontothere Phalanx. Note the thin, gray, micritic linings on many of the void walls, as well as the blocky calcite infilling the rest of these spaces.

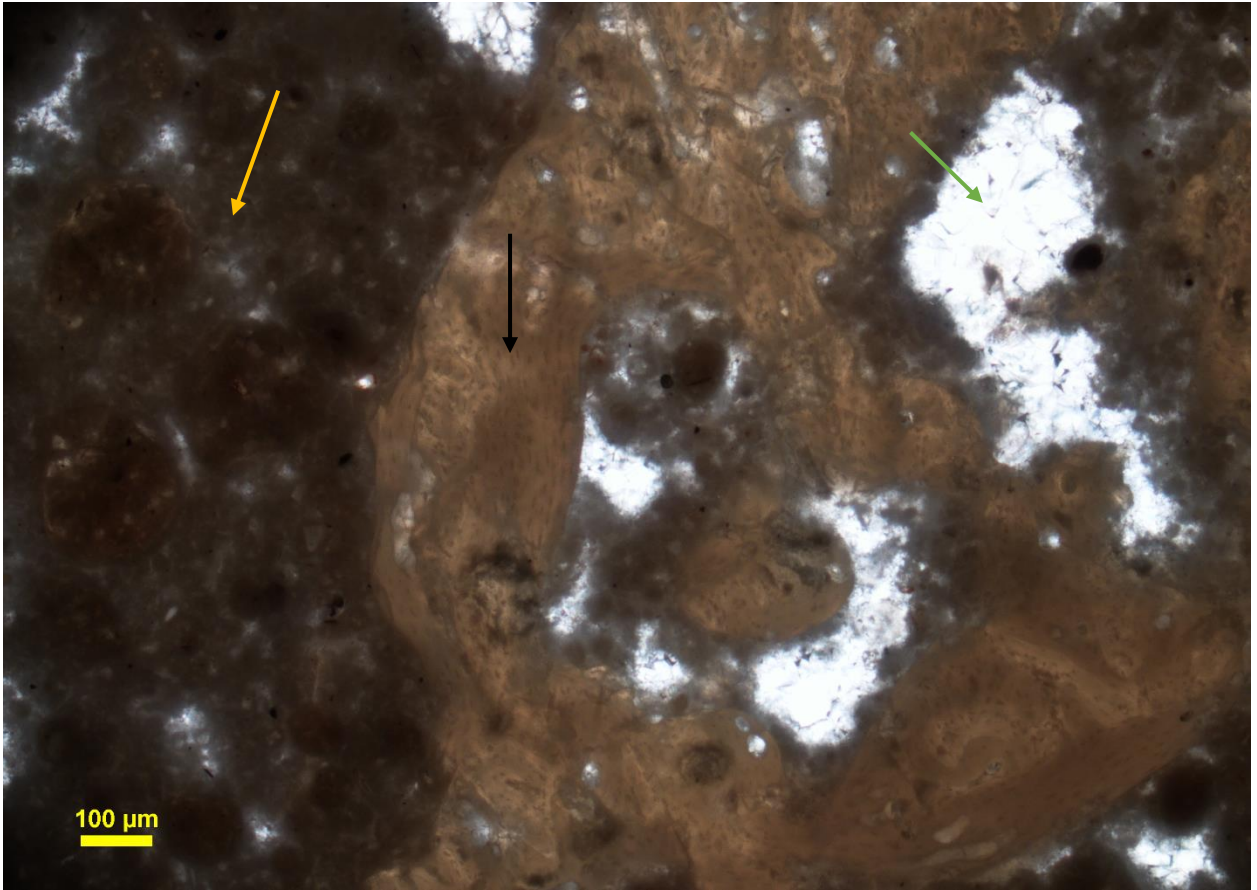


Figure 18. Thin Section Image of the Oreodont Dentary. This thin section shows well-preserved osteocytes (e.g., black arrow), diagenetic calcite void fill (green arrow), and infilling sediment (yellow arrow) in plane-polarized light.

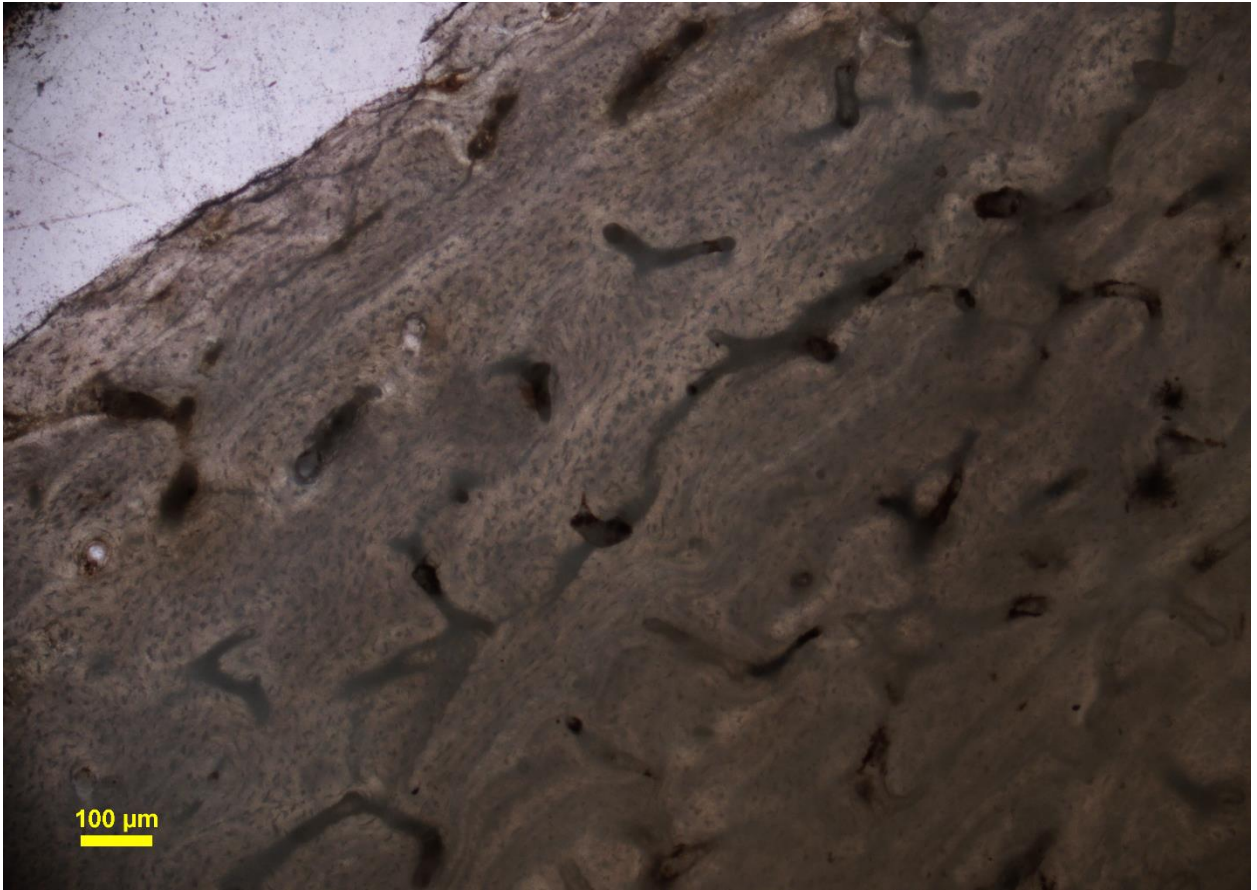


Figure 19. Thin Section Image of the Cortical Region Of The Tortoise Peripheral. This thin section highlights widespread osteocyte preservation (seen as tiny dark dots throughout the bone tissue at this magnification) and overall well-preserved bone fabric.

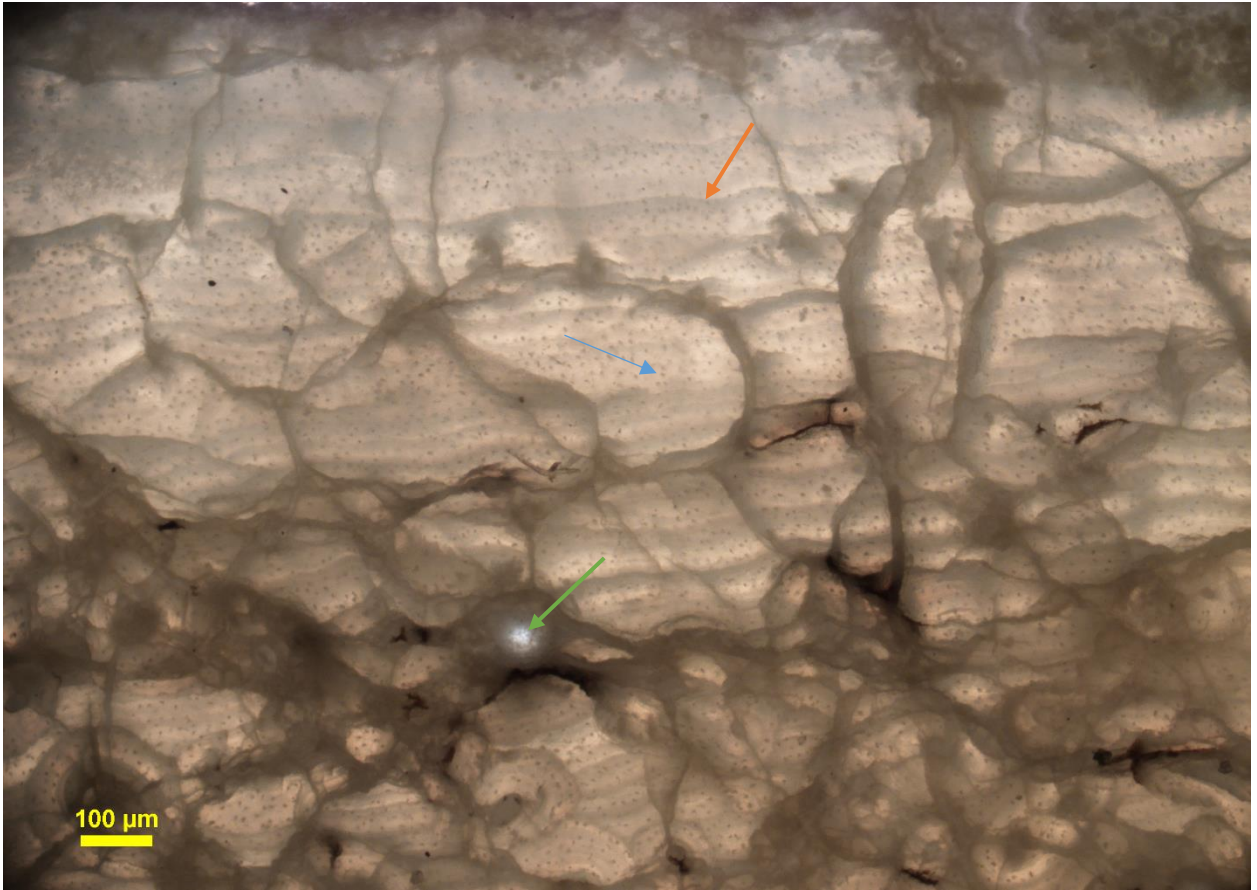


Figure 20. Thin Section Image of the Cortical Region of the Tortoise Scapula. This bone shows its widespread fracturing but otherwise excellent preservation of osteocytes (e.g., blue arrow), bone fabric, secondary osteons (e.g., green arrow), and possible lines of arrested growth (e.g., red arrow).

APPENDIX D
X-RAY DIFFRACTION DATA

Brontothere Subsample XRD Data, Background Subtracted.

BRC		BRT		BPC		BPT	
2θ	Intensity	2θ	Intensity	2θ	Intensity	2θ	Intensity
29.003	2.627	29.003	4.972	29.003	2.824	29.003	7.487
29.024	2.254	29.024	4.430	29.024	3.658	29.024	8.714
29.044	3.964	29.044	4.491	29.044	3.659	29.044	8.587
29.064	3.840	29.064	5.991	29.064	2.889	29.064	9.564
29.085	4.030	29.085	7.074	29.085	3.411	29.085	10.708
29.105	4.073	29.105	7.531	29.105	3.580	29.105	10.540
29.126	4.138	29.126	7.510	29.126	3.727	29.126	10.268
29.146	4.556	29.146	8.635	29.146	3.874	29.146	11.933
29.167	5.059	29.167	8.510	29.167	4.605	29.167	12.557
29.187	3.852	29.187	10.219	29.187	4.523	29.187	14.889
29.207	4.709	29.207	12.053	29.207	4.609	29.207	16.679
29.228	5.316	29.228	14.616	29.228	4.381	29.228	21.866
29.248	5.360	29.248	15.700	29.248	4.737	29.248	25.802
29.269	5.779	29.269	18.659	29.269	4.760	29.269	30.635
29.289	5.886	29.289	23.389	29.289	5.971	29.289	37.197
29.310	5.410	29.310	25.994	29.310	5.952	29.310	42.633
29.330	7.413	29.330	31.037	29.330	6.496	29.330	45.862
29.350	7.499	29.350	37.267	29.350	7.082	29.350	48.507
29.371	8.335	29.371	45.915	29.371	10.272	29.371	41.840
29.391	9.297	29.391	55.708	29.391	9.504	29.391	33.528
29.412	12.113	29.412	67.606	29.412	9.215	29.412	27.257
29.432	13.429	29.432	86.962	29.432	9.718	29.432	23.736
29.453	13.828	29.453	112.276	29.453	8.742	29.453	16.611
29.473	11.873	29.473	136.883	29.473	6.183	29.473	11.132
29.493	10.606	29.493	126.156	29.493	4.748	29.493	7.382
29.514	9.964	29.514	93.262	29.514	4.564	29.514	5.361
29.534	8.843	29.534	78.057	29.534	3.547	29.534	3.924
29.555	6.597	29.555	72.372	29.555	2.029	29.555	3.258
29.575	5.288	29.575	56.437	29.575	1.720	29.575	3.467
29.596	4.584	29.596	34.607	29.596	1.807	29.596	2.196
29.616	3.692	29.616	22.319	29.616	1.228	29.616	2.135
29.636	2.509	29.636	18.072	29.636	0.586	29.636	2.323
29.657	2.430	29.657	14.263	29.657	0.464	29.657	1.741
29.677	1.456	29.677	12.600	29.677	0.802	29.677	1.221
29.698	2.002	29.698	9.395	29.698	1.035	29.698	0.534
29.718	1.653	29.718	8.024	29.718	0.518	29.718	0.786

29.739	1.074	29.739	6.820	29.739	0.564	29.739	0.870
29.759	1.350	29.759	6.491	29.759	0.298	29.759	0.830
29.779	0.480	29.779	4.370	29.779	0.303	29.779	1.519
29.800	0.402	29.800	3.854	29.800	-0.110	29.800	0.437
29.820	0.782	29.820	2.046	29.820	0.666	29.820	0.022
29.841	0.579	29.841	3.051	29.841	0.462	29.841	0.774
29.861	0.501	29.861	2.577	29.861	0.446	29.861	-0.120
29.881	0.027	29.881	1.852	29.881	0.014	29.881	0.736
29.902	0.179	29.902	2.087	29.902	0.477	29.902	0.655
29.922	0.143	29.922	1.238	29.922	0.253	29.922	-0.322
29.943	0.065	29.943	1.556	29.943	0.071	29.943	0.243
29.963	0.175	29.963	0.957	29.963	0.306	29.963	-0.151
29.984	0.098	29.984	0.859	29.984	0.561	29.984	0.935
30.004	-0.584	30.004	0.865	30.004	0.442	30.004	0.833
30.024	0.152	30.024	1.017	30.024	0.406	30.024	0.502
30.045	-0.280	30.045	0.856	30.045	0.203	30.045	0.380
30.065	0.477	30.065	0.717	30.065	0.521	30.065	0.175
30.086	0.108	30.086	0.723	30.086	0.444	30.086	0.365
30.106	-0.031	30.106	0.251	30.106	0.179	30.106	-0.236
30.127	0.434	30.127	0.716	30.127	-0.086	30.127	0.017
30.147	0.316	30.147	0.327	30.147	0.233	30.147	0.645
30.167	-0.032	30.167	0.647	30.167	0.323	30.167	-0.310
30.188	-0.087	30.188	-0.284	30.188	0.350	30.188	-0.327
30.208	0.024	30.208	0.411	30.208	0.065	30.208	0.313
30.229	-0.261	30.229	0.127	30.229	0.405	30.229	0.246
30.249	-0.024	30.249	-0.115	30.249	0.828	30.249	0.262
30.270	-0.288	30.270	0.497	30.270	-0.311	30.270	-0.034
30.290	-0.124	30.290	0.234	30.290	0.800	30.290	0.065
30.310	-0.044	30.310	0.367	30.310	-0.110	30.310	0.727
30.331	-0.089	30.331	0.354	30.331	0.397	30.331	0.098
30.351	0.513	30.351	-0.075	30.351	-0.345	30.351	-0.052
30.372	0.093	30.372	0.371	30.372	-0.276	30.372	0.818
30.392	-0.097	30.392	0.088	30.392	-0.222	30.392	0.106
30.413	0.172	30.413	-0.008	30.413	0.540	30.413	0.643
30.433	0.377	30.433	0.356	30.433	0.281	30.433	-0.486
30.453	-0.521	30.453	0.115	30.453	0.731	30.453	0.281
30.474	0.164	30.474	-0.084	30.474	0.056	30.474	-0.368
30.494	0.141	30.494	0.050	30.494	0.172	30.494	0.920
30.515	-0.006	30.515	0.080	30.515	-0.003	30.515	-0.042
30.535	0.054	30.535	-0.264	30.535	-0.011	30.535	-0.296
30.556	-0.302	30.556	-0.214	30.556	0.397	30.556	-0.007
30.576	-0.039	30.576	0.441	30.576	0.514	30.576	0.281
30.596	-0.255	30.596	0.200	30.596	0.589	30.596	0.007

30.617	0.550	30.617	0.105	30.617	0.102	30.617	-0.163
30.637	0.147	30.637	-0.093	30.637	0.240	30.637	-0.603
30.658	0.014	30.658	-0.063	30.658	0.274	30.658	0.331
30.678	0.007	30.678	0.093	30.678	0.829	30.678	0.328
30.699	0.166	30.699	0.394	30.699	0.134	30.699	0.346
30.719	0.014	30.719	-0.012	30.719	0.814	30.719	-0.198
30.739	-0.056	30.739	-0.211	30.739	1.036	30.739	0.154
30.760	0.395	30.760	-0.117	30.760	0.508	30.760	0.005
30.780	0.159	30.780	-0.231	30.780	0.501	30.780	0.274
30.801	0.257	30.801	0.237	30.801	0.452	30.801	0.605
30.821	-0.250	30.821	-0.002	30.821	0.695	30.821	-0.002
30.842	-0.173	30.842	-0.012	30.842	0.230	30.842	0.475
30.862	0.633	30.862	0.666	30.862	0.265	30.862	0.557
30.882	0.335	30.882	0.240	30.882	1.175	30.882	0.388
30.903	0.516	30.903	-0.145	30.903	0.501	30.903	-0.030
30.923	0.656	30.923	0.887	30.923	1.162	30.923	0.447
30.944	1.067	30.944	0.024	30.944	0.676	30.944	0.091
30.964	0.873	30.964	0.140	30.964	1.045	30.964	0.902
30.985	0.492	30.985	-0.202	30.985	1.039	30.985	0.734
31.005	0.924	31.005	0.206	31.005	1.137	31.005	-0.101
31.025	1.127	31.025	0.447	31.025	0.547	31.025	0.836
31.046	1.246	31.046	0.355	31.046	0.708	31.046	0.918
31.066	0.407	31.066	0.326	31.066	1.577	31.066	1.563
31.087	0.985	31.087	0.589	31.087	1.259	31.087	1.541
31.107	1.126	31.107	0.205	31.107	1.545	31.107	1.686
31.128	1.558	31.128	0.073	31.128	1.123	31.128	1.477
31.148	1.115	31.148	0.565	31.148	1.784	31.148	2.309
31.168	1.235	31.168	0.432	31.168	2.050	31.168	1.163
31.189	1.855	31.189	0.716	31.189	2.023	31.189	2.162
31.209	1.996	31.209	0.542	31.209	1.935	31.209	2.641
31.230	2.158	31.230	0.973	31.230	2.513	31.230	1.641
31.250	2.070	31.250	0.549	31.250	2.362	31.250	3.182
31.271	1.732	31.271	1.042	31.271	2.962	31.271	2.619
31.291	2.124	31.291	2.327	31.291	2.499	31.291	2.369
31.311	2.078	31.311	2.237	31.311	3.077	31.311	2.765
31.332	3.157	31.332	2.314	31.332	3.969	31.332	4.328
31.352	3.049	31.352	1.474	31.352	3.443	31.352	5.536
31.373	3.086	31.373	1.843	31.373	4.064	31.373	4.620
31.393	3.499	31.393	2.962	31.393	4.185	31.393	5.371
31.414	3.912	31.414	3.060	31.414	5.285	31.414	6.496
31.434	4.366	31.434	3.262	31.434	5.010	31.434	6.184
31.454	5.592	31.454	4.694	31.454	5.797	31.454	6.956
31.475	5.921	31.475	4.314	31.475	6.877	31.475	6.519

31.495	5.689	31.495	6.600	31.495	6.414	31.495	7.145
31.516	5.810	31.516	6.032	31.516	6.473	31.516	7.667
31.536	7.286	31.536	5.215	31.536	7.532	31.536	6.543
31.557	6.991	31.557	6.960	31.557	8.570	31.557	8.148
31.577	8.613	31.577	6.080	31.577	8.754	31.577	9.129
31.597	8.277	31.597	6.055	31.597	8.834	31.597	8.547
31.618	8.128	31.618	6.071	31.618	10.164	31.618	9.569
31.638	10.084	31.638	6.942	31.638	12.911	31.638	10.216
31.659	10.414	31.659	7.479	31.659	12.117	31.659	10.218
31.679	10.682	31.679	8.037	31.679	13.093	31.679	11.449
31.700	12.472	31.700	7.763	31.700	14.965	31.700	11.117
31.720	12.907	31.720	8.800	31.720	15.691	31.720	12.682
31.740	13.842	31.740	9.526	31.740	16.168	31.740	13.350
31.761	15.735	31.761	10.585	31.761	16.749	31.761	13.748
31.781	14.525	31.781	11.144	31.781	19.225	31.781	15.063
31.802	15.190	31.802	11.120	31.802	20.723	31.802	15.149
31.822	17.125	31.822	13.221	31.822	21.033	31.822	15.776
31.843	19.186	31.843	12.281	31.843	21.010	31.843	14.820
31.863	20.267	31.863	13.361	31.863	22.404	31.863	14.302
31.883	22.578	31.883	14.192	31.883	22.402	31.883	15.596
31.904	20.472	31.904	13.690	31.904	22.754	31.904	14.120
31.924	25.033	31.924	13.979	31.924	24.127	31.924	14.498
31.945	23.657	31.945	14.268	31.945	24.625	31.945	14.355
31.965	25.197	31.965	13.995	31.965	23.145	31.965	14.629
31.986	24.759	31.986	15.014	31.986	23.206	31.986	12.903
32.006	23.403	32.006	14.679	32.006	23.996	32.006	13.281
32.026	25.361	32.026	14.886	32.026	23.578	32.026	12.847
32.047	23.235	32.047	13.176	32.047	22.327	32.047	12.496
32.067	23.734	32.067	14.550	32.067	22.575	32.067	12.416
32.088	23.067	32.088	13.048	32.088	21.908	32.088	11.107
32.108	23.587	32.108	13.902	32.108	21.511	32.108	12.152
32.129	22.857	32.129	13.296	32.129	19.260	32.129	10.927
32.149	21.898	32.149	13.066	32.149	20.572	32.149	10.910
32.169	21.690	32.169	12.253	32.169	19.884	32.169	10.643
32.190	21.148	32.190	12.482	32.190	19.321	32.190	9.043
32.210	20.002	32.210	10.940	32.210	17.424	32.210	8.422
32.231	20.252	32.231	12.981	32.231	15.799	32.231	8.260
32.251	18.668	32.251	10.044	32.251	16.549	32.251	7.473
32.272	18.106	32.272	10.940	32.272	15.965	32.272	6.352
32.292	16.940	32.292	9.252	32.292	13.923	32.292	6.023
32.312	15.919	32.312	9.294	32.312	12.298	32.312	5.236
32.333	14.732	32.333	8.066	32.333	11.298	32.333	4.949
32.353	12.712	32.353	7.504	32.353	10.257	32.353	4.892

32.374	11.358	32.374	6.546	32.374	9.382	32.374	4.147
32.394	11.317	32.394	6.381	32.394	8.362	32.394	4.089
32.415	9.755	32.415	5.632	32.415	8.383	32.415	3.282
32.435	8.756	32.435	5.279	32.435	7.717	32.435	3.287
32.455	8.382	32.455	3.280	32.455	6.218	32.455	2.938
32.476	8.092	32.476	3.657	32.476	5.864	32.476	2.589
32.496	7.593	32.496	3.262	32.496	5.969	32.496	3.636
32.517	5.761	32.517	3.639	32.517	4.512	32.517	2.996
32.537	5.491	32.537	3.058	32.537	5.284	32.537	3.314
32.558	6.055	32.558	2.685	32.558	4.931	32.558	3.216
32.578	5.828	32.578	2.937	32.578	5.161	32.578	2.784
32.598	5.163	32.598	2.669	32.598	5.600	32.598	2.936
32.619	4.414	32.619	2.755	32.619	4.018	32.619	3.567
32.639	4.729	32.639	2.736	32.639	5.582	32.639	2.427
32.660	4.377	32.660	2.572	32.660	4.563	32.660	3.475
32.680	4.524	32.680	2.450	32.680	4.940	32.680	3.919
32.701	5.027	32.701	2.578	32.701	4.254	32.701	4.071
32.721	5.383	32.721	2.728	32.721	4.672	32.721	4.640
32.741	5.344	32.741	2.877	32.741	5.508	32.741	5.251
32.762	5.263	32.762	2.484	32.762	5.697	32.762	4.799
32.782	5.744	32.782	3.259	32.782	5.658	32.782	5.056
32.803	5.664	32.803	3.304	32.803	7.702	32.803	4.792
32.823	5.500	32.823	3.912	32.823	6.704	32.823	4.987
32.844	5.940	32.844	4.000	32.844	7.186	32.844	5.931
32.864	6.651	32.864	4.525	32.864	7.522	32.864	6.063
32.884	6.488	32.884	4.050	32.884	8.274	32.884	6.091
32.905	6.824	32.905	4.784	32.905	7.923	32.905	5.724
32.925	7.244	32.925	5.518	32.925	8.259	32.925	6.023
32.946	8.476	32.946	4.689	32.946	7.825	32.946	6.801
32.966	8.230	32.966	5.715	32.966	9.432	32.966	6.725
32.987	8.796	32.987	5.637	32.987	9.727	32.987	6.358
33.007	9.258	33.007	5.788	33.007	9.272	33.007	6.116
33.027	8.449	33.027	6.105	33.027	9.421	33.027	5.811
33.048	9.890	33.048	6.798	33.048	10.195	33.048	5.861
33.068	8.956	33.068	6.096	33.068	10.053	33.068	5.286
33.089	9.939	33.089	5.685	33.089	10.494	33.089	5.440
33.109	10.881	33.109	6.024	33.109	9.810	33.109	5.906
33.130	11.343	33.130	6.197	33.130	9.960	33.130	5.248
33.150	9.639	33.150	6.557	33.150	9.547	33.150	5.486
33.170	11.081	33.170	5.772	33.170	9.613	33.170	3.973
33.191	10.523	33.191	6.195	33.191	8.701	33.191	4.836
33.211	10.048	33.211	5.785	33.211	8.497	33.211	4.512
33.232	8.782	33.232	4.875	33.232	7.918	33.232	3.583

33.252	8.558	33.252	4.278	33.252	7.693	33.252	2.300
33.273	7.813	33.273	4.202	33.273	7.781	33.273	3.101
33.293	8.692	33.293	3.730	33.293	7.077	33.293	3.277
33.313	8.239	33.313	3.466	33.313	5.498	33.313	2.661
33.334	6.244	33.334	2.849	33.334	5.920	33.334	2.233
33.354	6.812	33.354	2.648	33.354	5.133	33.354	1.055
33.375	5.963	33.375	2.489	33.375	5.284	33.375	0.898
33.395	6.281	33.395	2.789	33.395	4.747	33.395	2.074
33.416	5.682	33.416	1.755	33.416	4.502	33.416	1.271
33.436	4.334	33.436	1.993	33.436	4.049	33.436	1.239
33.456	4.402	33.456	2.147	33.456	2.971	33.456	1.770
33.477	4.783	33.477	1.239	33.477	3.227	33.477	0.634
33.497	2.997	33.497	1.414	33.497	3.232	33.497	1.227
33.518	2.482	33.518	0.881	33.518	2.259	33.518	0.737
33.538	2.925	33.538	1.036	33.538	1.952	33.538	1.394
33.559	2.911	33.559	1.066	33.559	2.145	33.559	1.112
33.579	3.354	33.579	0.658	33.579	2.214	33.579	1.435
33.599	2.840	33.599	1.147	33.599	2.095	33.599	1.029
33.620	1.576	33.620	0.469	33.620	1.872	33.620	1.040
33.640	2.103	33.640	0.104	33.640	1.815	33.640	0.946
33.661	1.339	33.661	0.343	33.661	1.863	33.661	0.790
33.681	1.991	33.681	0.540	33.681	2.307	33.681	0.822
33.702	2.352	33.702	0.363	33.702	2.230	33.702	1.125
33.722	2.192	33.722	0.102	33.722	1.466	33.722	1.427
33.742	2.054	33.742	0.904	33.742	1.535	33.742	0.897
33.763	1.311	33.763	0.581	33.763	2.354	33.763	1.158
33.783	2.047	33.783	0.363	33.783	2.882	33.783	1.982
33.804	2.304	33.804	0.373	33.804	2.639	33.804	2.473
33.824	2.020	33.824	1.530	33.824	2.271	33.824	2.047
33.845	2.403	33.845	0.708	33.845	2.862	33.845	1.913
33.865	2.535	33.865	0.802	33.865	3.056	33.865	2.091
33.885	2.709	33.885	1.147	33.885	3.209	33.885	3.165
33.906	2.530	33.906	0.971	33.906	3.196	33.906	2.802
33.926	2.683	33.926	1.462	33.926	3.954	33.926	3.106
33.947	2.712	33.947	1.953	33.947	3.774	33.947	2.889
33.967	3.387	33.967	1.736	33.967	4.011	33.967	2.609
33.988	3.645	33.988	2.560	33.988	4.393	33.988	3.268
34.008	3.403	34.008	2.073	34.008	4.881	34.008	3.593
34.028	4.078	34.028	1.793	34.028	4.701	34.028	3.647
34.049	4.045	34.049	2.493	34.049	4.709	34.049	3.013
34.069	5.012	34.069	3.235	34.069	4.905	34.069	2.880
34.090	4.916	34.090	2.915	34.090	5.226	34.090	2.643
34.110	4.779	34.110	2.782	34.110	5.901	34.110	2.010

34.131	4.934	34.131	2.482	34.131	4.326	34.131	1.794
34.151	5.297	34.151	2.600	34.151	5.064	34.151	1.703
34.171	5.035	34.171	2.363	34.171	4.218	34.171	2.278
34.192	4.982	34.192	2.481	34.192	3.831	34.192	1.250
34.212	4.283	34.212	2.640	34.212	4.069	34.212	1.117
34.233	4.292	34.233	2.487	34.233	3.307	34.233	1.298
34.253	4.135	34.253	1.835	34.253	3.587	34.253	0.978
34.274	3.665	34.274	2.286	34.274	2.846	34.274	0.679
34.294	2.654	34.294	2.779	34.294	2.647	34.294	0.859
34.314	2.788	34.314	1.856	34.314	2.407	34.314	0.623
34.335	2.506	34.335	1.308	34.335	1.353	34.335	0.908
34.355	2.120	34.355	1.740	34.355	1.738	34.355	0.088
34.376	3.110	34.376	1.234	34.376	1.477	34.376	0.332
34.396	2.203	34.396	0.624	34.396	1.299	34.396	0.054
34.417	0.942	34.417	0.534	34.417	1.142	34.417	-0.223
34.437	1.411	34.437	0.425	34.437	0.715	34.437	0.208
34.457	0.879	34.457	0.211	34.457	0.975	34.457	0.556
34.478	0.577	34.478	0.622	34.478	0.235	34.478	0.112
34.498	1.192	34.498	0.430	34.498	0.620	34.498	0.043
34.519	0.765	34.519	0.154	34.519	0.818	34.519	0.099
34.539	0.297	34.539	-0.039	34.539	-0.005	34.539	0.177
34.560	0.370	34.560	0.165	34.560	0.380	34.560	0.213
34.580	0.943	34.580	0.348	34.580	0.787	34.580	0.790
34.600	0.684	34.600	-0.053	34.600	-0.224	34.600	0.409
34.621	0.070	34.621	-0.119	34.621	0.037	34.621	0.279
34.641	0.560	34.641	0.126	34.641	0.090	34.641	0.482
34.662	-0.012	34.662	0.143	34.662	0.122	34.662	-0.149
34.682	0.666	34.682	-0.152	34.682	-0.180	34.682	-0.154
34.703	-0.239	34.703	-0.094	34.703	-0.106	34.703	0.486
34.723	-0.207	34.723	-0.243	34.723	-0.095	34.723	0.106
34.743	-0.070	34.743	-0.126	34.743	-0.167	34.743	0.247
34.764	-0.162	34.764	-0.009	34.764	0.261	34.764	0.138
34.784	-0.380	34.784	0.088	34.784	-0.081	34.784	0.050
34.805	0.736	34.805	-0.065	34.805	0.326	34.805	0.107
34.825	-0.210	34.825	0.115	34.825	0.109	34.825	-0.127
34.846	-0.406	34.846	-0.142	34.846	0.120	34.846	0.223
34.866	0.228	34.866	0.226	34.866	-0.264	34.866	0.239
34.886	0.279	34.886	0.052	34.886	-0.153	34.886	-0.119
34.907	0.018	34.907	0.254	34.907	-0.022	34.907	-0.040
34.927	-0.119	34.927	0.184	34.927	-0.162	34.927	0.226
34.948	0.558	34.948	-0.072	34.948	0.032	34.948	-0.069
34.968	0.067	34.968	0.297	34.968	0.018	34.968	-0.282
34.989	-0.173	34.989	-0.460	34.989	0.191	34.989	-0.216

35.009	-0.226	35.009	-0.007	35.009	0.052	35.009	0.163
35.029	0.326	35.029	-0.117	35.029	0.038	35.029	-0.084
35.050	-0.289	35.050	-0.144	35.050	-0.101	35.050	0.149
35.070	-0.237	35.070	-0.233	35.070	0.177	35.070	0.361
35.091	-0.268	35.091	0.039	35.091	0.038	35.091	0.032
35.111	0.240	35.111	0.290	35.111	0.316	35.111	-0.235
35.132	0.166	35.132	-0.250	35.132	0.719	35.132	0.186
35.152	0.321	35.152	0.314	35.152	0.080	35.152	1.044
35.172	0.330	35.172	-0.247	35.172	0.129	35.172	-0.035
35.193	-0.057	35.193	0.588	35.193	0.095	35.193	0.490
35.213	0.140	35.213	0.632	35.213	0.249	35.213	0.412
35.234	-0.184	35.234	0.071	35.234	0.006	35.234	0.562
35.254	-0.070	35.254	0.365	35.254	0.618	35.254	0.275
35.275	-0.103	35.275	0.222	35.275	0.147	35.275	0.196
35.295	-0.010	35.295	0.266	35.295	0.551	35.295	0.868
35.315	-0.437	35.315	0.227	35.315	0.392	35.315	0.435
35.336	0.029	35.336	-0.271	35.336	0.171	35.336	0.670
35.356	0.288	35.356	-0.207	35.356	-0.091	35.356	0.383
35.377	0.150	35.377	0.086	35.377	0.105	35.377	0.472
35.397	-0.070	35.397	0.505	35.397	-0.345	35.397	0.623
35.418	0.230	35.418	1.006	35.418	0.184	35.418	1.003
35.438	0.384	35.438	0.592	35.438	0.151	35.438	0.363
35.458	0.456	35.458	0.698	35.458	0.264	35.458	0.827
35.479	0.840	35.479	0.304	35.479	0.731	35.479	1.020
35.499	0.370	35.499	1.348	35.499	0.115	35.499	0.255
35.520	0.775	35.520	0.497	35.520	0.291	35.520	1.053
35.540	0.346	35.540	0.770	35.540	0.217	35.540	1.350
35.561	0.793	35.561	0.939	35.561	0.684	35.561	0.710
35.581	0.990	35.581	0.797	35.581	0.235	35.581	0.779
35.601	1.062	35.601	1.487	35.601	0.953	35.601	1.556
35.622	1.176	35.622	0.907	35.622	0.442	35.622	1.354
35.642	1.227	35.642	1.139	35.642	0.056	35.642	1.215
35.663	0.966	35.663	1.351	35.663	0.961	35.663	2.326
35.683	0.518	35.683	1.688	35.683	1.492	35.683	1.353
35.704	0.798	35.704	1.630	35.704	0.898	35.704	1.631
35.724	0.954	35.724	1.633	35.724	0.866	35.724	2.367
35.744	0.527	35.744	1.367	35.744	0.501	35.744	2.165
35.765	1.266	35.765	2.163	35.765	0.824	35.765	2.026
35.785	0.777	35.785	1.709	35.785	0.501	35.785	2.346
35.806	1.016	35.806	2.192	35.806	0.824	35.806	3.228
35.826	1.339	35.826	3.093	35.826	0.855	35.826	4.027
35.847	1.183	35.847	2.535	35.847	0.720	35.847	4.118
35.867	0.861	35.867	3.165	35.867	0.814	35.867	6.209

35.887	1.080	35.887	3.128	35.887	0.220	35.887	6.445
35.908	1.278	35.908	3.488	35.908	0.606	35.908	7.015
35.928	1.206	35.928	4.743	35.928	0.471	35.928	5.461
35.949	1.092	35.949	5.082	35.949	0.628	35.949	5.135
35.969	2.020	35.969	6.692	35.969	0.743	35.969	4.039
35.990	1.823	35.990	8.093	35.990	1.067	35.990	4.110
36.010	1.168	36.010	9.682	36.010	1.099	36.010	3.847

Oreodont Specimen XRD Data, Background Subtracted

ODC		ODT		ODT2		OLC		OLT	
2θ	Intensity	2θ	Intensity	2θ	Intensity	2θ	Intensity	2θ	Intensity
29.003	3.383	29.003	7.380	29.003	7.829	29.003	3.142	29.003	7.020
29.024	3.398	29.024	7.485	29.024	7.122	29.024	3.182	29.024	7.413
29.044	2.933	29.044	8.528	29.044	8.852	29.044	3.410	29.044	7.953
29.064	3.636	29.064	9.467	29.064	9.957	29.064	3.909	29.064	9.430
29.085	3.692	29.085	11.052	29.085	10.459	29.085	3.429	29.085	10.053
29.105	2.540	29.105	9.866	29.105	11.897	29.105	3.573	29.105	9.467
29.126	2.659	29.126	13.305	29.126	14.024	29.126	3.656	29.126	10.132
29.146	2.425	29.146	13.077	29.146	14.713	29.146	3.134	29.146	12.797
29.167	2.419	29.167	14.579	29.167	16.986	29.167	3.883	29.167	15.004
29.187	2.518	29.187	17.873	29.187	20.550	29.187	3.112	29.187	15.627
29.207	3.470	29.207	19.062	29.207	22.865	29.207	3.465	29.207	17.709
29.228	3.819	29.228	22.397	29.228	28.346	29.228	3.590	29.228	19.895
29.248	3.627	29.248	26.004	29.248	32.744	29.248	3.173	29.248	24.519
29.269	4.746	29.269	30.965	29.269	39.746	29.269	2.985	29.269	28.247
29.289	5.512	29.289	36.634	29.289	48.582	29.289	3.339	29.289	35.850
29.310	6.945	29.310	43.240	29.310	57.897	29.310	3.401	29.310	42.120
29.330	9.440	29.330	52.472	29.330	71.421	29.330	3.026	29.330	51.286
29.350	12.789	29.350	62.892	29.350	80.403	29.350	3.193	29.350	56.722
29.371	13.639	29.371	74.686	29.371	84.614	29.371	3.277	29.371	62.659
29.391	14.884	29.391	79.106	29.391	81.221	29.391	4.298	29.391	64.304
29.412	12.880	29.412	81.630	29.412	71.454	29.412	3.715	29.412	60.054
29.432	10.209	29.432	72.488	29.432	58.769	29.432	5.257	29.432	55.616
29.453	8.892	29.453	64.408	29.453	48.877	29.453	9.132	29.453	47.491
29.473	7.804	29.473	53.057	29.473	38.755	29.473	5.925	29.473	35.720
29.493	3.967	29.493	41.811	29.493	28.030	29.493	3.655	29.493	29.178
29.514	2.359	29.514	33.377	29.514	22.013	29.514	3.968	29.514	21.762
29.534	1.709	29.534	25.839	29.534	16.892	29.534	4.261	29.534	15.845
29.555	1.455	29.555	19.509	29.555	13.520	29.555	1.866	29.555	11.346
29.575	0.680	29.575	14.951	29.575	10.254	29.575	1.450	29.575	9.263
29.596	1.010	29.596	11.893	29.596	9.987	29.596	1.056	29.596	7.159

29.616	1.298	29.616	9.522	29.616	7.700	29.616	1.224	29.616	5.514
29.636	0.503	29.636	8.276	29.636	5.933	29.636	0.933	29.636	4.202
29.657	0.229	29.657	7.406	29.657	6.438	29.657	0.185	29.657	4.453
29.677	0.601	29.677	5.994	29.677	4.359	29.677	-0.709	29.677	4.037
29.698	-0.340	29.698	5.040	29.698	4.197	29.698	0.126	29.698	2.955
29.718	-0.385	29.718	4.941	29.718	3.806	29.718	0.086	29.718	2.060
29.739	0.779	29.739	3.696	29.739	3.624	29.739	0.421	29.739	2.332
29.759	0.984	29.759	3.784	29.759	3.025	29.759	0.027	29.759	2.396
29.779	1.044	29.779	3.831	29.779	2.613	29.779	0.571	29.779	1.793
29.800	-0.021	29.800	3.503	29.800	2.139	29.800	0.323	29.800	1.024
29.820	0.060	29.820	2.238	29.820	2.603	29.820	0.263	29.820	1.838
29.841	-0.047	29.841	2.306	29.841	1.796	29.841	0.370	29.841	1.777
29.861	0.096	29.861	1.770	29.861	1.552	29.861	0.164	29.861	1.633
29.881	0.636	29.881	1.817	29.881	1.724	29.881	0.146	29.881	1.760
29.902	-0.075	29.902	1.448	29.902	1.668	29.902	-0.060	29.902	1.366
29.922	0.069	29.922	1.058	29.922	1.716	29.922	0.172	29.922	0.931
29.943	0.338	29.943	1.210	29.943	1.034	29.943	-0.096	29.943	0.933
29.963	0.752	29.963	0.612	29.963	1.999	29.963	-0.031	29.963	0.435
29.984	1.271	29.984	1.702	29.984	1.130	29.984	0.285	29.984	0.209
30.004	0.207	30.004	0.937	30.004	0.928	30.004	-0.108	30.004	1.232
30.024	-0.065	30.024	1.069	30.024	0.935	30.024	0.062	30.024	0.255
30.045	0.558	30.045	2.096	30.045	1.567	30.045	0.440	30.045	1.196
30.065	0.807	30.065	0.874	30.065	1.178	30.065	-0.244	30.065	1.303
30.086	-0.341	30.086	0.339	30.086	1.164	30.086	-0.386	30.086	0.535
30.106	-0.342	30.106	1.242	30.106	1.608	30.106	0.347	30.106	-0.150
30.127	0.532	30.127	0.978	30.127	1.365	30.127	0.330	30.127	0.458
30.147	-0.073	30.147	1.131	30.147	-0.065	30.147	-0.271	30.147	0.482
30.167	-0.074	30.167	0.764	30.167	0.422	30.167	-0.312	30.167	1.214
30.188	0.341	30.188	0.563	30.188	1.221	30.188	0.286	30.188	0.947
30.208	-0.243	30.208	0.466	30.208	0.687	30.208	-0.117	30.208	0.534
30.229	-0.181	30.229	0.307	30.229	1.049	30.229	0.398	30.229	0.496
30.249	-0.015	30.249	0.523	30.249	0.390	30.249	-0.066	30.249	0.604
30.270	-0.119	30.270	0.739	30.270	0.148	30.270	-0.405	30.270	0.149
30.290	0.047	30.290	0.685	30.290	0.656	30.290	0.339	30.290	0.653
30.310	0.338	30.310	0.526	30.310	0.435	30.310	-0.375	30.310	0.157
30.331	0.046	30.331	0.930	30.331	0.235	30.331	0.369	30.331	0.703
30.351	0.754	30.351	-0.374	30.351	0.764	30.351	0.343	30.351	0.353
30.372	-0.037	30.372	0.489	30.372	0.585	30.372	-0.184	30.372	0.649
30.392	-0.183	30.392	0.289	30.392	-0.114	30.392	-0.272	30.392	-0.054
30.413	0.817	30.413	-0.056	30.413	0.249	30.413	-0.092	30.413	0.784
30.433	0.088	30.433	-0.173	30.433	0.278	30.433	-0.078	30.433	0.538
30.453	0.005	30.453	0.086	30.453	0.142	30.453	-0.189	30.453	0.460
30.474	0.151	30.474	0.262	30.474	0.734	30.474	-0.258	30.474	0.402

30.494	-0.390	30.494	0.396	30.494	0.827	30.494	0.027	30.494	0.074
30.515	-0.517	30.515	-0.324	30.515	0.294	30.515	0.041	30.515	0.975
30.535	1.064	30.535	0.727	30.535	0.700	30.535	0.409	30.535	-0.083
30.556	-0.605	30.556	-0.347	30.556	-0.395	30.556	0.465	30.556	-0.056
30.576	0.684	30.576	0.142	30.576	-0.427	30.576	-0.062	30.576	0.678
30.596	0.662	30.596	0.360	30.596	0.403	30.596	0.140	30.596	-0.191
30.617	0.597	30.617	0.537	30.617	0.087	30.617	-0.032	30.617	-0.373
30.637	0.241	30.637	-0.099	30.637	0.605	30.637	0.066	30.637	0.633
30.658	-0.240	30.658	-0.339	30.658	0.123	30.658	0.081	30.658	0.388
30.678	0.071	30.678	-0.011	30.678	-0.067	30.678	0.200	30.678	0.186
30.699	0.403	30.699	0.547	30.699	0.117	30.699	-0.223	30.699	-0.662
30.719	0.464	30.719	0.917	30.719	0.032	30.719	0.022	30.719	0.552
30.739	-0.017	30.739	0.121	30.739	0.175	30.739	0.558	30.739	0.579
30.760	0.253	30.760	-0.509	30.760	0.943	30.760	0.261	30.760	-0.477
30.780	0.189	30.780	0.132	30.780	-0.288	30.780	0.610	30.780	0.009
30.801	-0.041	30.801	0.795	30.801	0.272	30.801	0.063	30.801	0.870
30.821	0.479	30.821	-0.043	30.821	0.208	30.821	0.599	30.821	0.835
30.842	0.520	30.842	-0.359	30.842	0.164	30.842	0.448	30.842	0.446
30.862	1.123	30.862	0.407	30.862	0.308	30.862	0.235	30.862	0.473
30.882	-0.274	30.882	0.195	30.882	1.056	30.882	0.418	30.882	0.564
30.903	0.767	30.903	0.483	30.903	0.096	30.903	1.080	30.903	0.279
30.923	0.975	30.923	0.459	30.923	0.116	30.923	0.783	30.923	-0.130
30.944	1.016	30.944	0.268	30.944	0.177	30.944	0.216	30.944	0.585
30.964	1.391	30.964	0.368	30.964	-0.283	30.964	1.107	30.964	1.134
30.985	1.703	30.985	0.261	30.985	0.195	30.985	0.561	30.985	0.121
31.005	1.391	31.005	0.278	31.005	-0.076	31.005	0.640	31.005	-0.101
31.025	1.537	31.025	0.213	31.025	0.006	31.025	0.803	31.025	-0.406
31.046	1.662	31.046	0.543	31.046	0.005	31.046	1.278	31.046	-0.009
31.066	1.537	31.066	0.603	31.066	0.463	31.066	1.295	31.066	0.241
31.087	1.287	31.087	0.267	31.087	0.254	31.087	0.999	31.087	-0.279
31.107	2.058	31.107	0.639	31.107	0.670	31.107	1.266	31.107	0.201
31.128	1.829	31.128	0.678	31.128	-0.247	31.128	1.242	31.128	0.931
31.148	1.955	31.148	0.884	31.148	0.711	31.148	1.967	31.148	1.266
31.168	3.018	31.168	1.173	31.168	0.711	31.168	2.547	31.168	0.538
31.189	2.435	31.189	0.588	31.189	0.961	31.189	1.752	31.189	0.643
31.209	3.290	31.209	1.002	31.209	0.795	31.209	1.999	31.209	1.207
31.230	2.729	31.230	1.417	31.230	1.274	31.230	2.579	31.230	0.250
31.250	3.917	31.250	0.874	31.250	1.650	31.250	2.326	31.250	0.106
31.271	4.189	31.271	1.184	31.271	1.713	31.271	2.927	31.271	1.566
31.291	4.357	31.291	1.558	31.291	1.463	31.291	3.090	31.291	0.755
31.311	3.775	31.311	1.702	31.311	1.547	31.311	3.733	31.311	1.445
31.332	4.839	31.332	1.617	31.332	2.340	31.332	3.856	31.332	1.905
31.352	6.319	31.352	1.804	31.352	2.799	31.352	3.499	31.352	2.032

31.373	5.509	31.373	2.823	31.373	3.675	31.373	4.100	31.373	1.784
31.393	7.156	31.393	3.030	31.393	3.030	31.393	5.535	31.393	2.036
31.414	6.970	31.414	3.405	31.414	3.657	31.414	5.283	31.414	2.851
31.434	6.743	31.434	3.320	31.434	3.387	31.434	5.656	31.434	2.896
31.454	7.599	31.454	3.486	31.454	3.451	31.454	5.883	31.454	1.356
31.475	8.184	31.475	3.652	31.475	3.786	31.475	7.006	31.475	2.901
31.495	8.312	31.495	3.902	31.495	2.600	31.495	7.629	31.495	3.070
31.516	9.585	31.516	3.172	31.516	3.540	31.516	9.252	31.516	2.177
31.536	9.795	31.536	2.901	31.536	2.833	31.536	8.854	31.536	1.472
31.557	9.881	31.557	3.318	31.557	2.815	31.557	9.477	31.557	2.642
31.577	11.654	31.577	3.401	31.577	2.629	31.577	10.413	31.577	2.624
31.597	11.074	31.597	3.151	31.597	2.403	31.597	11.578	31.597	1.752
31.618	12.326	31.618	3.130	31.618	3.676	31.618	12.160	31.618	2.152
31.638	12.558	31.638	3.568	31.638	3.699	31.638	13.138	31.638	1.614
31.659	12.894	31.659	2.798	31.659	3.410	31.659	14.179	31.659	2.659
31.679	15.064	31.679	3.402	31.679	3.934	31.679	16.052	31.679	1.892
31.700	15.380	31.700	3.195	31.700	3.437	31.700	15.093	31.700	1.729
31.720	15.550	31.720	3.737	31.720	4.586	31.720	17.426	31.720	3.129
31.740	16.178	31.740	3.821	31.740	4.568	31.740	18.570	31.740	2.945
31.761	16.160	31.761	3.906	31.761	4.821	31.761	20.299	31.761	2.408
31.781	15.830	31.781	3.011	31.781	5.179	31.781	21.007	31.781	2.245
31.802	18.480	31.802	3.908	31.802	5.307	31.802	21.464	31.802	3.604
31.822	16.546	31.822	4.305	31.822	4.123	31.822	25.131	31.822	3.129
31.843	18.050	31.843	5.098	31.843	4.564	31.843	25.068	31.843	3.884
31.863	18.762	31.863	3.683	31.863	3.610	31.863	26.255	31.863	3.180
31.883	17.766	31.883	4.518	31.883	5.280	31.883	26.817	31.883	3.476
31.904	17.145	31.904	4.770	31.904	4.597	31.904	29.484	31.904	3.377
31.924	17.795	31.924	4.730	31.924	4.914	31.924	29.151	31.924	3.965
31.945	16.924	31.945	4.774	31.945	4.439	31.945	29.880	31.945	4.304
31.965	16.074	31.965	4.609	31.965	4.235	31.965	30.734	31.965	3.371
31.986	15.599	31.986	3.486	31.986	3.552	31.986	29.714	31.986	3.273
32.006	14.916	32.006	3.634	32.006	3.952	32.006	28.881	32.006	3.507
32.026	15.338	32.026	3.866	32.026	4.374	32.026	30.319	32.026	3.596
32.047	14.509	32.047	3.598	32.047	3.649	32.047	28.278	32.047	3.456
32.067	15.535	32.067	4.538	32.067	3.925	32.067	28.382	32.067	3.774
32.088	14.039	32.088	3.499	32.088	3.014	32.088	29.821	32.088	2.905
32.108	14.440	32.108	3.439	32.108	2.331	32.108	28.842	32.108	2.910
32.129	14.570	32.129	3.984	32.129	2.670	32.129	26.406	32.129	2.458
32.149	13.471	32.149	2.633	32.149	2.925	32.149	25.594	32.149	1.839
32.169	11.622	32.169	2.636	32.169	3.202	32.169	26.846	32.169	1.970
32.190	12.128	32.190	3.473	32.190	3.020	32.190	26.118	32.190	0.810
32.210	11.821	32.210	2.601	32.210	2.255	32.210	24.161	32.210	1.858
32.231	10.910	32.231	3.167	32.231	2.698	32.231	23.412	32.231	1.635

32.251	9.978	32.251	1.483	32.251	1.933	32.251	22.768	32.251	2.225
32.272	9.588	32.272	2.258	32.272	2.106	32.272	21.770	32.272	1.815
32.292	9.010	32.292	1.804	32.292	2.591	32.292	21.084	32.292	2.093
32.312	7.412	32.312	1.849	32.312	1.389	32.312	19.356	32.312	0.912
32.333	8.251	32.333	1.833	32.333	1.938	32.333	17.504	32.333	0.857
32.353	6.945	32.353	1.691	32.353	1.632	32.353	16.777	32.353	1.197
32.374	7.409	32.374	1.550	32.374	0.888	32.374	15.696	32.374	0.746
32.394	6.791	32.394	1.783	32.394	1.458	32.394	13.781	32.394	1.212
32.415	5.401	32.415	1.079	32.415	0.923	32.415	13.325	32.415	0.803
32.435	6.387	32.435	0.917	32.435	1.117	32.435	12.724	32.435	0.789
32.455	4.518	32.455	0.506	32.455	1.416	32.455	11.497	32.455	0.151
32.476	5.213	32.476	1.240	32.476	0.944	32.476	9.166	32.476	-0.216
32.496	4.886	32.496	0.849	32.496	0.347	32.496	8.544	32.496	-0.417
32.517	4.518	32.517	1.417	32.517	1.126	32.517	8.630	32.517	0.236
32.537	4.837	32.537	1.609	32.537	0.029	32.537	8.216	32.537	0.639
32.558	5.532	32.558	1.135	32.558	0.683	32.558	8.698	32.558	0.396
32.578	5.810	32.578	0.349	32.578	1.461	32.578	6.410	32.578	0.653
32.598	5.546	32.598	0.397	32.598	1.199	32.598	7.955	32.598	0.660
32.619	5.387	32.619	0.715	32.619	1.269	32.619	6.416	32.619	0.730
32.639	5.082	32.639	1.033	32.639	0.756	32.639	6.961	32.639	0.217
32.660	5.798	32.660	0.977	32.660	1.369	32.660	6.736	32.660	0.412
32.680	6.264	32.680	1.108	32.680	1.336	32.680	5.989	32.680	0.336
32.701	5.959	32.701	1.030	32.701	1.719	32.701	6.555	32.701	0.656
32.721	6.550	32.721	1.683	32.721	2.540	32.721	7.038	32.721	0.997
32.741	7.183	32.741	1.460	32.741	2.049	32.741	7.042	32.741	0.734
32.762	6.066	32.762	1.508	32.762	1.662	32.762	7.817	32.762	0.867
32.782	6.970	32.782	1.140	32.782	1.900	32.782	7.717	32.782	0.230
32.803	7.999	32.803	2.167	32.803	2.201	32.803	7.596	32.803	0.134
32.823	7.486	32.823	1.486	32.823	0.981	32.823	10.183	32.823	0.684
32.844	7.328	32.844	1.910	32.844	2.345	32.844	8.104	32.844	1.317
32.864	8.232	32.864	1.625	32.864	1.583	32.864	9.900	32.864	0.596
32.884	7.408	32.884	1.466	32.884	1.989	32.884	9.759	32.884	0.647
32.905	7.458	32.905	2.223	32.905	1.207	32.905	9.035	32.905	1.197
32.925	7.612	32.925	2.356	32.925	1.237	32.925	11.185	32.925	1.352
32.946	8.371	32.946	2.509	32.946	2.268	32.946	11.357	32.946	0.548
32.966	7.672	32.966	1.767	32.966	0.590	32.966	11.778	32.966	0.099
32.987	7.514	32.987	0.629	32.987	2.184	32.987	11.637	32.987	1.400
33.007	7.148	33.007	1.595	33.007	1.652	33.007	10.517	33.007	1.222
33.027	6.512	33.027	0.915	33.027	1.684	33.027	13.481	33.027	0.960
33.048	6.084	33.048	1.048	33.048	1.319	33.048	13.049	33.048	0.449
33.068	6.239	33.068	1.869	33.068	1.371	33.068	12.533	33.068	0.917
33.089	6.519	33.089	1.294	33.089	1.465	33.089	13.372	33.089	1.426
33.109	6.487	33.109	0.948	33.109	1.164	33.109	13.898	33.109	1.186

33.130	6.038	33.130	1.061	33.130	1.654	33.130	13.196	33.130	0.738
33.150	5.944	33.150	1.236	33.150	1.207	33.150	12.743	33.150	0.602
33.170	5.121	33.170	0.995	33.170	0.968	33.170	11.832	33.170	0.758
33.191	5.235	33.191	0.858	33.191	0.646	33.191	12.484	33.191	0.143
33.211	4.932	33.211	1.075	33.211	0.761	33.211	12.469	33.211	0.257
33.232	4.672	33.232	0.584	33.232	0.835	33.232	11.621	33.232	0.914
33.252	3.099	33.252	0.406	33.252	0.993	33.252	10.836	33.252	0.653
33.273	4.005	33.273	0.082	33.273	0.775	33.273	10.363	33.273	-0.024
33.293	3.411	33.293	0.112	33.293	0.829	33.293	9.599	33.293	0.862
33.313	2.005	33.313	0.414	33.313	0.841	33.313	9.126	33.313	0.415
33.334	3.245	33.334	0.527	33.334	1.478	33.334	8.404	33.334	-0.200
33.354	2.485	33.354	0.371	33.354	0.490	33.354	7.369	33.354	0.041
33.375	2.537	33.375	-0.265	33.375	0.481	33.375	6.730	33.375	0.531
33.395	2.694	33.395	-0.151	33.395	0.098	33.395	6.986	33.395	-0.125
33.416	2.288	33.416	0.359	33.416	0.465	33.416	6.202	33.416	-0.176
33.436	1.675	33.436	0.390	33.436	-0.023	33.436	5.792	33.436	-0.373
33.456	1.832	33.456	0.254	33.456	0.240	33.456	5.383	33.456	0.035
33.477	2.135	33.477	0.307	33.477	-0.247	33.477	4.661	33.477	-0.412
33.497	1.063	33.497	-0.162	33.497	-0.317	33.497	4.293	33.497	0.829
33.518	2.282	33.518	-0.026	33.518	-0.030	33.518	4.072	33.518	-0.534
33.538	1.877	33.538	0.172	33.538	0.341	33.538	3.517	33.538	-0.168
33.559	1.431	33.559	-0.192	33.559	0.129	33.559	3.628	33.559	-0.385
33.579	0.818	33.579	-0.014	33.579	-0.125	33.579	2.865	33.579	-0.065
33.599	1.454	33.599	-0.274	33.599	0.955	33.599	2.873	33.599	-0.036
33.620	1.862	33.620	-0.325	33.620	0.514	33.620	3.235	33.620	-0.445
33.640	0.541	33.640	-0.263	33.640	-0.448	33.640	2.702	33.640	0.542
33.661	1.220	33.661	0.070	33.661	-0.055	33.661	2.793	33.661	0.300
33.681	1.024	33.681	-0.347	33.681	0.046	33.681	2.635	33.681	0.287
33.702	2.911	33.702	0.090	33.702	0.480	33.702	2.268	33.702	-0.725
33.722	1.715	33.722	0.778	33.722	0.456	33.722	2.797	33.722	0.096
33.742	1.249	33.742	0.361	33.742	0.141	33.742	2.452	33.742	-0.417
33.763	2.261	33.763	-0.138	33.763	0.221	33.763	2.335	33.763	-0.079
33.783	2.816	33.783	-0.201	33.783	0.031	33.783	2.532	33.783	-0.136
33.804	1.995	33.804	0.300	33.804	0.716	33.804	2.561	33.804	0.139
33.824	2.487	33.824	0.238	33.824	1.089	33.824	2.279	33.824	0.582
33.845	0.958	33.845	0.426	33.845	0.857	33.845	3.183	33.845	-0.121
33.865	3.534	33.865	0.656	33.865	0.188	33.865	3.359	33.865	0.030
33.885	2.401	33.885	0.907	33.885	0.666	33.885	3.743	33.885	0.868
33.906	3.186	33.906	0.554	33.906	1.434	33.906	3.524	33.906	-0.085
33.926	2.532	33.926	-0.153	33.926	0.953	33.926	4.908	33.926	-0.121
33.947	2.483	33.947	1.161	33.947	0.910	33.947	3.855	33.947	-0.053
33.967	3.330	33.967	0.600	33.967	1.367	33.967	5.156	33.967	0.078
33.988	2.969	33.988	-0.086	33.988	0.949	33.988	4.958	33.988	0.084

34.008	3.983	34.008	0.499	34.008	0.364	34.008	5.488	34.008	0.485
34.028	3.080	34.028	0.125	34.028	0.654	34.028	5.040	34.028	0.158
34.049	3.219	34.049	-0.227	34.049	0.799	34.049	6.279	34.049	0.477
34.069	3.837	34.069	0.171	34.069	0.173	34.069	5.601	34.069	0.733
34.090	2.705	34.090	0.048	34.090	0.943	34.090	5.924	34.090	0.614
34.110	3.074	34.110	-0.054	34.110	0.942	34.110	7.455	34.110	0.350
34.131	3.421	34.131	-0.177	34.131	0.525	34.131	6.820	34.131	0.689
34.151	2.082	34.151	0.617	34.151	-0.142	34.151	6.205	34.151	1.363
34.171	2.284	34.171	-0.151	34.171	0.357	34.171	5.403	34.171	0.786
34.192	2.715	34.192	0.539	34.192	0.878	34.192	5.580	34.192	0.543
34.212	1.355	34.212	0.646	34.212	0.377	34.212	5.529	34.212	-0.117
34.233	1.620	34.233	0.815	34.233	0.544	34.233	5.540	34.233	0.494
34.253	0.864	34.253	0.131	34.253	1.002	34.253	4.821	34.253	0.022
34.274	1.483	34.274	0.217	34.274	0.252	34.274	4.353	34.274	0.321
34.294	1.081	34.294	0.262	34.294	0.211	34.294	3.927	34.294	0.224
34.314	1.117	34.314	-0.193	34.314	0.420	34.314	3.980	34.314	0.690
34.335	1.216	34.335	0.331	34.335	0.379	34.335	3.512	34.335	-0.302
34.355	1.065	34.355	-0.082	34.355	0.400	34.355	2.627	34.355	0.226
34.376	0.184	34.376	-0.161	34.376	0.088	34.376	2.722	34.376	-0.079
34.396	0.721	34.396	0.092	34.396	-0.140	34.396	2.171	34.396	0.346
34.417	0.215	34.417	0.638	34.417	0.236	34.417	1.496	34.417	0.125
34.437	0.481	34.437	-0.212	34.437	0.091	34.437	1.736	34.437	0.299
34.457	0.060	34.457	-0.062	34.457	0.363	34.457	1.353	34.457	0.141
34.478	1.450	34.478	-0.058	34.478	0.114	34.478	0.865	34.478	0.149
34.498	0.654	34.498	0.071	34.498	-0.343	34.498	1.314	34.498	0.782
34.519	0.316	34.519	-0.237	34.519	0.450	34.519	1.014	34.519	0.062
34.539	-0.064	34.539	0.309	34.539	-0.152	34.539	0.943	34.539	-0.263
34.560	-0.110	34.560	-0.665	34.560	0.245	34.560	0.518	34.560	0.016
34.580	-0.156	34.580	-0.119	34.580	0.685	34.580	0.593	34.580	0.734
34.600	0.152	34.600	-0.322	34.600	-0.251	34.600	0.397	34.600	-0.008
34.621	-0.039	34.621	0.053	34.621	-0.040	34.621	0.472	34.621	-0.186
34.641	-0.356	34.641	-0.030	34.641	0.503	34.641	0.735	34.641	0.469
34.662	0.119	34.662	-0.009	34.662	0.068	34.662	-0.065	34.662	0.061
34.682	0.240	34.682	-0.530	34.682	0.112	34.682	0.177	34.682	-0.096
34.703	0.049	34.703	0.283	34.703	0.282	34.703	0.169	34.703	0.122
34.723	-0.351	34.723	0.325	34.723	0.805	34.723	-0.463	34.723	0.548
34.743	0.708	34.743	-0.445	34.743	0.349	34.743	-0.075	34.743	0.474
34.764	0.496	34.764	0.285	34.764	0.582	34.764	0.396	34.764	0.921
34.784	0.284	34.784	0.702	34.784	0.418	34.784	-0.132	34.784	-0.027
34.805	0.427	34.805	-0.318	34.805	0.275	34.805	0.048	34.805	1.024
34.825	0.153	34.825	-0.087	34.825	0.320	34.825	-0.084	34.825	0.930
34.846	-0.517	34.846	0.664	34.846	0.261	34.846	0.034	34.846	0.315
34.866	0.751	34.866	0.436	34.866	-0.361	34.866	-0.244	34.866	0.638

34.886	-0.127	34.886	-0.438	34.886	0.643	34.886	-0.170	34.886	-0.185
34.907	-0.026	34.907	0.189	34.907	0.001	34.907	0.237	34.907	-0.446
34.927	-0.341	34.927	0.461	34.927	0.171	34.927	-0.023	34.927	0.357
34.948	0.093	34.948	0.317	34.948	0.279	34.948	-0.116	34.948	0.742
34.968	-0.222	34.968	0.132	34.968	-0.008	34.968	-0.042	34.968	0.191
34.989	0.422	34.989	1.050	34.989	0.058	34.989	-0.239	34.989	0.805
35.009	0.065	35.009	0.532	35.009	-0.125	35.009	-0.164	35.009	0.587
35.029	-0.396	35.029	-0.425	35.029	0.129	35.029	-0.007	35.029	-0.235
35.050	-0.054	35.050	0.536	35.050	0.134	35.050	-0.120	35.050	-0.370
35.070	0.308	35.070	0.330	35.070	0.763	35.070	-0.150	35.070	-0.136
35.091	0.295	35.091	-0.688	35.091	-0.169	35.091	0.070	35.091	0.348
35.111	-0.197	35.111	-0.144	35.111	-0.185	35.111	-0.355	35.111	0.749
35.132	-0.064	35.132	-0.079	35.132	0.195	35.132	0.136	35.132	0.753
35.152	0.278	35.152	0.070	35.152	-0.279	35.152	-0.018	35.152	0.404
35.172	0.245	35.172	-0.281	35.172	-0.024	35.172	-0.172	35.172	-0.028
35.193	0.107	35.193	-0.111	35.193	-0.061	35.193	0.236	35.193	0.185
35.213	0.345	35.213	0.350	35.213	0.299	35.213	0.165	35.213	-0.184
35.234	0.520	35.234	-0.396	35.234	0.804	35.234	0.241	35.234	-0.095
35.254	0.196	35.254	-0.143	35.254	-0.002	35.254	-0.059	35.254	-0.257
35.275	0.455	35.275	0.194	35.275	0.753	35.275	-0.234	35.275	0.103
35.295	0.485	35.295	0.135	35.295	0.051	35.295	-0.183	35.295	0.671
35.315	0.160	35.315	0.597	35.315	0.244	35.315	-0.069	35.315	0.552
35.336	-0.185	35.336	0.080	35.336	-0.125	35.336	0.628	35.336	0.308
35.356	0.595	35.356	0.459	35.356	0.298	35.356	0.513	35.356	0.127
35.377	0.209	35.377	0.068	35.377	0.950	35.377	0.398	35.377	0.883
35.397	0.177	35.397	0.259	35.397	0.686	35.397	0.533	35.397	0.868
35.418	0.061	35.418	-0.132	35.418	0.318	35.418	0.730	35.418	0.708
35.438	0.363	35.438	0.331	35.438	1.012	35.438	0.428	35.438	0.819
35.458	0.039	35.458	0.189	35.458	0.227	35.458	0.709	35.458	1.659
35.479	0.507	35.479	1.152	35.479	1.046	35.479	0.656	35.479	1.644
35.499	0.600	35.499	1.011	35.499	1.157	35.499	0.688	35.499	0.547
35.520	1.048	35.520	0.662	35.520	0.290	35.520	0.427	35.520	1.637
35.540	-0.046	35.540	1.646	35.540	1.047	35.540	0.980	35.540	1.477
35.561	0.318	35.561	1.172	35.561	0.971	35.561	0.490	35.561	0.630
35.581	0.516	35.581	0.990	35.581	1.728	35.581	0.543	35.581	1.450
35.601	1.339	35.601	0.849	35.601	0.757	35.601	0.720	35.601	1.166
35.622	0.120	35.622	0.772	35.622	1.744	35.622	0.502	35.622	1.965
35.642	0.464	35.642	0.881	35.642	0.856	35.642	0.867	35.642	1.472
35.663	0.371	35.663	0.616	35.663	1.322	35.663	1.024	35.663	1.459
35.683	0.215	35.683	1.997	35.683	1.455	35.683	0.640	35.683	0.737
35.704	0.705	35.704	1.607	35.704	1.255	35.704	0.672	35.704	1.308
35.724	0.758	35.724	1.967	35.724	1.763	35.724	0.662	35.724	1.295
35.744	-0.335	35.744	1.661	35.744	2.584	35.744	1.237	35.744	2.053

35.765	0.551	35.765	3.209	35.765	3.551	35.765	0.457	35.765	2.040
35.785	0.583	35.785	2.819	35.785	3.622	35.785	0.218	35.785	3.027
35.806	0.365	35.806	3.534	35.806	4.256	35.806	0.647	35.806	3.952
35.826	-0.040	35.826	3.395	35.826	4.369	35.826	0.825	35.826	4.315
35.847	0.534	35.847	3.777	35.847	5.794	35.847	0.837	35.847	4.448
35.867	0.691	35.867	5.034	35.867	7.595	35.867	0.808	35.867	5.790
35.887	0.620	35.887	6.707	35.887	8.146	35.887	0.653	35.887	6.237
35.908	2.027	35.908	8.131	35.908	8.884	35.908	0.228	35.908	6.766
35.928	1.581	35.928	7.805	35.928	10.644	35.928	0.907	35.928	7.546
35.949	1.530	35.949	9.437	35.949	9.903	35.949	0.649	35.949	9.034
35.969	1.730	35.969	9.944	35.969	8.455	35.969	0.703	35.969	8.627
35.990	1.701	35.990	8.181	35.990	8.006	35.990	0.466	35.990	6.594
36.010	1.525	36.010	7.751	36.010	6.912	36.010	0.583	36.010	6.854

Tortoise Subsample XRD Data, Background Subtracted

TPC		TPT		TSC		TST	
2θ	Intensity	2θ	Intensity	2θ	Intensity	2θ	Intensity
29.003	4.374	29.003	5.414	29.003	1.969	29.003	5.024
29.024	3.102	29.024	5.618	29.024	3.114	29.024	4.667
29.044	2.935	29.044	6.010	29.044	3.425	29.044	4.873
29.064	3.372	29.064	6.382	29.064	4.049	29.064	6.266
29.085	4.268	29.085	7.399	29.085	2.757	29.085	5.659
29.105	4.247	29.105	7.042	29.105	3.569	29.105	7.177
29.126	3.934	29.126	8.684	29.126	3.568	29.126	7.238
29.146	4.767	29.146	9.348	29.146	4.547	29.146	8.506
29.167	4.309	29.167	9.199	29.167	3.421	29.167	10.483
29.187	4.059	29.187	10.529	29.187	5.255	29.187	9.814
29.207	4.476	29.207	11.047	29.207	4.629	29.207	11.541
29.228	4.998	29.228	12.378	29.228	4.650	29.228	13.477
29.248	4.331	29.248	14.146	29.248	4.942	29.248	13.579
29.269	5.186	29.269	15.727	29.269	5.463	29.269	14.452
29.289	5.958	29.289	18.599	29.289	6.296	29.289	17.097
29.310	5.479	29.310	19.951	29.310	6.880	29.310	19.637
29.330	6.272	29.330	23.637	29.330	6.922	29.330	22.198
29.350	7.085	29.350	27.614	29.350	9.131	29.350	27.467
29.371	8.711	29.371	29.591	29.371	10.569	29.371	29.383
29.391	8.650	29.391	39.256	29.391	13.528	29.391	36.465
29.412	7.568	29.412	45.775	29.412	15.133	29.412	40.943
29.432	6.923	29.432	52.461	29.432	21.425	29.432	48.192
29.453	6.258	29.453	61.272	29.453	23.718	29.453	55.170
29.473	4.635	29.473	74.375	29.473	23.094	29.473	58.732
29.493	4.074	29.493	83.582	29.493	20.470	29.493	56.210

29.514	3.534	29.514	86.706	29.514	17.346	29.514	49.251
29.534	2.181	29.534	80.392	29.534	14.451	29.534	42.813
29.555	1.225	29.555	74.162	29.555	11.911	29.555	37.063
29.575	1.748	29.575	65.537	29.575	8.996	29.575	28.875
29.596	1.312	29.596	56.182	29.596	6.248	29.596	24.354
29.616	1.169	29.616	48.285	29.616	4.499	29.616	18.625
29.636	1.150	29.636	35.243	29.636	4.209	29.636	16.375
29.657	0.861	29.657	29.493	29.657	2.649	29.657	12.437
29.677	0.280	29.677	23.555	29.677	2.672	29.677	10.563
29.698	-0.051	29.698	20.493	29.698	1.570	29.698	8.938
29.718	0.994	29.718	15.076	29.718	1.738	29.718	7.605
29.739	0.434	29.739	14.076	29.739	1.657	29.739	6.668
29.759	0.478	29.759	11.014	29.759	1.076	29.759	5.460
29.779	0.398	29.779	9.306	29.779	1.079	29.779	4.482
29.800	0.505	29.800	8.077	29.800	0.602	29.800	4.566
29.820	0.196	29.820	6.932	29.820	0.563	29.820	3.566
29.841	0.116	29.841	5.620	29.841	0.420	29.841	3.151
29.861	-0.194	29.861	4.309	29.861	0.089	29.861	2.798
29.881	0.601	29.881	4.310	29.881	0.342	29.881	2.778
29.902	-0.083	29.902	4.040	29.902	0.491	29.902	2.654
29.922	0.379	29.922	3.770	29.922	0.473	29.922	1.405
29.943	-0.096	29.943	3.938	29.943	0.206	29.943	1.782
29.963	-0.009	29.963	2.398	29.963	0.647	29.963	1.888
29.984	0.016	29.984	1.837	29.984	0.150	29.984	1.785
30.004	0.207	30.004	2.588	30.004	0.653	30.004	0.724
30.024	0.170	30.024	2.215	30.024	0.157	30.024	1.059
30.045	0.153	30.045	1.217	30.045	-0.298	30.045	1.145
30.065	-0.301	30.065	2.115	30.065	-0.273	30.065	0.605
30.086	-0.537	30.086	1.284	30.086	0.064	30.086	0.815
30.106	0.436	30.106	1.057	30.106	0.006	30.106	0.422
30.127	0.805	30.127	1.059	30.127	0.426	30.127	-0.264
30.147	-0.285	30.147	1.061	30.147	-0.132	30.147	0.551
30.167	0.417	30.167	0.731	30.167	-0.190	30.167	0.387
30.188	-0.235	30.188	1.317	30.188	0.335	30.188	0.306
30.208	0.197	30.208	1.507	30.208	0.006	30.208	0.559
30.229	0.128	30.229	0.781	30.229	-0.302	30.229	0.708
30.249	-0.398	30.249	0.513	30.249	-0.089	30.249	0.273
30.270	-0.029	30.270	0.016	30.270	0.145	30.270	0.380
30.290	-0.180	30.290	1.103	30.290	0.150	30.290	0.612
30.310	-0.061	30.310	0.189	30.310	-0.158	30.310	0.469
30.331	-0.420	30.331	0.193	30.331	0.847	30.331	0.764
30.351	0.366	30.351	0.800	30.351	0.769	30.351	0.184
30.372	0.465	30.372	0.887	30.372	-0.080	30.372	0.250

30.392	-0.186	30.392	0.454	30.392	-0.304	30.392	-0.038
30.413	0.455	30.413	0.395	30.413	-0.041	30.413	-0.013
30.433	-0.612	30.433	-0.101	30.433	0.201	30.433	-0.197
30.453	-0.305	30.453	0.174	30.453	0.069	30.453	0.244
30.474	-0.144	30.474	0.137	30.474	0.228	30.474	0.790
30.494	-0.005	30.494	0.495	30.494	0.200	30.494	0.273
30.515	0.052	30.515	0.250	30.515	-0.183	30.515	0.194
30.535	0.212	30.535	-0.246	30.535	-0.023	30.535	0.614
30.556	0.102	30.556	-0.053	30.556	0.074	30.556	0.056
30.576	-0.091	30.576	0.202	30.576	0.379	30.576	-0.085
30.596	0.154	30.596	-0.085	30.596	0.497	30.596	0.253
30.617	0.502	30.617	-0.018	30.617	0.428	30.617	0.215
30.637	0.080	30.637	-0.137	30.637	0.275	30.637	0.554
30.658	0.887	30.658	0.430	30.658	0.081	30.658	0.308
30.678	0.486	30.678	-0.189	30.678	0.241	30.678	0.105
30.699	0.460	30.699	-0.163	30.699	0.152	30.699	-0.203
30.719	1.038	30.719	0.197	30.719	0.520	30.719	0.094
30.739	-0.092	30.739	0.244	30.739	0.097	30.739	-0.026
30.760	0.570	30.760	-0.291	30.760	0.570	30.760	-0.354
30.780	0.482	30.780	-0.235	30.780	0.585	30.780	0.037
30.801	0.269	30.801	-0.242	30.801	0.350	30.801	-0.010
30.821	0.201	30.821	-0.019	30.821	0.240	30.821	1.068
30.842	0.322	30.842	0.016	30.842	0.338	30.842	0.750
30.862	0.776	30.862	0.052	30.862	0.457	30.862	-0.088
30.882	0.834	30.882	0.463	30.882	0.660	30.882	0.991
30.903	0.725	30.903	0.478	30.903	1.196	30.903	0.632
30.923	0.930	30.923	0.159	30.923	0.920	30.923	0.544
30.944	0.571	30.944	-0.013	30.944	0.623	30.944	-0.002
30.964	1.338	30.964	0.127	30.964	0.347	30.964	0.431
30.985	1.376	30.985	0.039	30.985	0.258	30.985	0.801
31.005	0.976	31.005	0.679	31.005	0.399	31.005	0.401
31.025	0.764	31.025	0.466	31.025	0.894	31.025	1.022
31.046	1.657	31.046	0.273	31.046	0.827	31.046	0.393
31.066	0.632	31.066	0.372	31.066	0.760	31.066	0.660
31.087	0.900	31.087	0.076	31.087	1.172	31.087	0.531
31.107	1.250	31.107	0.155	31.107	1.709	31.107	0.360
31.128	1.685	31.128	0.379	31.128	1.600	31.128	0.690
31.148	1.473	31.148	0.562	31.148	0.992	31.148	0.562
31.168	1.512	31.168	0.162	31.168	1.571	31.168	0.766
31.189	1.842	31.189	0.741	31.189	1.483	31.189	0.867
31.209	2.152	31.209	0.341	31.209	1.375	31.209	0.906
31.230	1.816	31.230	0.795	31.230	0.787	31.230	0.965
31.250	2.438	31.250	0.708	31.250	1.700	31.250	1.378

31.271	2.352	31.271	0.954	31.271	2.155	31.271	1.209
31.291	2.829	31.291	0.867	31.291	2.151	31.291	1.018
31.311	3.327	31.311	0.885	31.311	2.064	31.311	2.536
31.332	3.074	31.332	1.235	31.332	2.560	31.332	1.638
31.352	3.197	31.352	2.065	31.352	2.807	31.352	2.260
31.373	3.653	31.373	1.041	31.373	2.825	31.373	2.508
31.393	4.297	31.393	1.372	31.393	2.946	31.393	2.401
31.414	5.254	31.414	0.952	31.414	3.047	31.414	2.649
31.434	5.481	31.434	1.887	31.434	3.732	31.434	2.771
31.454	5.875	31.454	2.092	31.454	3.708	31.454	3.144
31.475	6.186	31.475	1.944	31.475	4.643	31.475	3.288
31.495	7.497	31.495	2.816	31.495	4.786	31.495	4.161
31.516	7.558	31.516	3.376	31.516	4.575	31.516	4.118
31.536	7.515	31.536	2.957	31.536	4.843	31.536	4.408
31.557	8.972	31.557	3.288	31.557	6.174	31.557	4.593
31.577	9.367	31.577	3.182	31.577	6.963	31.577	4.988
31.597	9.699	31.597	4.055	31.597	6.898	31.597	4.069
31.618	10.906	31.618	3.928	31.618	8.042	31.618	5.526
31.638	13.093	31.638	3.635	31.638	8.415	31.638	6.233
31.659	12.196	31.659	3.675	31.659	8.954	31.659	6.316
31.679	13.862	31.679	3.194	31.679	9.098	31.679	5.981
31.700	14.862	31.700	4.630	31.700	10.263	31.700	7.418
31.720	15.299	31.720	4.129	31.720	12.199	31.720	7.979
31.740	16.465	31.740	4.732	31.740	12.843	31.740	7.937
31.761	18.590	31.761	4.773	31.761	12.570	31.761	8.728
31.781	21.381	31.781	5.584	31.781	14.027	31.781	9.644
31.802	21.985	31.802	4.834	31.802	15.776	31.802	10.289
31.822	23.277	31.822	5.916	31.822	15.358	31.822	10.580
31.843	25.568	31.843	6.249	31.843	16.399	31.843	10.851
31.863	24.610	31.863	6.832	31.863	18.293	31.863	12.538
31.883	27.360	31.883	7.498	31.883	18.980	31.883	13.226
31.904	27.111	31.904	7.602	31.904	20.666	31.904	13.309
31.924	26.632	31.924	9.331	31.924	22.707	31.924	14.663
31.945	28.383	31.945	9.123	31.945	23.498	31.945	14.622
31.965	27.758	31.965	10.748	31.965	22.810	31.965	14.622
31.986	28.259	31.986	11.311	31.986	23.435	31.986	15.851
32.006	26.281	32.006	10.853	32.006	24.080	32.006	16.623
32.026	26.490	32.026	11.540	32.026	24.205	32.026	16.436
32.047	27.387	32.047	11.562	32.047	23.371	32.047	15.228
32.067	25.909	32.067	11.479	32.067	23.871	32.067	16.458
32.088	24.847	32.088	11.272	32.088	23.600	32.088	14.563
32.108	23.182	32.108	10.814	32.108	23.204	32.108	14.814
32.129	23.975	32.129	12.232	32.129	22.059	32.129	14.419

32.149	22.747	32.149	10.546	32.149	22.246	32.149	13.337
32.169	21.624	32.169	9.547	32.169	20.330	32.169	14.984
32.190	20.959	32.190	10.152	32.190	19.456	32.190	12.902
32.210	18.565	32.210	9.633	32.210	19.289	32.210	14.195
32.231	20.129	32.231	10.072	32.231	19.602	32.231	12.238
32.251	17.881	32.251	9.053	32.251	17.832	32.251	11.323
32.272	15.529	32.272	9.492	32.272	18.396	32.272	11.429
32.292	14.719	32.292	8.515	32.292	16.980	32.292	11.118
32.312	13.221	32.312	8.496	32.312	15.502	32.312	9.786
32.333	11.556	32.333	7.311	32.333	14.024	32.333	9.455
32.353	10.955	32.353	7.271	32.353	12.358	32.353	8.832
32.374	10.416	32.374	6.336	32.374	11.776	32.374	7.584
32.394	9.106	32.394	6.922	32.394	10.819	32.394	6.753
32.415	8.650	32.415	5.821	32.415	10.237	32.415	6.422
32.435	7.569	32.435	3.969	32.435	9.156	32.435	6.383
32.455	7.010	32.455	4.035	32.455	9.074	32.455	6.198
32.476	7.242	32.476	4.204	32.476	7.617	32.476	4.597
32.496	5.391	32.496	3.291	32.496	7.161	32.496	4.391
32.517	4.769	32.517	2.752	32.517	5.913	32.517	3.831
32.537	4.918	32.537	2.755	32.537	5.227	32.537	3.397
32.558	4.630	32.558	2.571	32.558	4.813	32.558	3.150
32.578	4.092	32.578	1.637	32.578	4.752	32.578	3.028
32.598	4.574	32.598	1.974	32.598	4.484	32.598	2.719
32.619	4.578	32.619	1.645	32.619	4.028	32.619	2.701
32.639	5.144	32.639	1.524	32.639	3.781	32.639	3.100
32.660	4.231	32.660	1.382	32.660	3.804	32.660	2.208
32.680	4.444	32.680	1.719	32.680	4.786	32.680	2.357
32.701	4.906	32.701	1.119	32.701	4.747	32.701	2.236
32.721	5.931	32.721	1.332	32.721	5.062	32.721	2.282
32.741	5.852	32.741	1.128	32.741	3.753	32.741	2.285
32.762	6.419	32.762	1.029	32.762	4.173	32.762	2.602
32.782	6.381	32.782	1.304	32.782	3.530	32.782	2.356
32.803	6.052	32.803	1.267	32.803	3.950	32.803	2.964
32.823	6.328	32.823	1.480	32.823	5.037	32.823	2.385
32.844	6.895	32.844	1.402	32.844	4.415	32.844	3.348
32.864	6.817	32.864	1.386	32.864	5.544	32.864	3.227
32.884	7.905	32.884	2.413	32.884	5.818	32.884	3.753
32.905	8.181	32.905	1.710	32.905	6.468	32.905	3.612
32.925	8.727	32.925	2.507	32.925	6.346	32.925	3.575
32.946	9.107	32.946	2.221	32.946	6.829	32.946	3.496
32.966	9.467	32.966	2.643	32.966	7.375	32.966	4.376
32.987	9.368	32.987	2.461	32.987	7.463	32.987	4.965
33.007	11.228	33.007	2.551	33.007	8.383	33.007	4.907

33.027	10.921	33.027	3.327	33.027	9.596	33.027	4.600
33.048	12.155	33.048	3.563	33.048	9.309	33.048	5.918
33.068	12.474	33.068	3.777	33.068	9.313	33.068	6.277
33.089	11.792	33.089	3.221	33.089	10.380	33.089	6.699
33.109	11.548	33.109	3.936	33.109	10.198	33.109	5.497
33.130	11.679	33.130	3.672	33.130	9.577	33.130	6.482
33.150	11.206	33.150	4.595	33.150	11.145	33.150	6.529
33.170	11.920	33.170	3.894	33.170	10.712	33.170	7.618
33.191	10.781	33.191	4.547	33.191	10.467	33.191	6.854
33.211	9.391	33.211	4.325	33.211	10.827	33.211	7.276
33.232	9.773	33.232	4.707	33.232	10.561	33.232	6.678
33.252	9.404	33.252	3.777	33.252	9.025	33.252	6.372
33.273	9.140	33.273	4.701	33.273	9.947	33.273	5.878
33.293	7.313	33.293	4.062	33.293	8.911	33.293	5.385
33.313	7.612	33.313	4.237	33.313	8.500	33.313	4.725
33.334	6.494	33.334	4.161	33.334	8.443	33.334	4.815
33.354	6.605	33.354	4.002	33.354	7.949	33.354	4.572
33.375	5.737	33.375	2.073	33.375	7.225	33.375	3.995
33.395	4.786	33.395	3.393	33.395	5.502	33.395	4.023
33.416	4.877	33.416	2.089	33.416	5.383	33.416	3.780
33.436	3.967	33.436	2.868	33.436	5.244	33.436	3.516
33.456	4.392	33.456	2.377	33.456	4.687	33.456	3.169
33.477	3.649	33.477	2.240	33.477	4.486	33.477	2.885
33.497	3.594	33.497	1.290	33.497	4.304	33.497	1.976
33.518	2.644	33.518	1.778	33.518	3.686	33.518	2.629
33.538	2.631	33.538	1.578	33.538	3.859	33.538	2.158
33.559	2.118	33.559	1.608	33.559	2.699	33.559	1.540
33.579	3.147	33.579	0.867	33.579	1.956	33.579	1.381
33.599	2.655	33.599	1.606	33.599	2.422	33.599	1.452
33.620	2.101	33.620	0.490	33.620	2.283	33.620	1.439
33.640	2.338	33.640	0.479	33.640	2.144	33.640	1.405
33.661	3.118	33.661	1.030	33.661	1.985	33.661	1.518
33.681	1.939	33.681	0.144	33.681	2.159	33.681	1.151
33.702	2.156	33.702	0.550	33.702	2.354	33.702	0.930
33.722	2.143	33.722	0.726	33.722	2.257	33.722	1.064
33.742	2.611	33.742	0.382	33.742	1.640	33.742	1.343
33.763	2.869	33.763	0.455	33.763	1.897	33.763	1.081
33.783	3.274	33.783	0.569	33.783	2.155	33.783	1.361
33.804	3.158	33.804	1.038	33.804	1.746	33.804	2.161
33.824	2.522	33.824	0.965	33.824	1.900	33.824	1.566
33.845	2.906	33.845	0.309	33.845	2.554	33.845	1.283
33.865	3.707	33.865	0.758	33.865	2.250	33.865	1.230
33.885	4.404	33.885	0.768	33.885	1.445	33.885	1.802

33.906	3.872	33.906	0.863	33.906	2.850	33.906	1.811
33.926	4.715	33.926	0.811	33.926	2.483	33.926	1.633
33.947	5.704	33.947	1.177	33.947	2.887	33.947	1.747
33.967	5.526	33.967	1.146	33.967	3.334	33.967	2.361
33.988	5.599	33.988	1.095	33.988	3.072	33.988	1.829
34.008	5.796	34.008	1.023	34.008	3.935	34.008	2.505
34.028	5.702	34.028	1.556	34.028	3.902	34.028	2.494
34.049	6.087	34.049	1.609	34.049	4.848	34.049	2.379
34.069	6.598	34.069	2.350	34.069	5.066	34.069	2.327
34.090	6.671	34.090	2.112	34.090	5.554	34.090	3.004
34.110	6.410	34.110	2.395	34.110	4.626	34.110	3.160
34.131	6.046	34.131	2.512	34.131	5.031	34.131	3.149
34.151	6.119	34.151	1.837	34.151	5.520	34.151	3.410
34.171	5.151	34.171	1.870	34.171	5.634	34.171	3.837
34.192	4.703	34.192	2.487	34.192	5.331	34.192	3.139
34.212	5.277	34.212	1.937	34.212	5.403	34.212	2.546
34.233	4.705	34.233	2.345	34.233	3.496	34.233	2.994
34.253	4.424	34.253	1.692	34.253	4.423	34.253	2.276
34.274	2.977	34.274	2.371	34.274	4.246	34.274	3.058
34.294	3.113	34.294	1.822	34.294	3.172	34.294	1.861
34.314	2.812	34.314	1.565	34.314	3.203	34.314	2.039
34.335	2.011	34.335	1.620	34.335	2.651	34.335	1.967
34.355	1.690	34.355	1.654	34.355	2.099	34.355	0.958
34.376	2.076	34.376	1.105	34.376	2.172	34.376	1.469
34.396	1.067	34.396	0.848	34.396	1.266	34.396	1.147
34.417	1.017	34.417	0.612	34.417	1.610	34.417	1.513
34.437	1.570	34.437	0.730	34.437	1.329	34.437	0.483
34.457	1.270	34.457	1.036	34.457	1.278	34.457	0.766
34.478	1.116	34.478	0.466	34.478	1.706	34.478	0.653
34.498	1.315	34.498	0.189	34.498	0.737	34.498	0.145
34.519	0.203	34.519	0.599	34.519	0.665	34.519	0.761
34.539	0.611	34.539	0.489	34.539	0.822	34.539	0.565
34.560	0.686	34.560	0.420	34.560	0.271	34.560	0.327
34.580	-0.239	34.580	0.102	34.580	0.574	34.580	0.423
34.600	0.253	34.600	0.158	34.600	-0.185	34.600	-0.064
34.621	0.100	34.621	0.444	34.621	0.556	34.621	0.157
34.641	-0.096	34.641	0.355	34.641	-0.036	34.641	0.232
34.662	0.688	34.662	-0.130	34.662	0.205	34.662	0.328
34.682	0.597	34.682	0.344	34.682	0.300	34.682	-0.075
34.703	0.131	34.703	-0.058	34.703	-0.146	34.703	-0.375
34.723	0.144	34.723	-0.438	34.723	-0.072	34.723	0.086
34.743	0.158	34.743	0.328	34.743	0.961	34.743	0.026
34.764	0.109	34.764	-0.031	34.764	0.161	34.764	0.049

34.784	0.247	34.784	0.005	34.784	0.215	34.784	-0.011
34.805	0.386	34.805	0.126	34.805	0.020	34.805	0.659
34.825	-0.121	34.825	0.287	34.825	-0.114	34.825	0.078
34.846	0.206	34.846	0.054	34.846	-0.601	34.846	-0.127
34.866	-0.093	34.866	0.070	34.866	0.224	34.866	-0.020
34.886	0.067	34.886	-0.018	34.886	0.050	34.886	-0.204
34.907	0.185	34.907	-0.105	34.907	-0.437	34.907	-0.430
34.927	0.450	34.927	0.224	34.927	-0.028	34.927	0.511
34.948	-0.036	34.948	0.220	34.948	-0.202	34.948	-0.257
34.968	-0.209	34.968	0.258	34.968	0.311	34.968	0.372
34.989	-0.236	34.989	-0.121	34.989	-0.217	34.989	0.292
35.009	0.591	35.009	-0.333	35.009	0.109	35.009	-0.517
35.029	0.689	35.029	0.121	35.029	-0.065	35.029	-0.075
35.050	-0.129	35.050	0.159	35.050	-0.030	35.050	-0.446
35.070	0.052	35.070	-0.157	35.070	-0.287	35.070	0.433
35.091	-0.183	35.091	0.298	35.091	0.165	35.091	0.437
35.111	0.207	35.111	0.149	35.111	-0.155	35.111	-0.080
35.132	-0.048	35.132	0.271	35.132	0.401	35.132	-0.055
35.152	0.071	35.152	-0.190	35.152	0.207	35.152	0.179
35.172	-0.268	35.172	0.202	35.172	0.242	35.172	-0.234
35.193	-0.095	35.193	0.075	35.193	-0.347	35.193	-0.416
35.213	-0.027	35.213	0.197	35.213	0.188	35.213	0.254
35.234	-0.167	35.234	0.173	35.234	-0.276	35.234	0.134
35.254	0.297	35.254	0.212	35.254	-0.250	35.254	0.117
35.275	0.615	35.275	0.668	35.275	0.130	35.275	-0.191
35.295	0.038	35.295	0.166	35.295	0.511	35.295	0.085
35.315	0.356	35.315	0.497	35.315	0.412	35.315	0.152
35.336	0.696	35.336	0.391	35.336	0.210	35.336	0.011
35.356	0.202	35.356	0.202	35.356	-0.263	35.356	0.558
35.377	-0.021	35.377	0.512	35.377	0.743	35.377	0.250
35.397	0.403	35.397	0.906	35.397	0.478	35.397	0.318
35.418	0.534	35.418	0.717	35.418	0.734	35.418	0.344
35.438	0.416	35.438	0.341	35.438	0.074	35.438	0.537
35.458	0.714	35.458	0.694	35.458	0.392	35.458	0.771
35.479	0.513	35.479	0.922	35.479	0.503	35.479	0.339
35.499	0.436	35.499	0.525	35.499	0.218	35.499	0.428
35.520	0.777	35.520	0.732	35.520	0.391	35.520	0.288
35.540	0.805	35.540	0.148	35.540	0.794	35.540	0.856
35.561	1.124	35.561	0.543	35.561	0.613	35.561	0.195
35.581	0.736	35.581	1.125	35.581	0.766	35.581	0.868
35.601	0.597	35.601	1.083	35.601	0.731	35.601	0.957
35.622	1.230	35.622	0.520	35.622	0.697	35.622	1.276
35.642	0.862	35.642	0.874	35.642	1.183	35.642	1.115

35.663	0.662	35.663	1.353	35.663	0.795	35.663	1.164
35.683	0.503	35.683	1.082	35.683	0.823	35.683	0.774
35.704	1.053	35.704	1.165	35.704	1.226	35.704	0.822
35.724	0.519	35.724	0.769	35.724	0.817	35.724	1.454
35.744	0.694	35.744	1.207	35.744	0.783	35.744	1.711
35.765	0.868	35.765	1.520	35.765	1.082	35.765	1.551
35.785	0.897	35.785	1.625	35.785	0.799	35.785	1.724
35.806	0.802	35.806	1.271	35.806	0.723	35.806	1.836
35.826	0.685	35.826	2.563	35.826	0.960	35.826	2.343
35.847	0.881	35.847	2.252	35.847	1.677	35.847	2.600
35.867	0.411	35.867	2.607	35.867	0.852	35.867	1.941
35.887	1.044	35.887	3.150	35.887	0.777	35.887	2.406
35.908	1.720	35.908	2.359	35.908	1.077	35.908	2.601
35.928	0.958	35.928	2.985	35.928	0.502	35.928	3.067
35.949	1.634	35.949	4.424	35.949	2.573	35.949	3.367
35.969	0.580	35.969	5.176	35.969	2.124	35.969	4.562
35.990	1.069	35.990	5.677	35.990	1.612	35.990	5.674
36.010	0.411	36.010	6.721	36.010	2.621	36.010	5.682

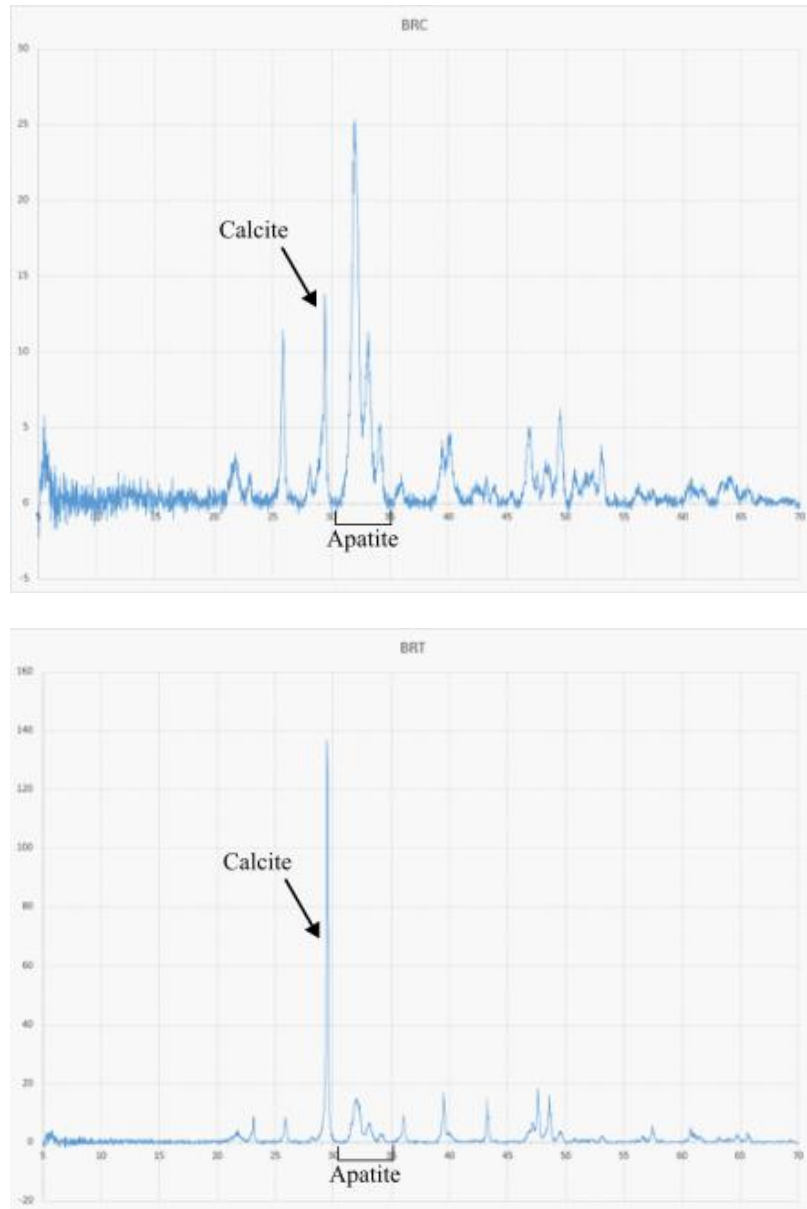


Figure 21: X-Ray Diffractograms for Brontothere Rib Subsamples. These charts show XRD profiles for cortical and trabecular subsamples of brontothere rib, highlighting disparities in calcite and apatite peaks.

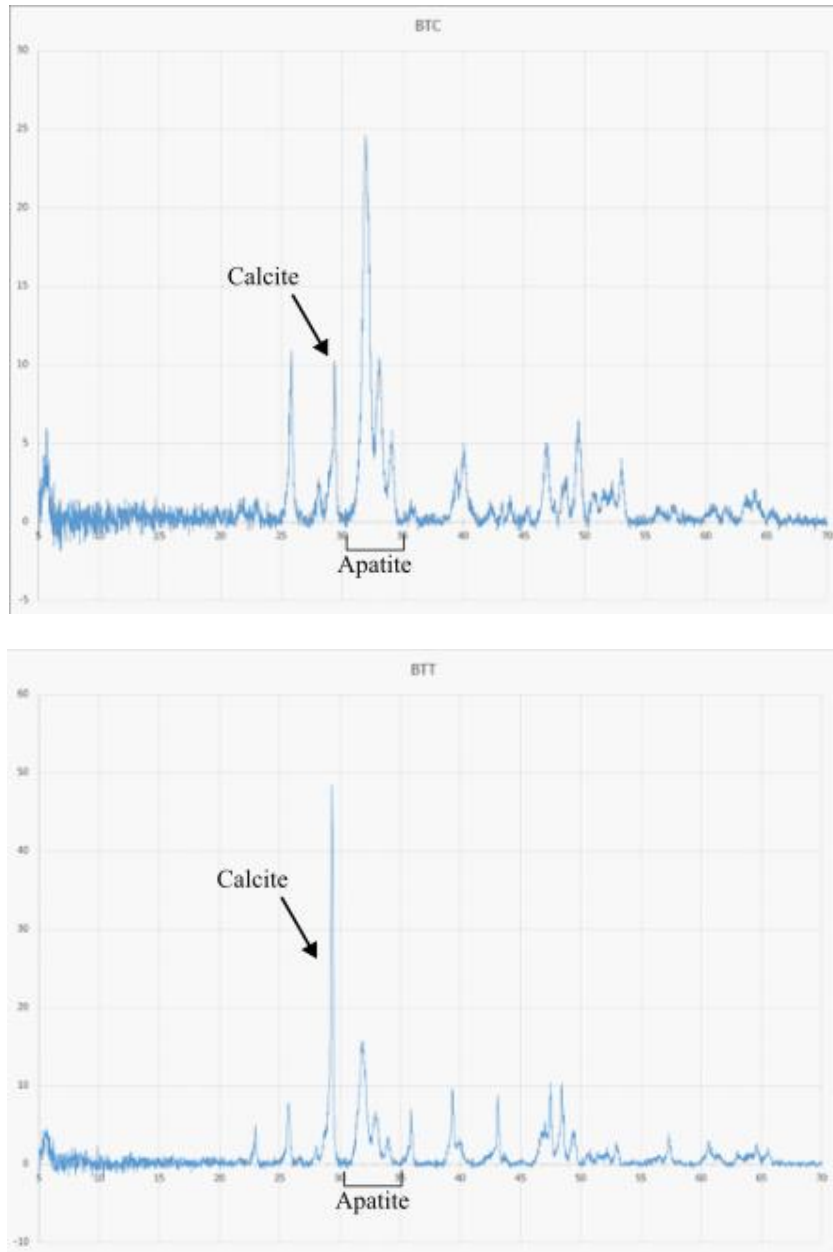


Figure 22: X-Ray Diffractograms for Brontothere Phalanx Subsamples. These charts show XRD profiles for cortical and trabecular subsamples of brontothere phalanx, highlighting disparities in calcite and apatite peaks.

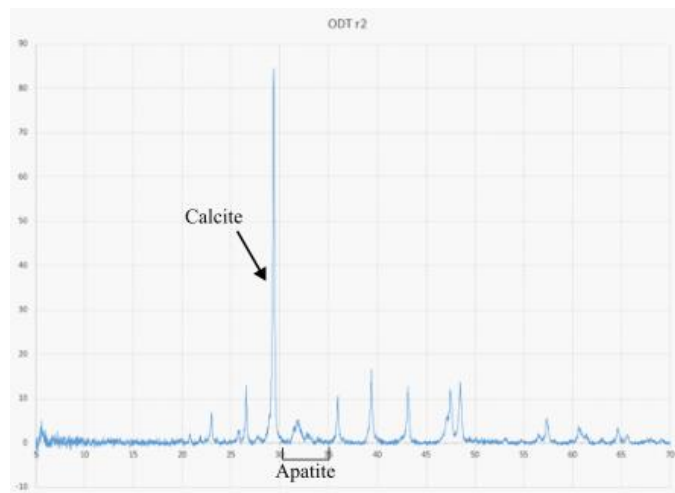
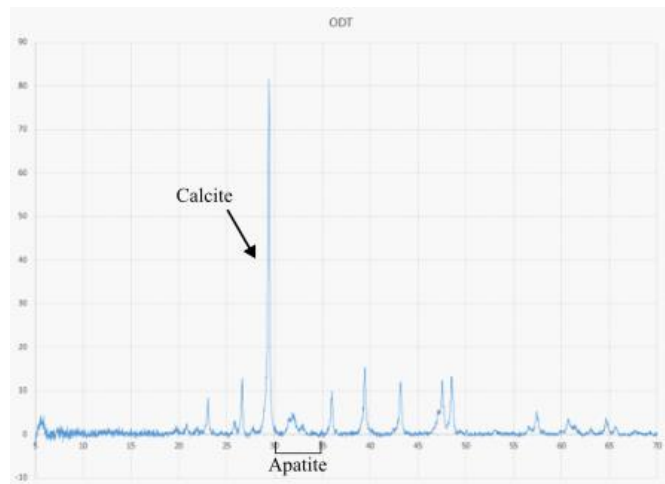
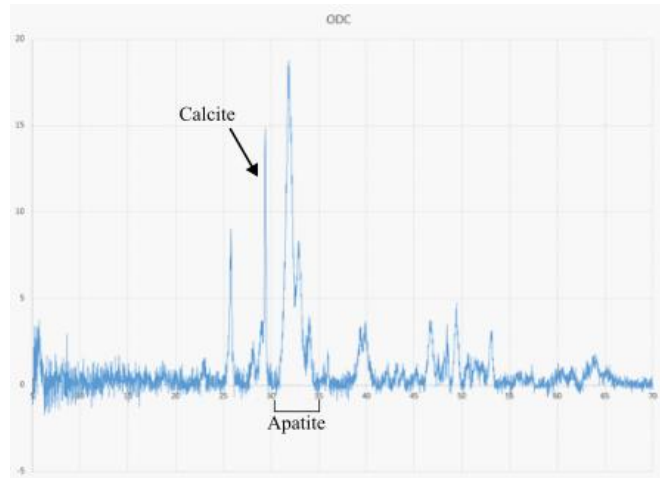


Figure 23: X-Ray Diffractograms for Oreodont Dental Subsamples. These charts show XRD profiles for cortical and trabecular subsamples of oreodont dentary, highlighting disparities in calcite and apatite peaks.

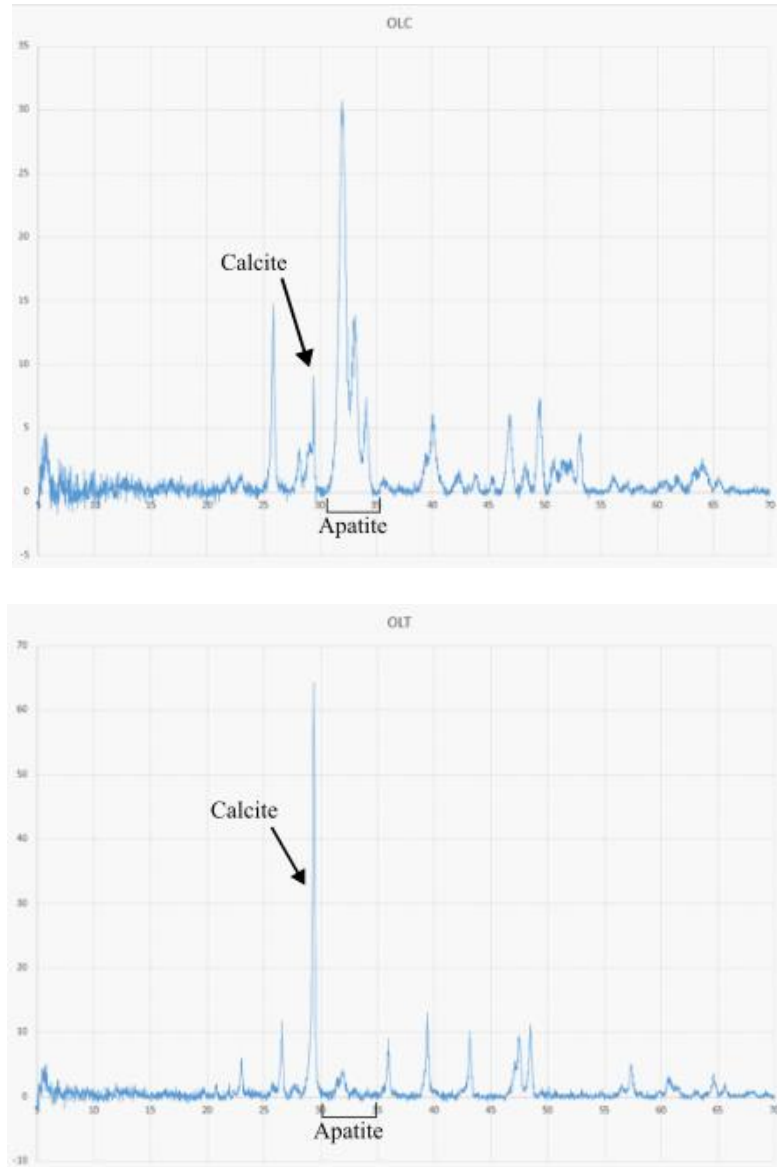


Figure 24: X-Ray Diffractograms for Oreodont Limb Subsamples. These charts show XRD profiles for cortical and trabecular subsamples of oreodont limb, highlighting disparities in calcite and apatite peaks.

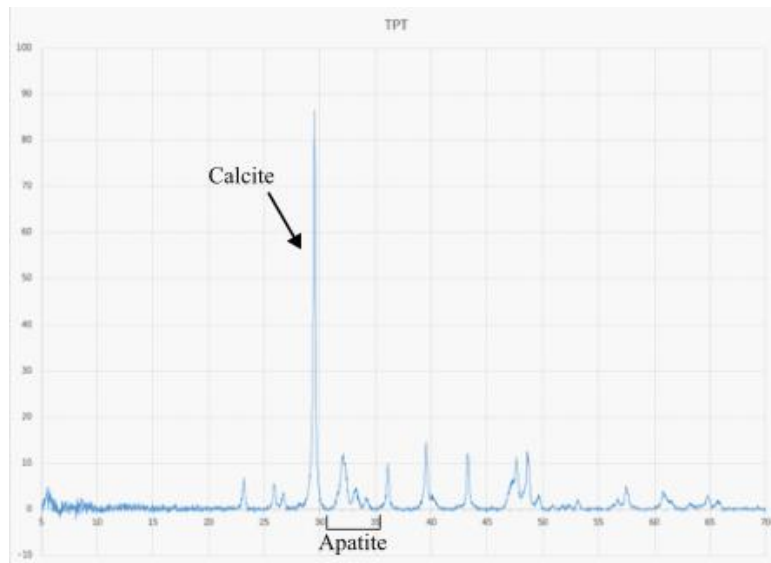
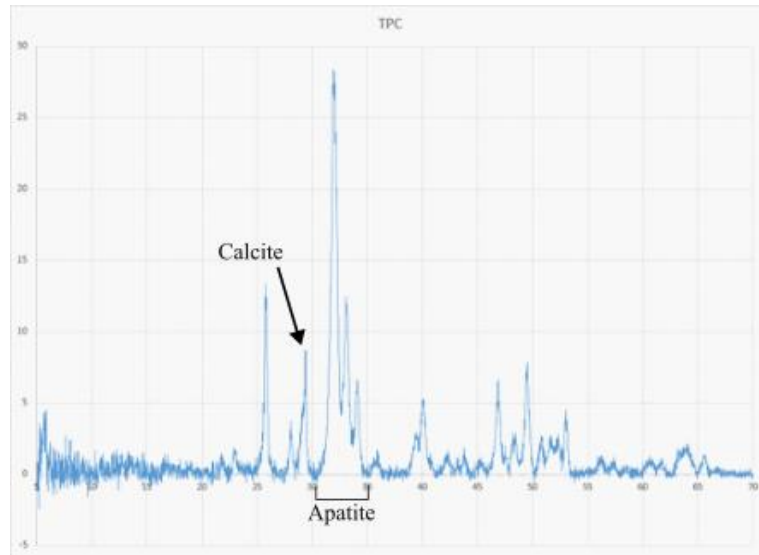


Figure 25: X-Ray Diffractograms for Tortoise Peripheral Subsamples. These charts show XRD profiles for cortical and trabecular subsamples of tortoise peripheral, highlighting disparities in calcite and apatite peaks.

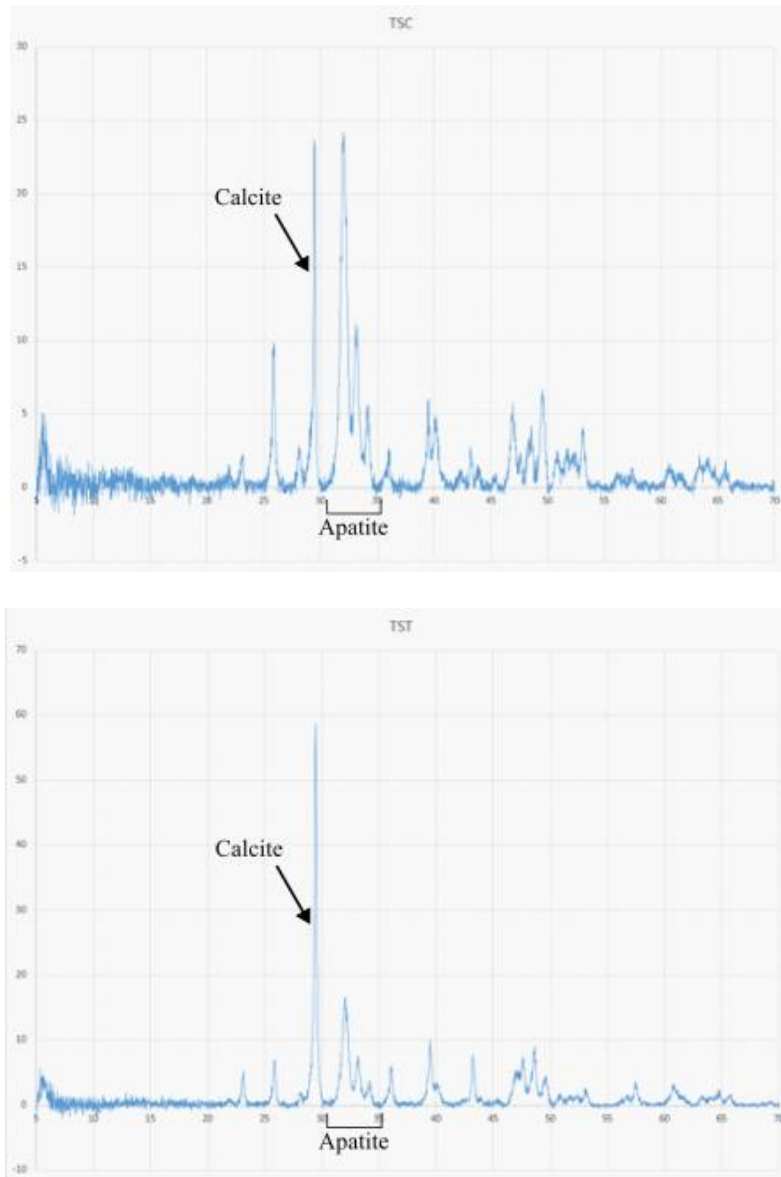


Figure 26: X-Ray Diffractograms for Tortoise Scapula Subsamples. These charts show XRD profiles for cortical and trabecular subsamples of tortoise scapula, highlighting disparities in calcite and apatite peaks.

APPENDIX E

SEM IMAGES AND EDS DATA

Electron Image 3

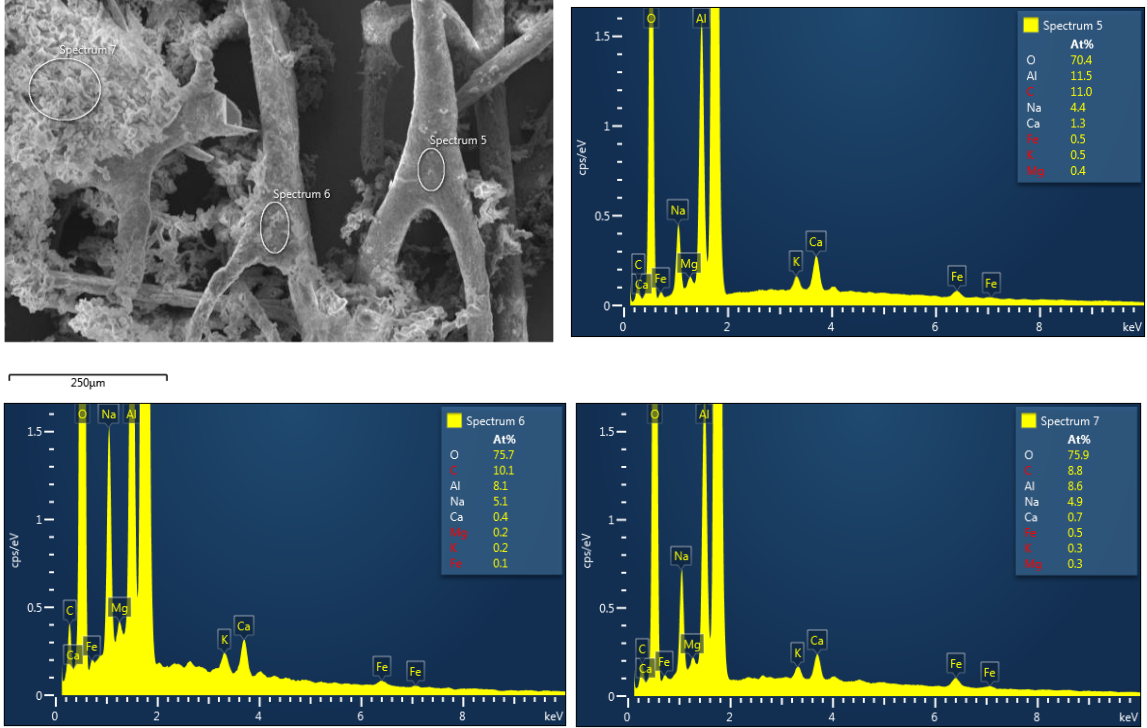


Figure 27. Structures and EDS Spectra from *Brontothere Phalanx Cortical Bone*. These plots highlight elemental composition of selected sites in the secondary electron image (top). Each shows high abundance of silicon (unlabeled peak at 1.8keV), oxygen, and aluminum.

Electron Image 4

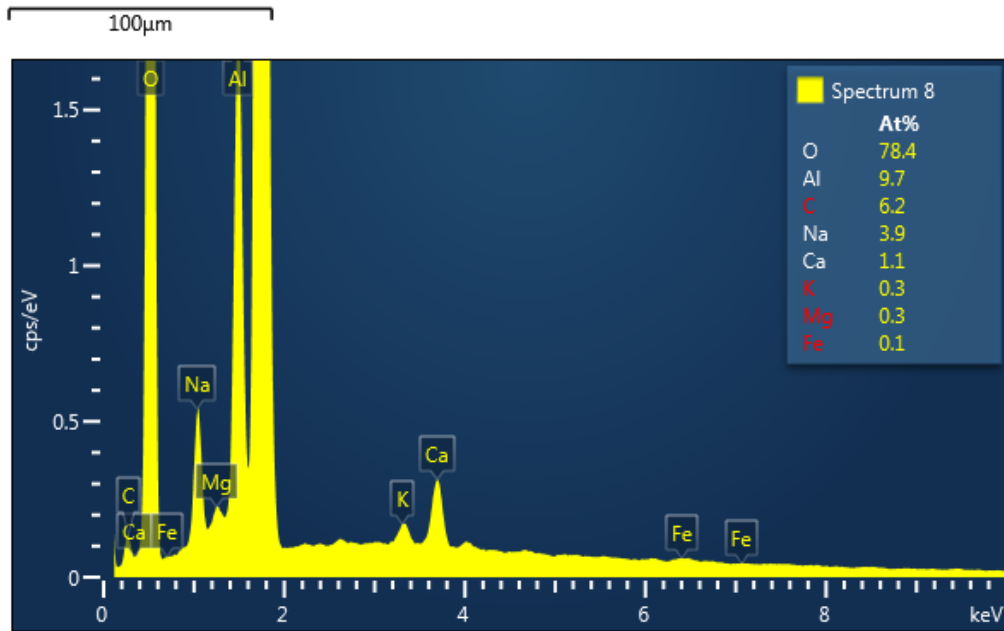
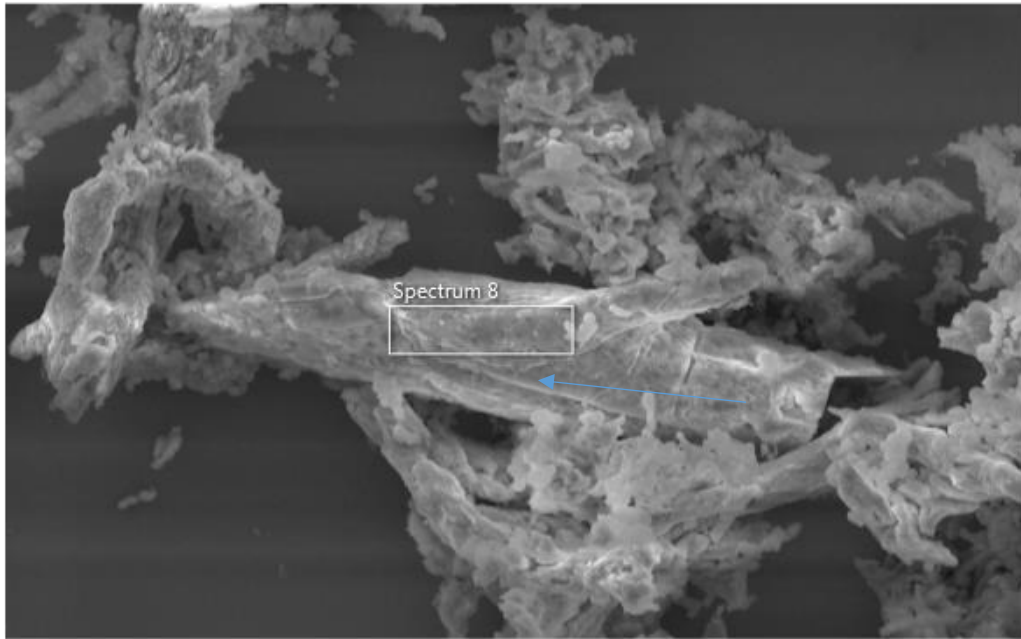


Figure 28. Preserved Vessel from *Brontothere Phalanx Trabecular Bone*. Blue arrow indicates suspected fungal hyphae preserved on a permineralized blood vessel.

Electron Image 2

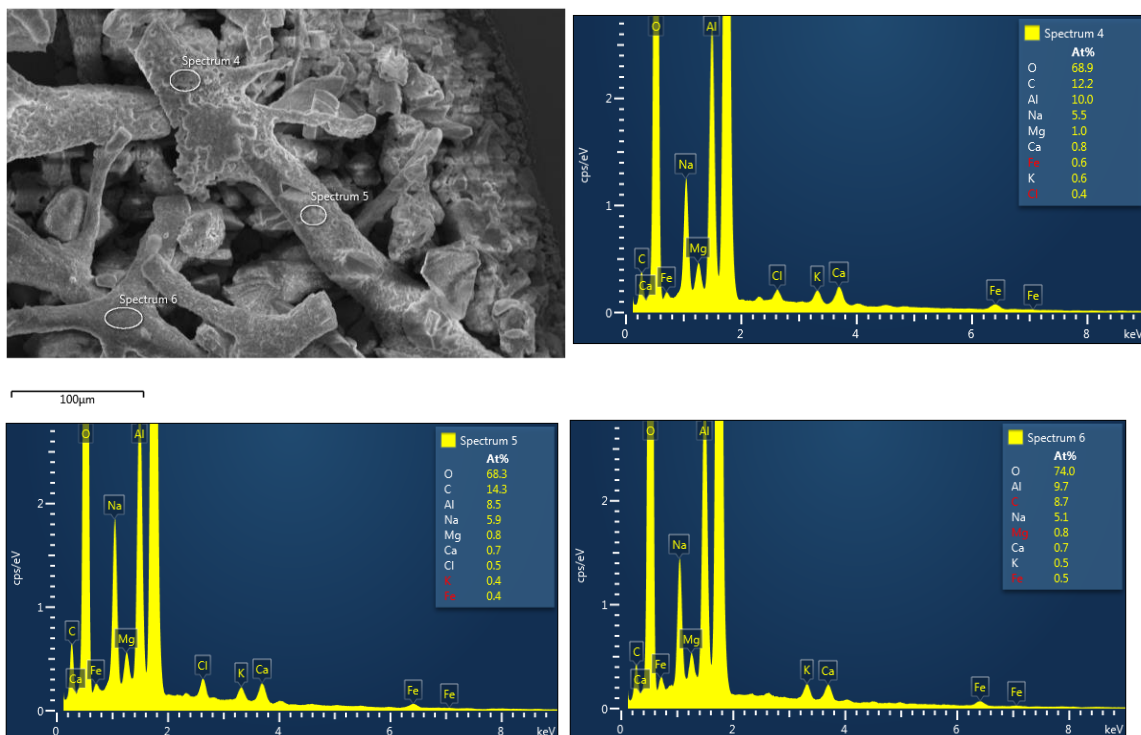


Figure 29. Structures and EDS Spectra from Oreodont Limb Cortical Bone. These plots highlight elemental composition of selected sites in the secondary electron image (top). Each shows high abundance of silicon (unlabeled peak at 1.8keV), oxygen, and aluminum.

Electron Image 4

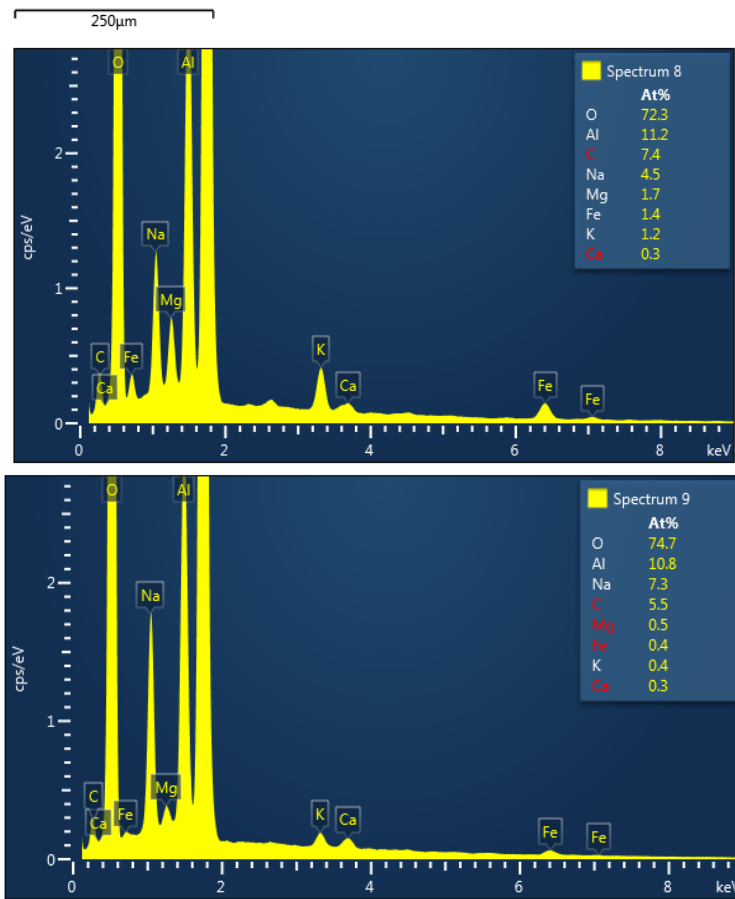
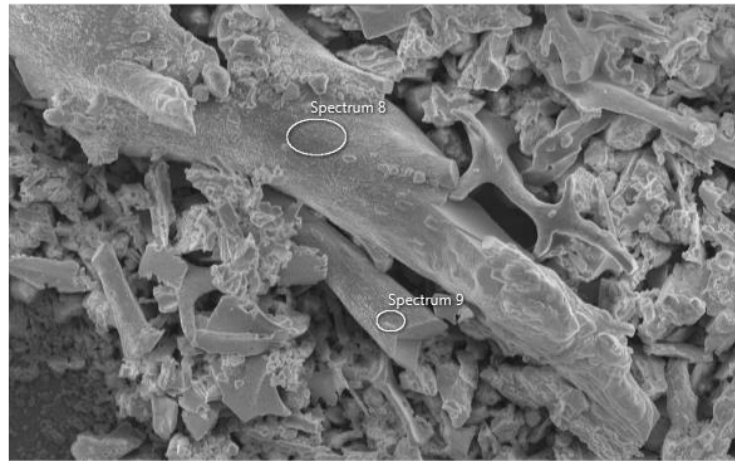


Figure 30. Structures and EDS Spectra from Oreodont Limb Trabecular Bone. These plots highlight elemental composition of selected sites in the secondary electron image (top). Each shows high abundance of silicon (unlabeled peak at 1.8keV), oxygen, and aluminum.

Electron Image 6

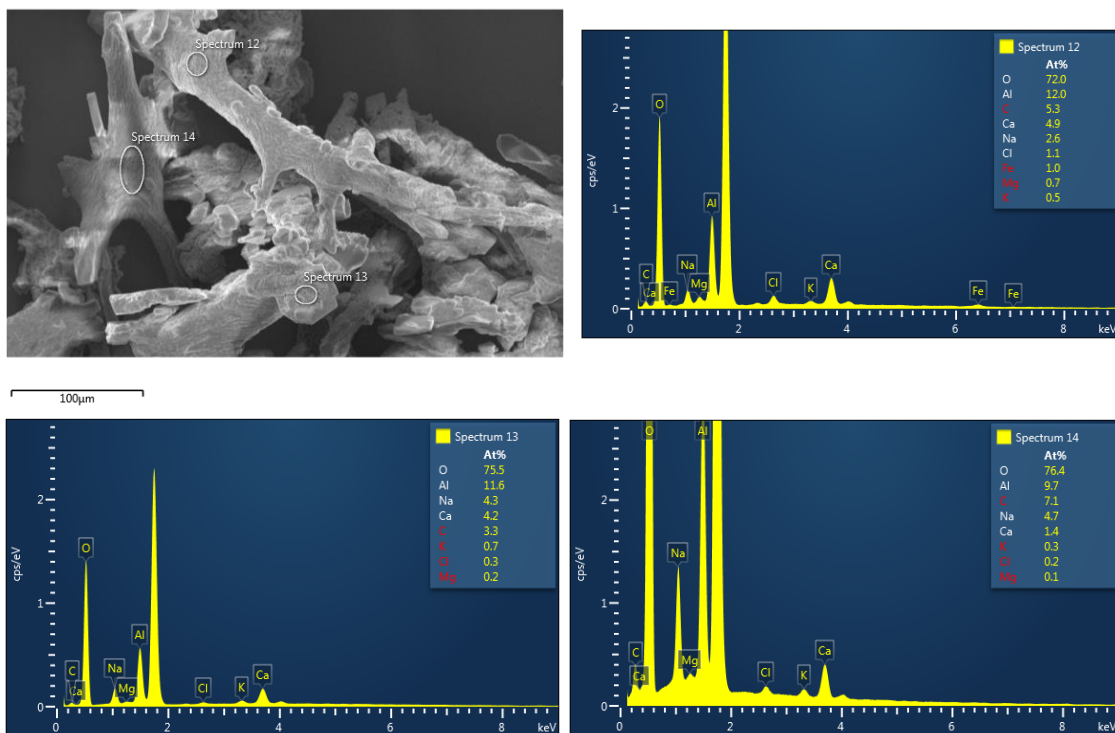


Figure 31. Structures and EDS Spectra from Oreodont Dentary Cortical Bone. These plots highlight elemental composition of selected sites in the secondary electron image (top). Each shows high abundance of silicon (unlabeled peak at 1.8keV), oxygen, and aluminum.

APPENDIX F
SEM-EDS MAPPING
EDS Layered Image 1

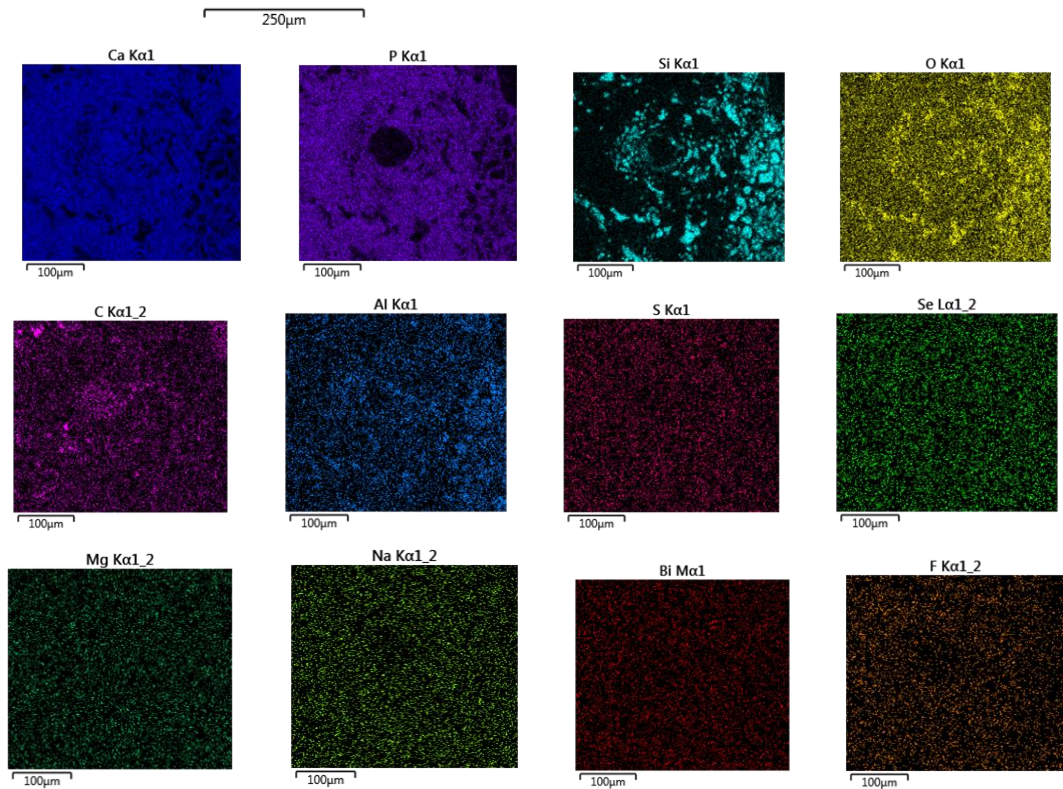
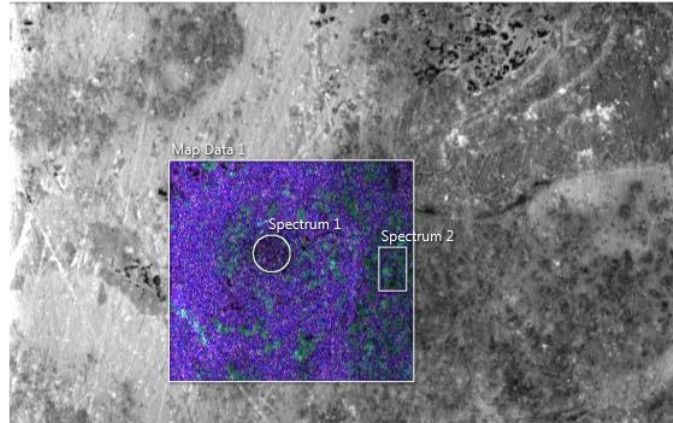


Figure 32. Brontothere Rib EDS Map Set. These images combine to produce a geochemical profile of the mapped area of the brontothere rib thin section, shown in the blue box on the SEM image, with each color representing a different detected element.

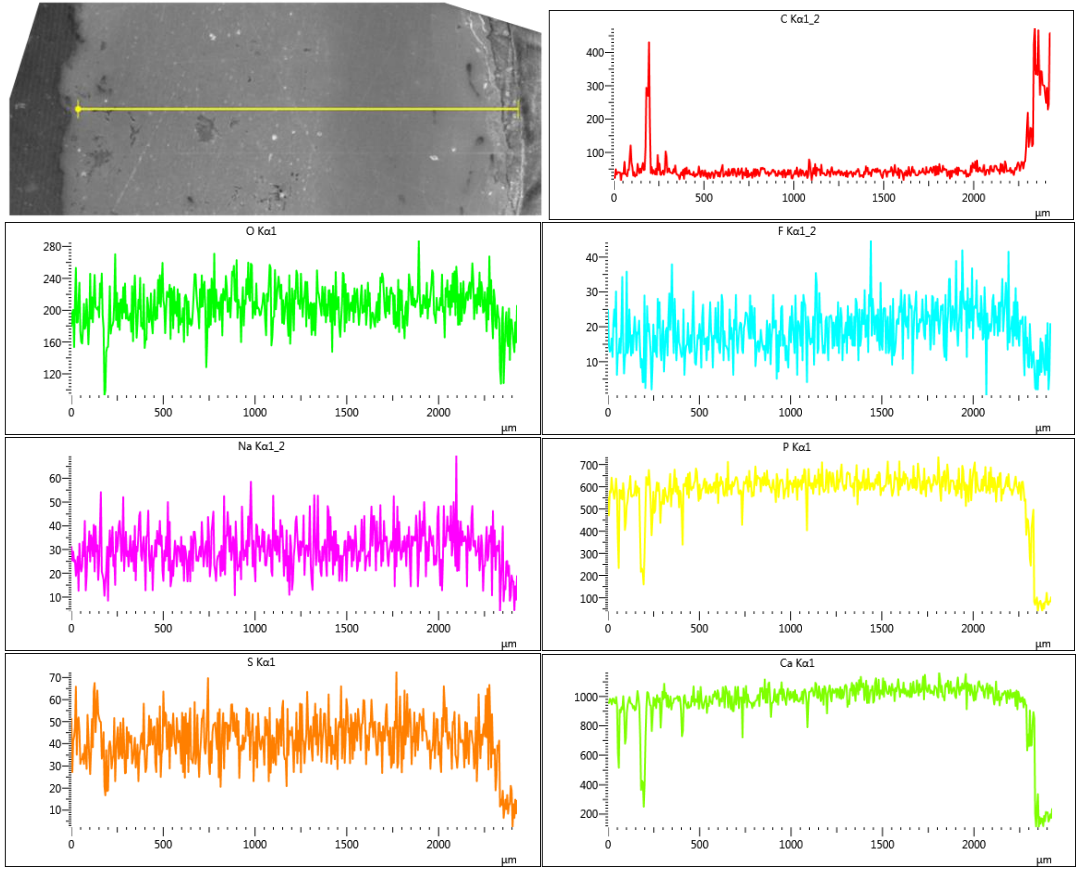


Figure 33. Oreodont Limb Bone EDS Line Scan. The left edge of image extends into medullary cavity (dark); right is the cortical margin, with signatures at the end from embedding resin.

EDS Layered Image 5

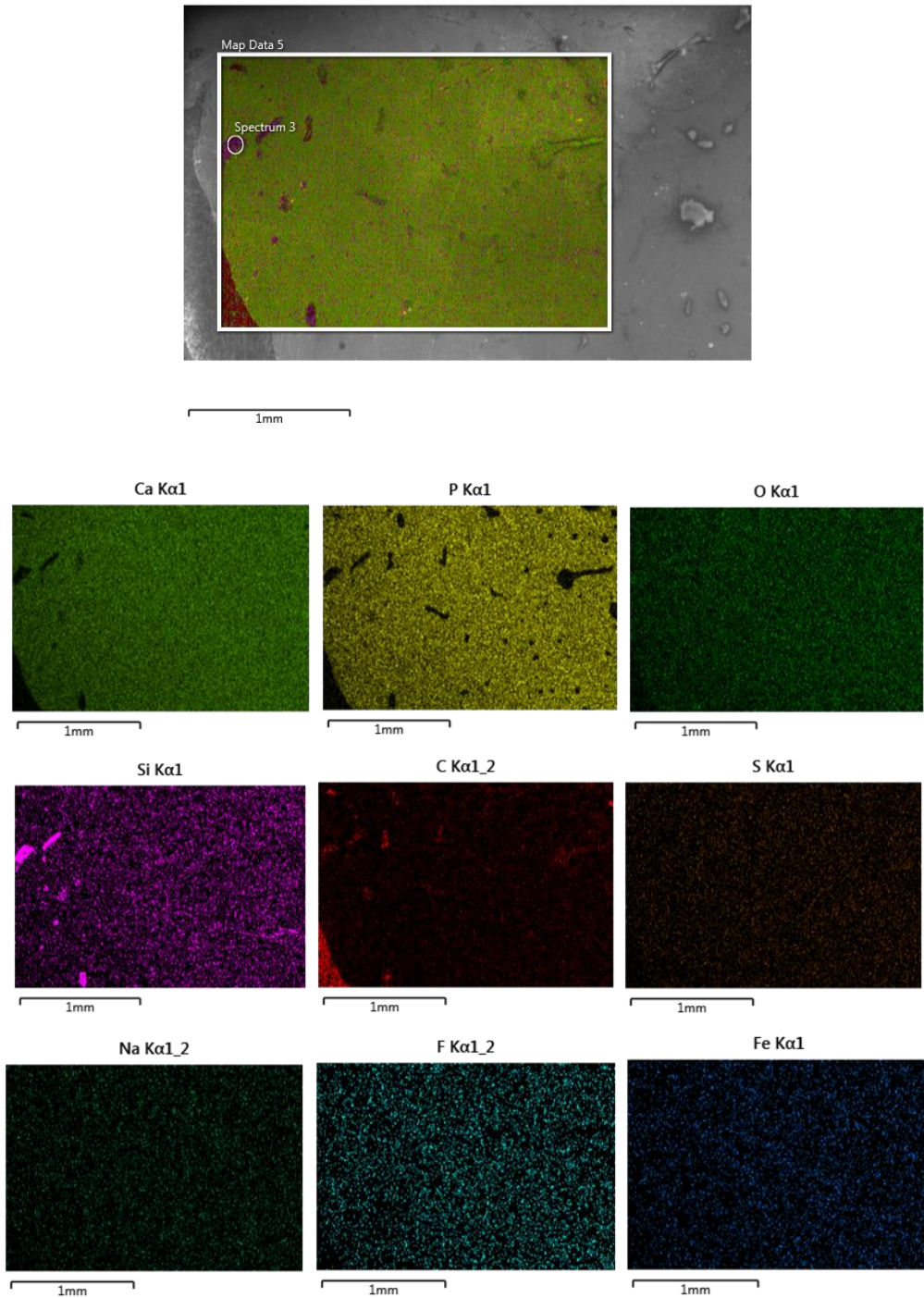


Figure 34. Tortoise Peripheral EDS Map Set. These images combine to produce a geochemical profile of the mapped area of the tortoise peripheral thin section, shown in the blue box on the SEM image, with each color representing a different detected element.